Annual Report 2010

Institute for Pulsed Power and Microwave Technology

Jahresbericht 2010

Institut für Hochleistungsimpuls- und Mikrowellentechnik (IHM)

Manfred Thumm (ed.)

KIT Scientific Publishing

Manfred Thumm (ed.)

Annual Report 2010

Institute for Pulsed Power and Microwave Technology

Jahresbericht 2010

Institut für Hochleistungsimpuls- und Mikrowellentechnik (IHM)

Karlsruhe Institute of Technology

KIT SCIENTIFIC REPORTS 7590

Annual Report 2010

Institute for Pulsed Power and Microwave Technology

Jahresbericht 2010

Institut für Hochleistungsimpuls- und Mikrowellentechnik (IHM)

edited by
Manfred Thumm

Report-Nr. KIT-SR 7590

Institute for Pulsed Power and Microwave Technology

(Institut für Hochleistungsimpuls- und Mikrowellentechnik (IHM))

Director (acting):   Prof. Dr. Dr. h.c. Manfred Thumm

The main working fields of the IHM have been research, development, academic education and, in collaboration with the KIT Division IMA and industrial partners, the technology transfer in the areas of pulsed power technology and microwave technology at high power levels. The projects of the IHM have been conducted within six HGF Programs: Renewable Energies (EE), FUSION, NUKLEAR, NANOMIKRO, Efficient Energy Conversion and Use (REUN) and Technology-Innovation and Society (TIG). R&D work has been done in the following topics: theoretical and experimental basics of pulsed power and high power microwave technology; theory and experiments on the generation of intensive electron beams, strong electromagnetic fields and waves and their interaction with plants, materials and plasmas; application of these methods in the area of generation of energy through controlled thermonuclear fusion in magnetically confined plasmas, in materials processing and in energy technology. Research in both divisions of the IHM require the application of modern electron beam optics, high voltage technology and high voltage measurement techniques. A short description of the R&D program of the IHM is as follows:

Pulsed Power Division (Head: Dr. Georg Müller):

In environmental- and bio-technology the research and development is devoted to pulsed power technology with repetition rates up to 20 Hz, power in the Giga-Watt range and electric field strengths of 10^5-10^7 V/m. The research is concerned with short pulse (µs) - and with ultra-short pulse (ns) treatment of biological cells (electroporation).The focus is related to large-scale applications, treatment of large volumes, to the realization of a high component life time and to the overall process integration. Main directions of work in this field are the electroporation of biological cells for extraction of cell contents (KEA process), the dewatering and drying of green biomass, the treatment of micro algae for further energetic use and sustainable reduction of bacteria in contaminated effluents. Another key research topic is related to the surface modification and corrosion protection of metals and alloys using high-energy, large-area pulsed electron beams (GESA process). The research is focused on electron beam physics, the interaction of electron beams with material surfaces and the corresponding material specific characterization investigations. The goal is to develop a corrosion barrier for improved compatibility of structural nuclear reactor materials in contact with heavy liquid metal coolants (Pb or PbBi) (Programs: EE, NUKLEAR, TIG).

— The commissioning of an annular gap photobioreactor has been completed. Due to media optimization an algea cell density of at least 5 g/l (dry mass) has been reproduced in monthly runs. The cell density and lipid status were monitored in time using photometric and fluorescent optical methods. It was shown that the maximum lipid content does not coincide with the highest cell density. Therefore, the development of a proper lipid diagnostic is a key issue for the energetic use of micro algea (Programs: EE, TIG).

— To measure the effectiveness of electroporaton assisted extraction from micro algae fast photometric and fluorescence optical tests were established. For quantitative measurement of intracellular lipids, the Nile-Red staining of the lipids and the coupled diagnostics was improved. Extraction results from initiated studies show that a combined process of pulse treatment, drying and ethanol as

a solvent the lipid yield can be increased by a factor of 2-3. The protein content in the extracellular medium can also be doubled after electric pulse treatment (Program: EE).

— Basic studies on the influence of intracellular processes in plant cells using ultra-short (ns) pulsed electric fields (PEF) were performed. Previous results on electroporation assisted growth stimulation in fungi spawn have been confirmed by further experiments. Moreover, it was obtained that nsPEF-treatment also improves the development of rhizomorphic mycelium, which is responsible for the formation of fruiting bodies. First results indicate an increase of mushroom yield by a factor of 2 compared to the control (Program: EE, KIT-Shared Research Group).

— An effective long-term protection against corrosion in Pb and PbBi-cooled systems was confirmed at high temperatures (550 to 650 °C) by alloying aluminum into the steel surfaces or re-melting of FeCrAlY coatings by the GESA process. However, for selective formation of pure Al_2O_3 at low temperatures of 400 to 500 °C, the Al and/or Cr content must be increased. At a concentration of 15 wt% Cr and 11 wt% Al, formation of thin alumina layers can be guaranteed over the entire temperature range (400-650 °C) (Program NUKLEAR).

**High Power Microwave Division
(Head (acting): Dr. Gerd Gantenbein):**

The activities on high-power microwave technology are being performed in the fields of heating of magnetically confined nuclear fusion plasmas and microwave materials processing.

— Planning, construction and testing of the entire 10 MW, 140 GHz electron cyclotron resonance heating ECRH system for continuous wave operation (CW) on the new stellarator W7-X at IPP Greifswald. In particular, a 1 MW, 140 GHz, CW gyrotron has been developed in cooperation with the CRPP EPFL Lausanne and Thales Electron Devices (TED), Paris, and the quasi-optical transmission system as well as the high-voltage modulator for the gyrotron has been developed with IPF, University of Stuttgart. The first series tube delivered world record parameters in long-pulse operation with 0.92 MW at 30 min pulse lengths, an efficiency of nearly 45% and a mode purity of 97.5%. Recently, the series tube SN4R reached 1.02 MW. With the ECRH system KIT makes a significant contribution to W7-X (Programm FUSION).

— Development and testing of 2 MW, 170 GHz gyrotron tubes with coaxial resonator and step-tunable 1 MW gyrotrons (105-143 GHz), including edge-cooled microwave vacuum window made of synthetic diamond for ECRH systems of large-scale tokamak experiments (ITER, ASDEX Upgrade). A pre-prototype tube of IHM for the European 2 MW, 170 GHz ITER gyrotron achieved a record output power of 2.2 MW at 30% efficiency (without depressed collector for energy recovery). The gyrotron and the components are currently installed in an industrial prototype tube in collaboration with CRPP and TED and will be tested in 2011. These KIT works within an international cooperation fulfill an obligation of the EU with respect to ITER (Programm FUSION).

- Experimental and theoretical studies on the plasma-wall interaction at the first wall and divertor of tokamak fusion reactors (Programm FUSION).

- Sintering of advanced functional and structural ceramics, in particular of nanostructured ceramics and metal powders and process technology in nano-mineralogy by means of high power millimeter waves at a frequency of 30 GHz delivered by a gyrotron. In further experiments, fundamental new non-thermal microwave effects are validated (Program NANOMIKRO).

- System studies on microwave applicators for various applications at the ISM (Industrial, Scientific, Medical) frequencies 0.915 GHz, 2.45 GHz and 5.8 GHz, such as for energy-efficient production of aircraft components made of carbon fiber composites by microwave process technology at 2.45 GHz. The new HEPHAISTOS CA3 system with a payload capacity of 7000 l and a microwave power of 25 kW is already in routine operation. This will, in development with industry, offer various applications and processes on a service basis. With the new facilities of the 2.45 GHz HEPHAISTOS-line significantly shorter processing times at slightly improved material properties compared with the conventional production in autoclaves have been achieved (Programm REUN, TIG and IMA).

For the conduction of R&D in all of these theoretical and experimental fields the IHM is equipped with a workstation cluster and a large number of experimental installations: KEA, KEA-ZAR, three GESA machines, eight COSTA devices, one abrasion and one erosion teststand, two gyrotron test facilities with one common power supply and microwave-tight measurement chamber, one compact technology gyrotron (30 GHz, 15 kW, continuous wave (CW)), several 2.45 GHz applicators of the HEPHAISTOS series, one 0,915 GHz, 60 kW magnetron system and one und 5.8 GHz, 3 kW klystron installation.

The director (acting) of IHM Prof. Dr. rer.nat. Dr. h.c. Manfred Thumm also is Full Professor for Microwave Measurement Techniques at the Institute of High Frequency Techniques and Electronics in the Faculty of Electrical Engineering and Information Technology of KIT with 4 teaching courses (one at the International Department). PD Dr.-Ing. habil Lambert Feher and Dr.-Ing. Martin Sack each hold one lecture course at KIT and Dr. Rudolf Schneider two courses at the University of Applied Sciences in Karlsruhe.

At the end of 2010 the total IHM staff with regular positions amounted to 41 (20 academic staff members, 3 engineers and 18 technical staff member and others).

In addition 12 academic staff members and 11 technical staff members (and others) were financed by acquired third party budget.

In course of 2010 8 guest scientists, 8 PhD students (5 of KIT-Campus South, 3 of KIT-Campus North), 3 master students, 3 bachelor students, 6 internship students and 7 trainees in the mechanical and electronics workshops worked in the IHM.

Strategical Events, Scientific Honors and Awards

Time schedule of the calling procedure "Successor of Prof. Thumm":

30 April 2008	Deadline for applications (9 applications)
20 May 2008	1st meeting (selection of 3 candidates for invitation to scientific talks)
15 July 2008	Scientific talks
15 July 2008	2nd meeting (selection of 2 candidates for invitation to sample lectures)
21 Oktober 2008	Sample lecture for graduate students
21 Oktober 2008	3rd meeting (decision on a calling list)

The appointment negotiations early 2009 and therefore this first calling procedure could not be finished successfully.

April/Mai 2010	New advertisement of a professor ship in the field of "High Power Microwave Engineering" according to the so-called "Jülich Model"
20 July 2010	Scientific talks and sample lectures of 3 candidates
18 November 2010	Scientific talk and sample lecture of one additional candidate
26 January 2011	Decision of the calling commission on a new calling list.

Dr. Georg Müller, Head of the Pulsed Power Division, organized in collaboration with the International Society on Pulsed Power Applications e.V. an International Pulsed Power PhD Congress (17-18 February 2010) at KIT with 40 participants.

At the 3rd Euro-Asian Pulsed Power Conference (EAPPC) in Korea Dr. Georg Müller has been elected for the International Organizing Committee. He will be the General Chair of the next EAPPC in combination with the 19th International Conference on High-Power Particle Beams (BEAMS) in 2012 in Karlsruhe.

At the 2010 IEEE International Vacuum Electronics Conference (IVEC 2010), which was organized from 18 – 20 March in Monterey, CA, USA, by the Institute of Electrical and Electronics Engineers (IEEE), Dipl.-Ing. Andreas Schlaich, a PhD student of the Institute for Pulsed Power and Microwave Technology (IHM), CN, and at the Institute of High Frequency Techniques and Electronics (IHE), CS, received the "Best Student Paper Award" for his contribution "Investigations on Parasitic Oscillations in Megawatt Gyrotrons". Two PhD students of the MIT got rank 2 and 3. Nearly 400 participants attended the conference.

At the IEEE 37th International Conference on Plasma Science in Norfolk, VA, USA (20-24 June 2010), Prof. Dr. rer.nat. Dr. h.c. Manfred Thumm received the Plasma Science and Applications Award 2010 "For outstanding contributions to the development of high power microwave sources (in particular gyrotrons) for application in magnetically confined fusion plasma devices as well as for stimulation and establishing of extensive international co-operations".

Longlasting Co-operations with Industries, Universities and Research Institutes

- Basics of the interaction between electrical fields and cells (Bioelectrics) in the frame of the International Bioelectrics Consortium with Old Dominion University Norfolk, USA; Kumamoto University, Japan; University of Missouri Columbia, USA; Institute Gustave-Roussy and University of Paris XI, Villejuif, France; University of Toulouse, Toulouse, France, Leibnitz Institute for Plasma Science and Technology, Greifswald, Germany

- Desinfection of hospital wastewater by pulsed electric field treatment in cooperation with University of Mainz and Eisenmann AG

- Integration of the electroporation process for sugar production with SÜDZUCKER AG

- Development of protection against corrosion in liquid metal cooled reactor systems in the following EU-Projectes: LEADER, GETMAT, MATTER, HELIMNET, ESFR (Partner: CEA, ENEA, SCK-CEN, CIEMAT)

- Development of core- and structure materials for liquid lead reactor cooling systems in collaboration with the Japanese Atomic Energy Agency (JAEA)

- Development of large area pulsed electron beam devices in collaboration with the Efremov Institute, St. Petersburg, Russia

- Experiments on liquid Pb and PbBi-cooling of reactor systems with the Institute for Physics and Power Engineering (IPPE), Obninsk, Russia

- Development, installation and test of the complete 10 MW, 140 GHz ECRH Systems for continuous wave operation at the stellarator Wendelstein W7-X in collaboration with the Max-Planck-Institute for Plasmaphysiks (IPP) Greifswald and the Institute for Plasmaresearch (IPF) of the University of Stuttgart

- Development of the European ITER Gyrotrons in collaboration in the frame of the European Gyrotron Consortiums EGYC and coordinated by Fusion for Energy (F4E). The other members of the Consortium are CRPP, EPFL Lausanne, Switzerland, CNR Milano, Italy, ENEA, Frascati, Italy, HELLAS-Assoc. EURATOM (NTUA/NKUA Athens), Greece. The industrial partner is the microwave tube company Thales Electron Devices (TED) in Paris, France

- Virtual Helmholtz-Institute VH-VI-259 „Advanced ECRH for ITER" in collaboration with IPP Garching and Greifswald, IPF Stuttgart, Institute of Applied Physics, Russian Academy of Sciences, Nizhny Novgorod, Russia and CNR Milano, Italy

- Improvement of electron guns for gyrotrons and cavity interaction calculations in collaboration with the St. Petersburg Polytechical University, Russia and the University of Latvia, Latvia

- Basic investigations of plasma-wall interaction in fusion reactors in collaboration with the State Research Center of Russian Federation Troitsk Institute for Innovation and Fusion Research (TRINITI), Troitsk, Russia and the Institute of Plasma Physics, Kharkov, Ukraine

- Fundamentals of application of gyrotrons for microwave materials processing in collaboration with the National Institute for Fusion Science (NIFS) in Toki, Japan and the University of Fukui, Japan

- Development of Microwave Systems of the HEPHAISTOS Series for materials processing with microwaves with the Company Vötsch Industrietechnik GmbH, Reiskirchen.

FUSION: Program Nuclear Fusion

Plasma Wall Interaction (PWI)

(EFDA Task WP10-PWI-05-02-01/KIT/BS+PS: Development of the PWI basis in support of integrated high-Z scenarios for ITER and demonstration of liquid plasma-facing components.)

In the future tokamak ITER the plasma edge localized modes (ELMs) and the disruptions of plasma confinement may produce vaporization and melting at the divertor and first wall surfaces of metallic targets of reference ITER materials beryllium and tungsten. Also transient heat loads below the melting threshold the surface cracking should be accounted for in the ITER design. In addition, the thermoconductivity of carbon fibre composites (CFC) near the surface remains an issue in lifetime estimations.

For modelling of tungsten melt motion damage including bulk heat transport the incompressible fluid dynamics code MEMOS was applied. The validation of MEMOS by experiments at the plasma gun installation QSPA-T and the applications of the code for supportive numerical modelling of the melt damage to the W targets in ITER simulation experiments at the tokamak TEXTOR have been continued. Also new calculations with MEMOS were carried out, being focused mainly on the magnitudes and thresholds of melt splashing of Be and W under pulsed heat loads.

Brittle destruction (cracking) of tungsten armour under action of ELMs is considered as a serious problem for the ITER divertor. The cracking can produce W dust with characteristic sizes of particles ranged as 1 to 10 µm. The particles can leave the surface with velocities up to 10 m/s, then they cross the scrape-off layer (SOL) and are evaporated in the confined plasma.

For W surface cracking under the loads below the melting threshold the thermo-mechanics code PEGASUS was earlier applied. The code PEGASUS describes such processes in W and CFC as crack formation, thermal conduction and dust production. In 2010 analytical calculations aiming at interpretation of experimental observation at the plasma gun device QSPA-Kh-50 and further validation and improvements of PEGASUS models have been developed.

Validation of MEMOS and simulations of melt motion damages for ITER

The code MEMOS describes fluid motion on molten surfaces taking into account such material properties as surface tension and viscosity. In the code the plasma pressure variations along the surface, as well as the gradient of surface tension and the JxB force caused by the currents crossing the melt layer immersed in strong magnetic field as well as by the eddy currents generated due to the poloidal field evolution, produce the melt acceleration.

To validate MEMOS against experimental data, two-dimensional simulations with account of the macrobrush structure of the targets were performed. The W macrobrush structure can effectively prevent gross melt layer displacement thus decreasing the erosion both for single and multiple transient loads.

For TEXTOR relevant calculations the energy deposition function of time t was obtained by comparison of experimental surface temperature $T_{exp}(t)$ and calculated T(t) at the most heated place (hot spot). Calculating the melt motion driven by the JxB force for the current density J the Child-Langmuir law

was assumed (i.e. the thermoelectric current is limited by the space charge in front of the target). The simulations of surface damage were performed for heat load duration τ = 5 s, plasma pressure 10^{-3} bar, magnetic field B = 2.5 T, brush size D = 1 cm and gap width a = 0.5 cm. A good agreement between the calculations and the experimental data for heat load and surface temperature is obtained (figures below). The calculated melt layer depth of ~ 1.5 mm per one pulse of load is in reasonable agreement with the TEXTOR experiments. However, the experimental amount of resolidified tungsten of ~2 mm per shot were overestimated by a factor of 2 in the corresponding MEMOS simulations.
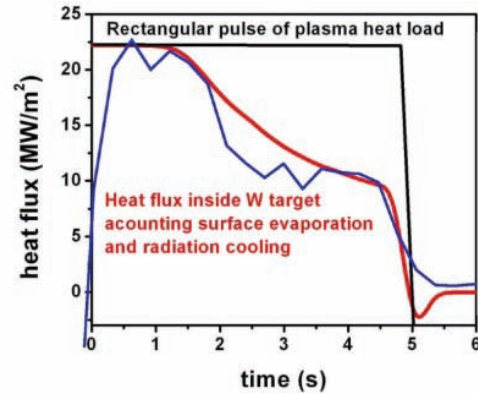

Time dependence of experimental (blue) and simulated heat flux at the target surface for TEXTOR.
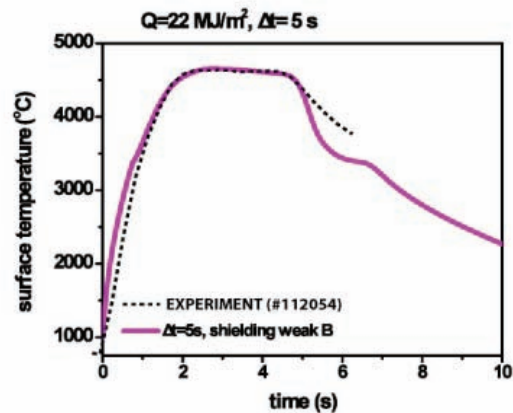
Time dependence of experimental and simulated surface temperature for TEXTOR.

Also new MEMOS simulations for effective thermoconductivity of CFC material deteriorated after multi-pulsed loads have been performed. The conclusion is that a degradation threshold appears if CFC is heated to temperatures above approximately 3600 K. Those high temperatures can be reached at rather low deposited energy Q ~0.5 MJ/m², which is usually considered as still a tolerable ELM size in the ITER design. Thus we assume the complex structure of CFC degenerates above the threshold, resulting in a carbon sub-surface layer of a few tens of microns. The effective heat conductivity of degenerated layers has been validated against experiments at the plasma gun QSPA-T (TRINITI, Troitsk, Russia) and it can be used for further numerical simulations for tokamaks (figure on the next page).

It is concluded that the obtained thermal conductivity in the degenerated layer correlates well with that of fine grain graphite.
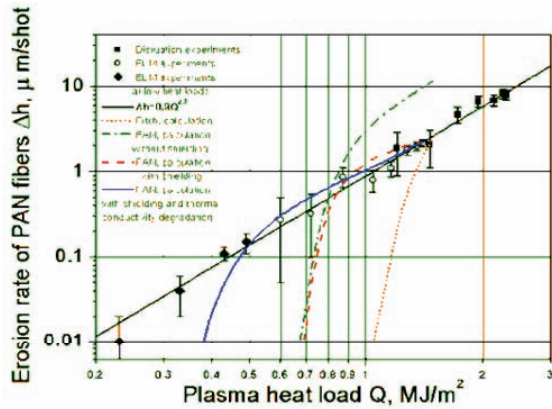
Dependence of CFC erosion rate on Q. MEMOS simulations agree better with the experimental points if assuming decreased thermal conductivity in a sub-surface layer.

Simulation of tungsten armour cracking after repetitive ELM-like heat loads with the code PEGASUS

Numerical investigations of tungsten behaviour under the transient heat loads expected in ITER with PEGASUS need experimental verifications. For this purpose a dedicated series of experiments has been performed with the quasi-stationary plasma accelerator QSPA Kh–50 (Kharkov, Ukraine) for pulsed repetitive ELM-like plasma impacts on tungsten targets of ITER grade. Measurements of residual stress below and above the melting threshold were done and compared with corresponding results of PEGASUS.

The main plasma parameters of QSPA Kh-50 are as follows: ion energy about 0.4 keV, averaged pressure during the pulse ~2 bar, and pulse duration τ ~0.25 ms (triangular shape). The heat load Q was varied as 0.2, 0.3, 0.45 (no melting) and 0.75 MJ/m^2 (slightly above the melting threshold). The initial W target temperature T_{init} was varied as well in the range 200-600 C. The samples were exposed to a perpendicular plasma stream. To study the micro-structural evolution of exposed targets the X-ray diffraction technique (XRD) was used. The lattice parameter 0.3164 nm measured in a stress-free state is close to the reference value 0.3165 nm, which is an indication of negligible number of vacancies in the W lattice.

If the surface melts, residual tensile stress appears after the pulse due to fast resolidification of the melt before the final cooling of the target. If there was no melting during the pulse, the stress is due to plastic deformations of the heated material. If the tensile stress exceeds some maximum value, cracks appear in a thin sub-surface layer, which can occur after a number of pulses. Cracking should significantly reduce initial resolidification stress, and the residual stress only is practically measurable. The minimum pulse number necessary for cracking depends on Q.

In the experiments the cracks can appear after a small number of pulses. For instance, after 5 shots the cracks appear at $Q > 0.3$ MJ/m^2. In presence of tungsten cracking the stress of 0.3-0.4 GPa was measured. Macroscopically the damaged target becomes covered with a net of random cells formed by the cracks (next figure). The typical depth of the cracks is 0.2-0.3 mm, and the cell sizes are of order of 1 mm. The crack width depends on T_{init} and Q varying in a wide range 0.3 to 8 μm (see the Table for example).

The obtained experimental results are going to be used for validation of PEGASUS. In 2010 we performed analytical estimations which allowed a prediction that the threshold for tungsten cracking of $Q_{thr} \approx 0.3$ MJ/m^2, which was measured after 5-10 shots, is not a universal value. The analysis which
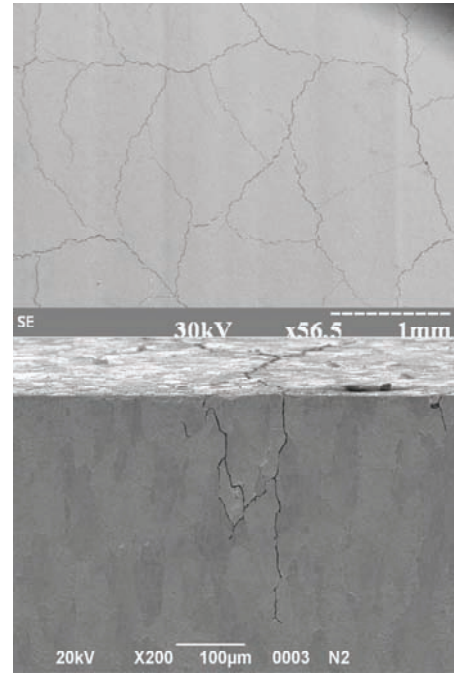
Cracking at W surface after 5 pulses at Q = 0.45 MJ/m^2 (upper panel) and a normal cut showing crack depth ~ 0.3 mm.

accounts for the load magnitude Q and pulse duration τ, leads to the conclusion that increasing pulse number results eventually in the appearance of cracks even at $Q << 0.3$ MJ/m^2, i.e. the value of the Q_{thr} substantially decreases (material fatigue) going down to Q_{thr} ~ 0.1 MJ/m^2 for τ = 0.25 ms. The fatigue reason is the growing of plastic deformations and thus the residual stress should also increase from shot to shot up to the mentioned maximum value necessary for cracking.

So far it was not possible to perform a more detailed analysis of the cracking threshold, because an analytical solution for the dynamics of residual stress obtained in the estimations showed that the maximum pulse number of cracking onset depends also on the viscosity coefficient ν at the mean temperature of the target during the pulse. The data on ν at the high temperatures in question (~ 3×10^3 K) is not available. Perhaps the lacking information can be extracted from the dependence of the cracks width from the number of shots, which is not done yet.

EFDA Task WP10-PWI-07-02-01/KIT/BS: Mitigation of disruption and investigation on ELM and inter-ELM heat loads

A significant issue for ITER operation with high fusion gain is the occurrence of disruptions, which can limit the lifetime of plasma facing components (PFCs). Disruption mitigations can result in generation of runaway electrons (RE) which can also damage the first wall. Numerical simulations for the consequences of RE impact on the PFCs have been carried out in 2010 for JET and ITER conditions. For JET the work was focused on the benchmarking of the codes ENDEP and MEMOS by experimental observations of RE beams. Reasonable qualitative and quantitative agreement between numerical simulations and experiments at JET was obtained. For ITER a predictive modelling with these codes for beryllium first wall melt damage was performed.

Another activity has concerned modelling of massive gas injection (MGI) with the radiative MHD code TOKES. In the simulations the injected noble gas gets ionized in the core and then the contamination results in fast loss of plasma energy by radiation emission. For MGI modelling TOKES was upgraded

with a toroidally symmetric two-dimensional plasma model and with magnetic flux coordinates covering the whole volume of the tokamak vessel. The new model has been successfully compared with an argon experiment on the tokamak DIII-D.

Modelling of runaway electrons impact for ITER and JET

Relativistic runaway electrons (RE) can appear during the thermal quench of a disruption and by massive gas injection (MGI). In ITER RE will mainly be generated by avalanches. The RE density can be estimated as 1016 m-3, their kinetic energy as 10-20 MeV and the associated magnetic energy can be of order of the thermal energy of the plasma (in ITER ~ 1 GJ).

To estimate RE damage to the ITER first wall and to support JET experiments, dedicated numerical simulations have been done with the energy deposition Monte-Carlo code ENDEP for CFC, Be and W targets. Heating with melting of a Be target for ITER and heating only of CFC for JET was performed with the melt motion code MEMOS. Beam parameters used in the calculations were agreed with the teams of both tokamaks.

For these tasks the code ENDEP was upgraded in order to take into account the effect of electron gyration in the magnetic field on the incident angle and the effect of the polarization of bound electrons of target material by the RE which resulted is slightly smaller stopping power. The energy distribution of RE is assumed to be exponential as $\exp(-E/E_0)$. For a CFC target in a magnetic field of 3.5 T (JET case) the characteristic energy E_0 equals 5, 8 and 10 MeV. For a Be target (ITER) $E_0 = 12.5$ MeV, and a sandwich target with 1 cm Be PFC and 1 cm copper substrate is assumed. The main incident angle was varied from 1 up to 10 degrees. The transversal energy of RE was varied up to 5% of the total energy. The figures show the obtained energy deposition profiles for the different targets.

A typical penetration depth of the RE into a CFC target is 1 mm. At large inclination angles α in the case of JET the influence of the transversal energy E_{tr} is small (CFC target), in contrast to the ITER case (Be target) when α is small, which decreases also the penetration depth of the RE (~0.5 mm). The Be melt layer exists for about 0.5 s. It is to note that during this time the Rayleigh-Taylor instability caused by eddy currents can develop on the molten surface resulting in significant splashing.

In case of the W target, which can be interesting for the ITER design, despite the obtained larger stopping power (see upper figure). The deposition function has not increased compared to that of Be, because the RE energy is reradiated from W more effectively (~50%) than from Be (20%). The reflected energy can be attributed mainly to the secondary electrons (~40%) and the X-ray radiation (~10%).

Energy depositions of ENDEP are used in MEMOS to get melting in ITER, starting the heating from a wall temperature of 800 K and heating in JET (room temperature). For ITER a Gaussian profile of the spatial energy distribution with a characteristic width of 10 cm was assumed. For instance, at a RE heat load of 25 MJ/m^2 the surface temperature of W target exceeds the melting temperature 1540 K after 10 ms.

In MEMOS simulations the melting thresholds in case of RE heating at large pulse durations of 10 ms are obtained: Be melts above 5 MJ/m^2 and W melts above 65 MJ/m^2 This ratio (W/Be = 13) is much larger than that of plasma impact (~ 3) after ELMs with surface heating only. The simulations showed that the evaporation at the beryllium surface significantly (by several times) decreases the melting threshold, which is favourable for the ITER first wall armour.
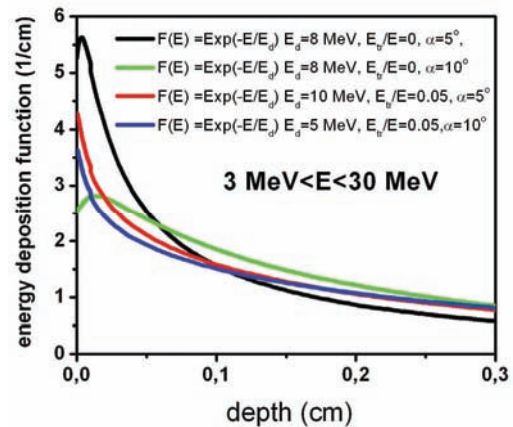
At the regime with beryllium melting, the final depth of the melt pool exceeds 1 mm at a heat load Q > 35 MJ/m^2 (figure on next page).
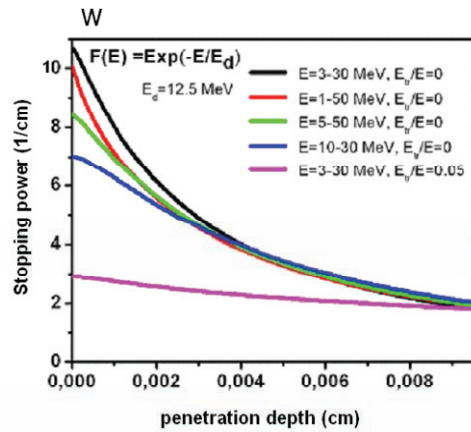
Energy deposition of runaway electrons in tungsten target for different energy spectra and transversal energy.
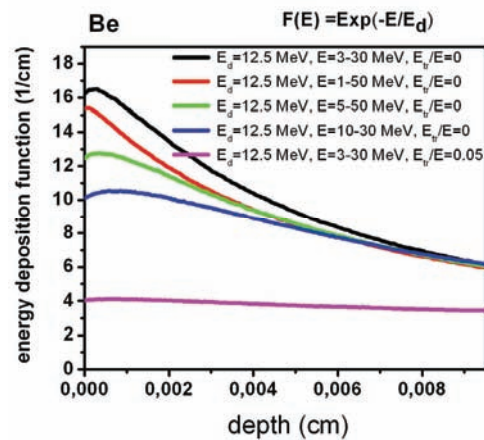

Energy deposition of runaway electrons in beryllium target for different energy spectra and transversal energy.

Energy deposition of runaway electrons in beryllium target for different energy spectra and transversal energy.

Noticeable evaporation starts for heat loads Q > 12 MJ/m^2. At Q = 40 MJ/m^2 the evaporation depth reaches about ~50 μm. The melting continues for a long while (~0.2 s) which could cause splashing away of whole melt layer by the **J**×**B** force.

For JET, simulations of the impact of runaway electrons generated during MGI experiments are performed in order to apply and, if possible, validate using available experimental data, the codes ENDEP and MEMOS. The code MEMOS was applied for the calculations of temperature distributions inside the target, however without the melting. Detailed temperature evolution and spatial distributions over CFC tiles installed in JET
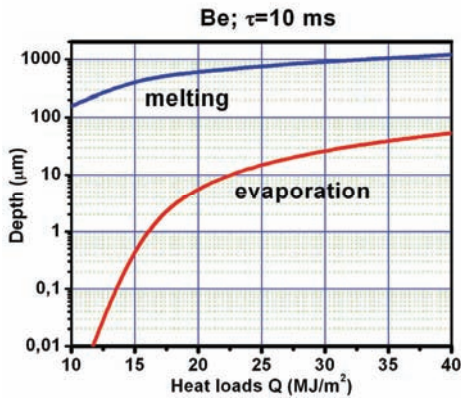
Melting thickness and the amount of vaporized beryllium (in terms of solid tangsten layer removed due to vaporization) versus deposited energy of load pulse.

during the RE impact were calculated as functions of heat load density and compared with the experimental data, which are available as functions of the runaway current. The dependence of the surface temperature on heat loads was transformed to the dependence of the surface temperature on the RE current using a dedicated model that is based on Ohm's law and some assumptions of contributions from magnetic and kinetic energies of the RE. Varying the heat load the simulated dependence of surface temperature T_w was fitted to direct measurements of T_w. By this way the RE energy density in JET was estimated as 3-4 MJ/m^2.

Simulation of massive gas injection (MGI) with tokamak code TOKES

Tokamak experiments demonstrated effective ionization of injected atoms G (G = Ne, Ar, He) during MGI, the following MHD activity which causes the thermal quench (TQ) within a few ms when the ionization front reached the magnetic surface of safety factor $q = 2$, and the toroidally well symmetric radiation flush. On the short time scale the ionization of G-atoms localized near the jet entry can result in plasma parameters strongly varying on the poloidal coordinate y. For example the electron temperature T_e decreases drastically near the jet. This can significantly decrease the ionization rate resulting in deep jet penetration.
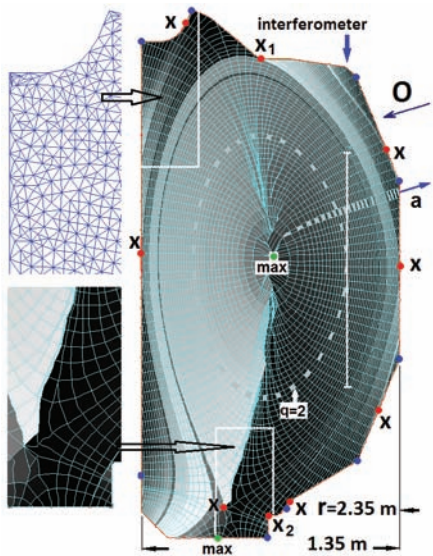

Layout of tokamak DIII-D and numerical meshes (triangular and magnetic flux coordinate on poloidal plane) of code TOKES.

In 2010 the modelling with the tokamak code TOKES has been focused upon further development of the code aiming MGI simulations. After significant elaborations of the generator of magnetic flux coordinates two-dimensional description of the plasma in the whole vessel was achieved (figure above), The model of a 2D toroidally symmetric multi-fluid plasma includes fast cross-diffusion and non-equilibrium expansion of the plasma along the magnetic field lines.

TOKES was successfully used for validation against DIII-D experiments on argon MGI. The figure below demonstrates the comparison of simulated and experimental centre temperature $T_{e0}(t)$. The fit is achieved tuning up a few parameters which are not precisely known in the experiment but strongly influence $T_{e0}(t)$: 1) position of $q = 2$ magnetic surface which locates approximately as it can be expected in DIII−D. 2) Electron thermal conductivities of hot plasma before (k_{eini}) and after (k_{efin}) reaching the surface of q = 2 by the cooling front, which happened at $t = t_{q2} \approx 2$ ms after starting the gas injection.

The good fitting indicates that the simulation reproduces the main processes of a TQ. The first consequence of core instabilities appears to be small deteriorations of toroidal symmetry and thus slight overlapping of nested magnetic surfaces, which drastically increases electron cross-transport by thermal conductivity along entangled magnetic field lines. After start of plasma cooling periphery the instabilities can develop at many rational values of q in the core, but we assume they remain moderate until $t > t_{q2}$, due to which $k_{eini} << k_{efin}$ follows. The long tail of T_{e0} on the figure is due to a long electron-ion thermal energy exchange time, because centre ion temperature remains high until t = 4 ms.
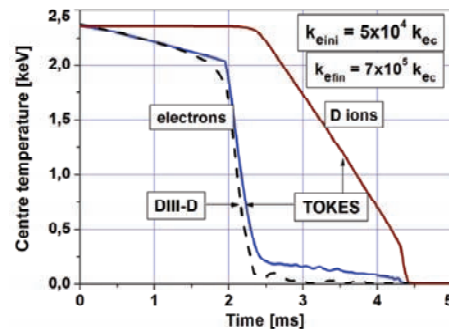
Validation of TOKES by DIII-D electron temperature T_{e0}. k_{ec} is electron classical thermal conductivity.

Conclusions

A series of dedicated experiments with the plasma gun QSPA Kh-50 has been performed for verification of the tungsten brittle destruction model used in the code PEGASUS in order to predict ITER divertor damage by ELMs of various powers and time durations. The residual tensile stress at the W target was measured after a few shots with energy depositions up to the melting threshold. The measurements are complemented with an analytical model for residual stress dependence on the number of pulses. The obtained analytical solution was fitted to the experimental data. The estimations predict that at large number of load pulses the threshold value should decrease from $Q_{thr} = 0.3$ down to $Q \sim 0.1$ MJ/m^2.

Numerical simulations of Be and W armour damage under the runaway electron heat loads are carried out using the codes ENDEP and MEMOS validated against JET experiments. The melting thresholds for Be and W armour were determined. The numerical simulation estimated typical parameters and demonstrated that the mechanism of the surface evaporation

significantly influences the melt layer thickness for metallic PFCs under RE impact.

The results obtained with TOKES provide useful benchmarks of MGI simulations, but more work is needed for further development of the code in order to reach reliable integrated modelling including plasma and surface aspects as well as the injector gas dynamics in the vessel.

Microwave Heating for Wendelstein 7-X

Introduction

In the recent years electron cyclotron resonance systems have been established as a standard method for localised heating (ECRH) or current drive (ECCD) in fusion relevant plasmas. Thus ECRH will be the basic day-one heating system for the stellarator W7-X which is currently under construction at IPP Greifswald. In the first stage W7-X will be equipped with a 10 MW ECRH system operating at 140 GHz in continuous wave (CW). The complete ECRH system will be provided by KIT, which in 1998 established, together with EU partners, the 'Project for Microwave Heating on W7-X' (PMW). The responsibility covers the design, development, construction, installation and integrated tests of all components required for stationary plasma heating on site at IPP Greifswald. PMW also coordinates the contributions from Institut für Plasmaforschung (IPF) of the University of Stuttgart, which is responsible for the microwave transmission system and parts of the HV-system, and from the team at IPP Greifswald, which is responsible for the in-vessel components and for the in-house auxiliary systems. PMW benefits also from the collaboration with Centre de Recherche de Physique des Plasmas (CRPP) Lausanne, Commissariat à l´Energie Atomique (CEA) in Cadarache and Thales Electron Devices (TED) in Vélizy.

A contract between CRPP Lausanne, FZK Karlsruhe (now KIT) and TED, Vélizy, had been settled to develop and build the continuously operating series gyrotrons. The first step of this collaboration was the development of a prototype gyrotron for W7-X with an output power of 1 MW for CW operation at 140 GHz. This step has been finished successfully.

At the industrial company TED seven series gyrotrons have been ordered. First operation and long pulse conditioning of these gyrotrons will take place at the teststand at KIT, where pulses up to 180 s at full power are possible (factory acceptance test, FAT), 30 minutes shots at full power are possible at IPP (site acceptance test, SAT). Including the pre-prototype tube, the prototype tube and the 140 GHz CPI-tube, ten gyrotrons will be available for W7-X. To operate these gyrotrons, in addition to the Oxford Instruments and Accel gyrotron magnets, eight superconducting magnetic systems were delivered by Cryomagnetics Inc., Oak Ridge, USA.

The completion of the project made further progress in 2010. Most of the components of the transmission system, HV-systems and in-vessel-components have been ordered, manufactured, delivered and are ready for operation at IPP Greifswald. A part of the existing ECRH system is already used to test new concepts and components for ECRH. Some delay arose in the project during the last 1-2 years due to unexpected difficulties in the operation of the series gyrotrons.

Series gyrotrons

The first TED series gyrotron SN1 has been tested successfully at FZK and IPP in 2005 (920 kW/1800 s). It fulfilled all the specifications, during the acceptance test no specific limitations were observed. In order to keep the warranty this gyrotron has been sealed, the two prototype gyrotrons are routinely used for test experiments on novel transmission line components.

The next series gyrotrons showed a more or less different behavior with respect to parasitic oscillations excited in the beam tunnel region. These oscillations result in an excessive heating of the beam tunnel components, in particular of the absorbing ceramic rings. The gyrotrons re-opened after operation showed significant damages due to overheating at the ceramic rings and the brazing of the rings. This limited in general the pulse length in high-power operation to a few ms.

In order to avoid this problem it was decided to test the series gyrotron SN3a at reduced output power, well below the threshold for excitation of the parasitic oscillations. The experiments showed that it is possible to operate the tube at a maximum output power of about 700 kW without oscillations in the beam tunnel. The gyrotron was optimized in short pulse short pulse regime with a typical pulse length of a few ms. The operation and the dependence of the output power and stable oscillating region of the design mode ($TE_{28,8}$) on different parameters was investigated. In particular, scans of the output power versus the accelerating voltage have been performed for different magnetic field values in the cavity and the electron gun region (see figure). Since this gyrotron is still equipped with a beam tunnel which allows parasitic oscillations the maximum achievable output power is limited. The operation of the gyrotron beyond this limit is usually associated with a strong reduction of output power, enhanced stray radiation and an increased amount of absorbed RF power in the beam tunnel region which may result in a thermal overload. It has been found that about 700 kW RF power can be generated at a beam current of about 40 A very reliably, avoiding any evidence of spurious oscillations.
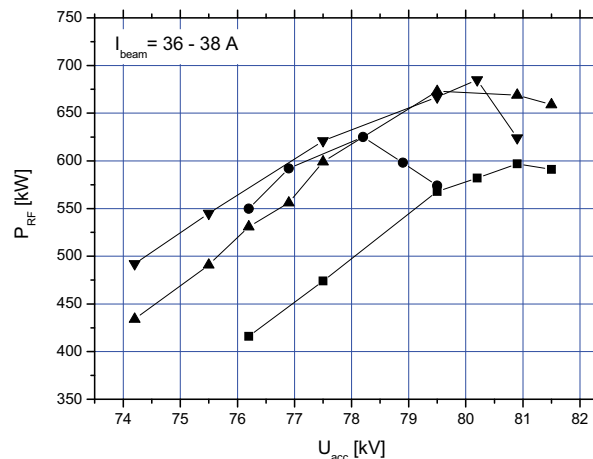

Output power of series gyrotron SN3a, measured in short pulse operation at a beam current of about 36 – 38 A, the different curves correspond to different magnetic settings. The flattening of the curves at the maximum indicates the occurrence of parasitic oscillations.

Thermographic measurement and analysis of the output beam gave a TEM_{00} mode content of 97%, which verifies the high quality of the internal mode converter and mirror system.

Long pulses up to 3 minutes were performed with a CW load at full power (700 kW) at an efficiency of 37 % in depressed collector mode for energy recovery. The temperature increase of

several cooling channels are given in the next figure for a shot with constant parameters. Note that the beam current is decreasing at the beginning of the pulse due to the cathode cooling effect of the extracted electrons and that the control system needs about 60 s to adjust a constant current. It can be seen that the calorimetric measurement shows a constant output power at the end of the pulse, after some regulation oscillations in the first 90 s.

The increasing temperature of the cavity is associated with an expansion of the cavity diameter and has therefore an influence on the oscillation frequency. The typical drop of the frequency during the first second of the pulse is about 260 MHz (to be compared with 140.33 GHz at the start).
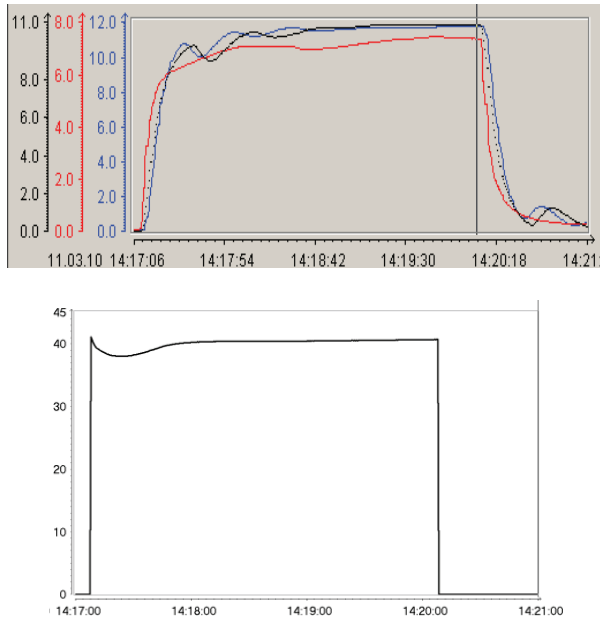

Top: Temperature increase of cooling channels for 3 minutes operation at 700 kW (black: collector, red: cavity and body, blue: absorber load). The oscillations during the first 90 s are due to the secondary cooling system. Bottom: Beam current behaviour.

As a standard procedure the W7-X gyrotrons have to pass a reliability test during the acceptance tests showing a reproducible and stable operation within a pulse sequence.

The following figure shows the beam current during this reliability study. The gyrotron has been operated in 3 min pulses at a power level of around 700 kW and a duty cycle of 10 %. Repetitive and very reliable operation of the gyrotron was possible with a pulse length of 3 min. During this sequence all parameters were kept constant, except the average beam current: it was increased slightly from 38.7 A (in the morning) to 40.2 A (in the evening), the measured power was in the narrow range of 690 – 714 kW. All pulses were successful, one pulse was pre-terminated due to an arc in the pre-load.

At KIT a pulse length of up to 30 min (and even longer) is only possible at a beam current of less then 30 A due to the limitation of the power supply. Tests at full power were performed at IPP Greifswald after transferring the gyrotron. The next figure shows the total RF power during a 28 min pulse. It shows a very stable behaviour, the variation of the output power between 17 and 23 min is caused by adjusting the body voltage and optimizing the boosting procedure to stabilize the beam current. The gyrotron passed both, FAT and SAT, and is in regular operation at IPP Greifswald for test of new transmission line components.
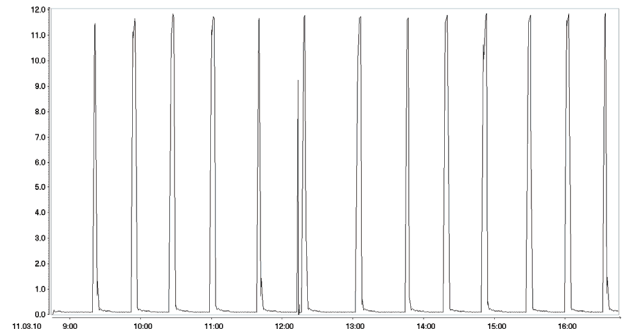
Beam current for 13 pulses with 3 min length each (duty cycle 10%). One short pulse was due to an arc in the pre-load.
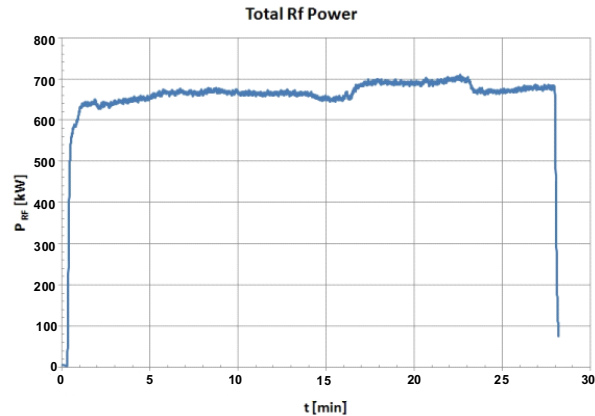

Total RF power at 28 min pulse. Variation of the power after 16 min is due to adjustment of body voltage and beam current.

During the experiments it was observed that the stainless steel housing of the gyrotron in the beam tunnel/cavity/uptaper area becomes hot. This is most probably due to stray radiation inside the vacuum tube which is absorbed at the non-cooled surfaces of the housing and which makes operation with high duty over a long time inconvenient. To reduce the absorption down to tolerable values the inner side of the tube will be covered with a highly reflective copper layer.

In order to avoid any possible problems with corrosion in the window cooling circuit the water has been replaced by inert silicone oil. A numerical study showed that the additional temperature increase of the diamond disk is uncritical. The high power experiments with the gyrotron showed that the increase of the oil temperature in regular operation is about 3 °C and saturates after approximately 3 min.

The first W7-X gyrotron which is equipped with an improved beam tunnel was delivered and tested at KIT until end of 2010 (SN4R). As the main difference to the usual beam tunnel this design features longitudinal corrugations in the copper rings which handicap the excitation of parasitic modes (as shown in an experimental campaign with two modular test gyrotrons in 2009). During the tests at KIT no parasitic oscillations originating from the beam tunnel region were observed. However, it has been observed that the dependence of the output power on beam current shows a saturation, well below the currents observed in previous tubes. Even for a beam current of 48 A it was not possible to obtain more then 960 kW. Possible reasons for this behaviour like poor e-beam properties, misalignment of the magnet-gyrotron system and interaction in the after cavity region are under investigation. Nevertheless, long pulse operation with 180 s/ 860 kW and 1800 s/ 580 kW was possible, however at reduced efficiency of ~ 35%. As an example the time traces of output power, beam current and accelerating voltage are shown in the next figure for a 180 s pulse.
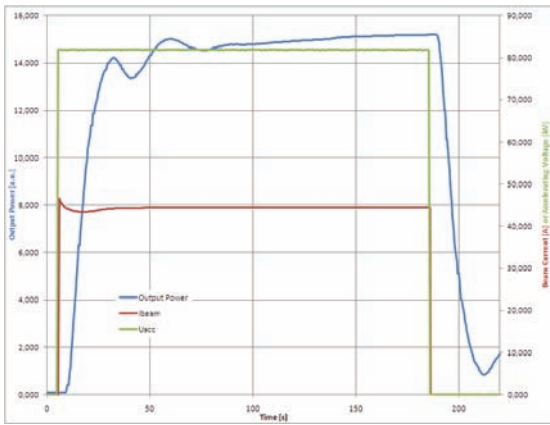
Output power, beam current and accelerating voltage of series gyrotron SN4R for a 180 s /860 kW pulse.

The measurement and analysis of the output beam gave a Gaussian mode content as high as 97%. After successful reliability tests the FAT procedure was terminated and the gyrotron was shipped to IPP Greifswald.

Design, construction and first tests of a high-power stainless steel load

The load is a critical, required component of the test stand for high-power CW gyrotrons. It both has to absorb and to measure the microwave power in an accurate and reliable way. Up to now cylindrical, ceramic-coated loads have been used at IHM, which show a good absorption behavior. Unfortunately this type of loads has the drawback that the ceramic layer may degrade and even may flake off due to local overheating. To avoid this problem, a load has been designed and constructed that is purely made of stainless steel. To enlarge the absorbing surface, the load is filled with an additional structure made of stainless steel pipes (next figure).
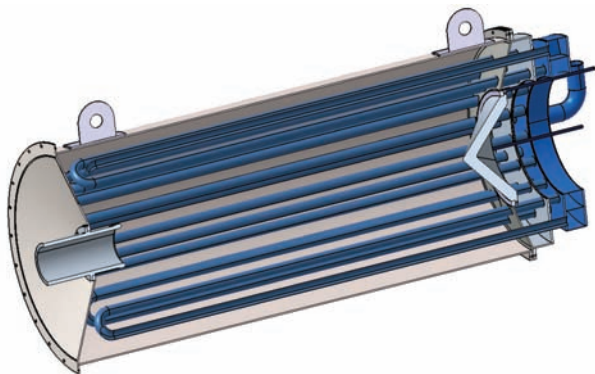

CAD cross section drawing of the stainless steel load.

In 2010, measurements with a preliminary load (next figure) without active cooling showed that 700 kW of microwave power with a pulse length of two seconds could be absorbed. During the measurement sequence, the load heated up to temperatures of 100°C at the outer surface and up to 250°C at the inner structure which is a critical value in terms of arcing due to outgasing. In the experiments a water-cooled pre-load showed that the back-reflected power is approximately 2%, which is a very good value.

At the moment, the load is equipped with an assembly that allows water-cooling of the inner structure. The outer structure (cylinder, top and bottom sections and the conical mirror) are still not actively cooled. The measurements with this modified setup showed a much better behaviour concerning arcs, compared to the results of the former measurement campaign.

The tolerated pulse length could be significantly increased up to 30 seconds at a gyrotron output power of 550 kW and up to 20 seconds at a power level of 780 kW. Calorimetric measurements showed that the internal pipe structure absorbed approximately two thirds of the microwave power. This corresponds well to the ratio of the surface areas under consideration.
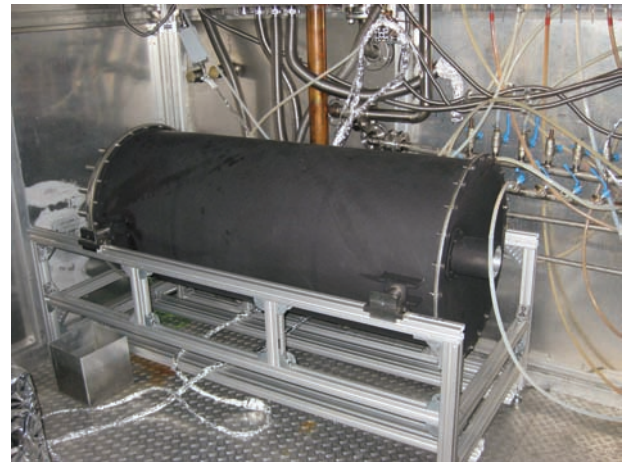
Stailess steel load after installation in the measurement box.

Transmission line

The transmission line consists of single-beam waveguide (SBWG) and multi-beam waveguide (MBWG) elements. For each gyrotron, a beam conditioning assembly of five single-beam mirrors is used. Two of these mirrors match the gyrotron output to a Gaussian beam with the correct beam parameters, two others are used to set the appropriate polarization needed for optimum absorption of the radiation in the plasma. A fifth mirror directs the beam to a plane mirror array, the beam combining optics, which is situated at the input plane of a multi-beam wave guide. This MBWG is designed to transmit up to seven beams (five 140 GHz beams, one 70 GHz beam plus an additional spare channel) from the gyrotron area (entrance plane) to the stellarator hall (exit plane). To transmit the power of all gyrotrons, two symmetrically arranged MBWGs are used. At the output planes of the MBWGs, two mirror arrays (beam distribution optic, BDO) separate the beams again and distribute them via two other mirrors and CVD-diamond vacuum barrier windows to individually movable antennas (launchers) in the torus. The BDOs and the successive mirrors are mounted in so-called antenna towers with "pinnacles" on top.
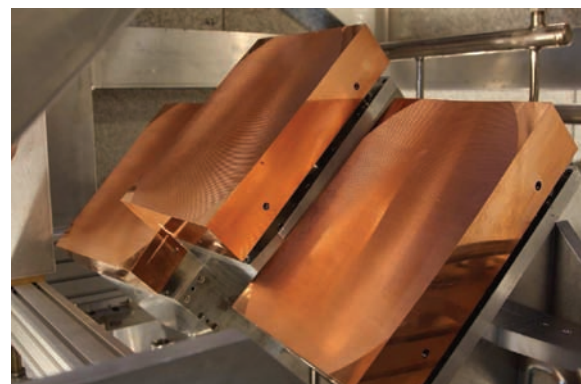

Assembly of 3 mirrors type M13 installed in an ECRH antenna tower.

The manufacturing and installation of the components of the basic transmission system is finished now. The figure shows an assembly of 3 mirrors of type M13 installed in an ECRH antenna tower. In 2010, gyrotron SN3a was installed in Greifswald, and

beam characterization and the subsequent design and manu-facturing of the surfaces of the two matching mirrors for this tube have been performed. SN4R is presently under test at KIT Karlsruhe, where the beam parameters have been measured.

Further remaining work includes diagnostics and power measurement of the gyrotron beams. The receivers attributed to the directional couplers on the mirrors M14 have been designed, and are under fabrication; related alignment control is in development. Owing to the aging of the available absorber loads from CCR, which led to increased arcing problems at higher power, a replacement of these loads was pursued. For module 1, a water-cooled version of the "'long load'", which consists of a 24 m long absorbing stainless-steel waveguide, was designed and ordered in industry; delivery is scheduled for end of 2010. In module 5, a cylindrical stainless-steel load from GYCOM was installed, and the system of coupling mirrors was upgraded to allow routing of the beam either to the old CCR load or to the new GYCOM load. Within the parameters used up to now (700 kW, 15 min), the GYCOM load performs well.

As in the past years, the ECRH system could be used for test of special components. Among others, the high-power tests of the compact long-pulse diplexer "Mk II" continued. This device (see next figure) is equipped with HE_{11} mode interfaces, and thus is compatible with waveguide transmission systems. It is developed for use as a combiner for the power of two gyrotrons as well as a fast directional switch (FADIS) between two outputs, and it is therefore of potential interest for ITER.
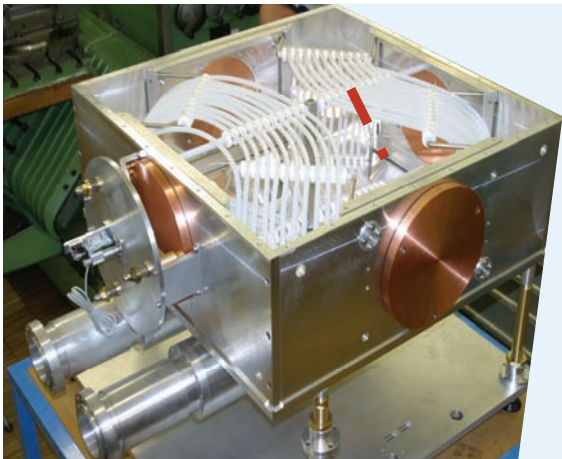
Diplexer which has been investigated in the ECRH system for W7-X. At the bottom, one can see the two HE11-mode waveguide outputs. The top plate is removed to reveal the resonator geometry and the stray radiation absorbing hoses.

The output power diagnostics as well as the drive (developed by TNO in Delft) for the resonator mirror was optimized; as a result, tracking of the slope or the peak of the diplexer resonance to the gyrotron frequency now works on a 20-ms time scale. With this system, demonstration of several diplexer applications was possible, including "'slow'" switching between two output channels by controlled mirror movement, fast switching by frequency-shift keying of the gyrotron (using few kV voltage modulation of the body) with optimum contrast, and tracking the notch of the diplexer to the gyrotron as is needed for in-line ECE experiments. When feeding two gyrotrons to the diplexer, stable power combination with an output contrast of 90% could be reached. A power combination experiment is shown in the following figure.

For two of the N-ports of W7-X, "remote-steering" (RS) launchers are foreseen. This is due to the fact, that front steering launchers as used in the A and E ports (see chapter on launchers) will not fit into these narrow ports. The remote-
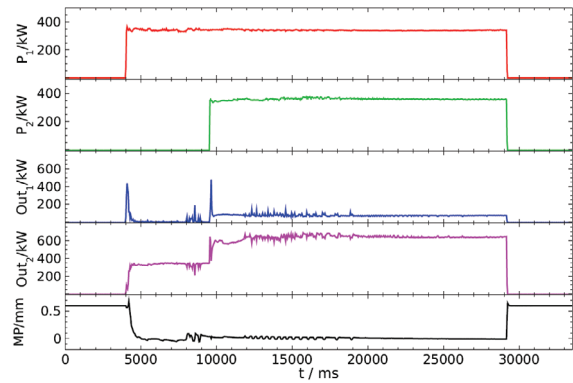
Beam combination of two gyrotrons operating at slightly different frequencies with diplexer frequency tracking to dip. The RF power of gyrotron 1 (P1, top) at input 1 and gyrotron 2 (P2, 2nd from top) at input 2, respectively, are displayed together with the output power in channel OUT1 (3rd from top) and OUT2 (4th from top) as a function of time. The feedback controlled diplexer mirror position MP is shown at the bottom.

steering properties are based on multi-mode interference in a square waveguide leading to imaging effects: For a proper length of the waveguide, a microwave beam at the input of the waveguide (with a defined direction set by a mirror system outside of the plasma vacuum) will exit the waveguide (near the plasma) in the same direction. For W7-X, the vacuum window, a vacuum valve as well as a mitre bend must be incorporated into the 4.6 m long waveguide.

A conceptual design for the two RS-launchers in module 1 and module 5 was performed. The waveguide will be fabricated by an electroforming process, thereby integrating the water-cooling channels. To enlarge the steering range, systematic investiga-tions of small deformations for the basically square corrugated waveguide were started to find an optimised cross-section. In parallel, further calculations of the losses in the gap needed for installation of the vacuum valve continued. In conjunction with the optimised waveguide cross-section, a significant reduction of the gap losses especially for larger scanning angles is expected.

Low-power experimental investigations on a prototype waveguide have been started to benchmark the calculations.

HV-systems

For the operation of gyrotrons with depressed collector, a precisely controlled beam acceleration voltage is necessary, which is supplied by the body-voltage modulator. The beam current of the gyrotrons is controlled by the cathode heater supply, which is on cathode potential (about -55 kV). In case of arcing inside the gyrotron, a thyratron crowbar protects the tubes from being damaged.

All ten body-voltage modulators and the protection units are now ready for operation. With growing experience with the complete system, some final optimization issues concerning the system diagnostics in case of a gyrotron fault are implemented.

In-vessel components

The first refurbished ECRH-plug-in launcher was successfully tested for vacuum tightness in the large MISTRAL vacuum chamber. In addition extensive mechanical tests of the mirror drive mechanism were performed successfully. Thus the refurbishment of the remaining three launchers can go-on on track.

The N-Port-launcher design was refined. Now, production drawing could be provided, if the decision for manufacture is done.

The electron cyclotron absorption (ECA) diagnostics, which measures the transmitted ECRH power and the beam position and polarization, was partially completed. The four B-port plug-in parts were fabricated and are currently tested for vacuum tightness. The design of the in-vessel parts, which consist of 4 waveguide bundles, could not be terminated, since the assembly test of a prototype bundle is pending. In addition a waveguide re-routing became necessary, since the piping of the in-vessel components was changed.

A new small material test chamber was build-up, which enables to estimate the microwave stray radiation absorption properties of different materials at 140 GHz. Even though the chamber is fed with a power of 14 W only, it helps to select the materials for W7-X in-vessel components prior to the extensive high power tests at the MISTRAL chamber.

ITER ECRF Advanced Source Development – Coaxial Cavity Gyrotron, Backup Design and Test Facility

Introduction

The development of a 2 MW, CW, 170 GHz coaxial cavity gyrotron for ITER is pursued within the European Gyrotron Consortium (EGYC, consisting of CRPP, Switzerland; KIT, Germany; HELLAS, Greece; CNR and, within F4E Grant GRT-08, ENEA; Italy), which acts as scientific partner for F4E, and in cooperation with ISSP, Latvia. The goal of the development is the supply of sources for 170 GHz ECH & CD in ITER providing 8 MW CW power, to cover the EU contingent on ECH & CD sources at ITER. In contrast to other contributors to ECH & CD on ITER, the EU plans to provide sources with 2 MW RF power per unit (ITER minimum specification: 1 MW) for reduced cost and space requirements, to be able to double the system power if requested and to establish the - essentially more powerful - coaxial cavity technology.

While the industrial gyrotron prototype, built by Thales Electron Devices (TED, France), is tested at CRPP, KIT provides support to the development and the tests through component design, scientific investigations and collaboration as well as low and high power tests. The latter are done with the modular short-pulse pre-prototype gyrotron at KIT (see figure). In particular, KIT is solely responsible for the design of cavity, uptaper and mode converter system, and is involved in gun, beam tunnel and collector design.

In parallel to the coaxial 2 MW gyrotron activities, a 1 MW conventional cavity design is in preparation as fallback solution. This backup design intends to support the strategic decision about keeping the 2 MW design or switching to a conventional 1 MW design, which will be taken in mid 2011 after the next prototype experiments.

Status of work at the beginning of 2010

After the experiments with the first coaxial 2 MW prototype at CRPP were stopped without major success in autumn 2008, the efforts in 2009 concentrated on the demonstration of efficient high power operation with the pre-prototype at KIT, on the improvement of critical components and on a deeper understanding of the various problems. After the KIT Oxford Instruments magnet was enhanced using an additional normal conducting coil, it could finally operate (in pulses of tens of seconds) at the nominal field strength of 6.87 T. In combination with an adapted design of the electron gun and improved designs for beam tunnel and output launcher antenna, the KIT pre-prototype finally reached a world record power of 2.2 MW at 170 GHz, at an efficiency of 30% (without energy recovery). This short-pulse experiment (1 ms) proved the feasibility of a stable and highly efficient single-mode gyrotron interaction at the chosen high order mode $TE_{34,19}$. At the same time, the new structure of the corrugated beam tunnel was verified (see the internal mirror line report on gyrotrons for W7-X), and the launcher antenna with wall perturbations was also successfully tested with an RF output beam with 96% fundamental Gaussian beam content. The goal of this experiment, to demonstrate gyrotron operation at ITER parameters in short pulse, was fully reached. In particular, the output power and the RF beam quality exceeded ITER specifications (2 MW and 95% Gaussian content), while the efficiency without energy recovery matched the expectations – the ITER gyrotron specification calls for 50% efficiency with energy recovery, which appears reasonable with 30% non-recovered efficiency, but was not demonstrated.
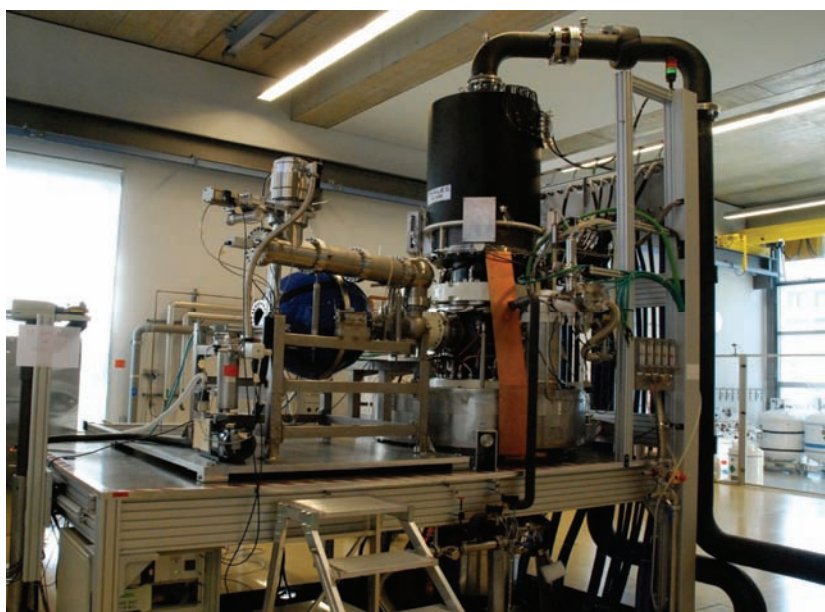

Coaxial 2.2 MW 170 GHz short pulse pre-prototype gyrotron at KIT (left) and the industrial long pulse prototype, installed at the CRPP test stand (right). The blue sphere is the CNR 2 MW RF load.

In addition, the gyrotron was equipped with a broadband silicon nitride Brewster window which permitted experiments at different operation modes and the corresponding different frequencies. These experiments could not be finalized in the available time, but supported the theoretical prediction that with such a window, the 2 MW gyrotron could well be used as a step-tunable millimetre wave source over a wide frequency range (140–210 GHz). Unfortunately, it was not possible to go on with these experiments due to a crack in a ceramic insulator of the electron gun.

On theoretical side, the three important achievements of 2009 were the finalisation of a new launcher synthesis code which permits the design of an output launcher with arbitrary wall perturbations, as well as an improved understanding of parasitic oscillations and of the relevance of particle traps for long pulse gun designs. The new launcher replaced the former launcher antenna with harmonic wall distortions, which turned out to be not suitable for a typical coaxial gyrotron mode (this is perfectly suitable for modes with caustic radius at the half cavity radius, but coaxial-cavity modes typically have smaller caustic radii). The launcher was successfully tested at low and finally high power, as reported above. The activities on parasitic oscillations and electron gun design were carried further in 2010 and will be described subsequently.

High power tests and redesigns of the pre-prototype

During the whole year 2010, it was tried in several ways to operate the short-pulse pre-prototype gyrotron at KIT. First attempt was to fix the crack in the gun insulator by an appropriate liquid sealant. This was successful first, the tube was vacuum tight, but it turned out that the sealant was dissolved by the insulating oil surrounding the gun contacts. Next, a similar electron gun from the former 165 GHz gyrotron experiment was employed, after a damage at the filament heater contact of this gun was diagnosed and repaired. Again, the conditioning of the gyrotron equipped with the old gun proceeded well, but unfortunately an indium sealing ring was melting and the old gun was polluted by oil. Towards the end of 2010, the pre-prototype was re-assembled with the old gun and successfully conditioned, so a next experimental campaign will probably be possible (see next figures). Since no high power experiments during 2010 could be done, the plans for these experiments were shifted to 2011 and beyond, as described in the next paragraph.
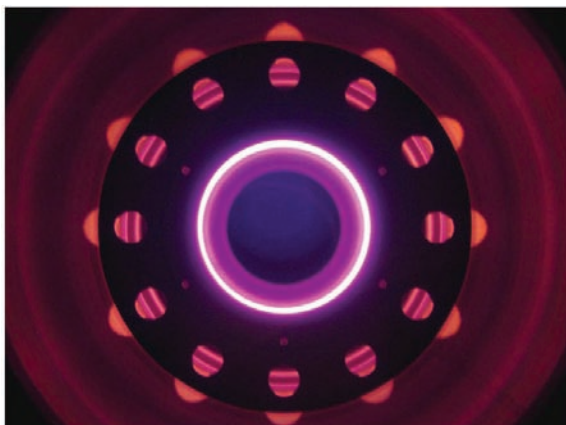
View inside the 165 GHz electron gun test assembly with heated emitter ring.
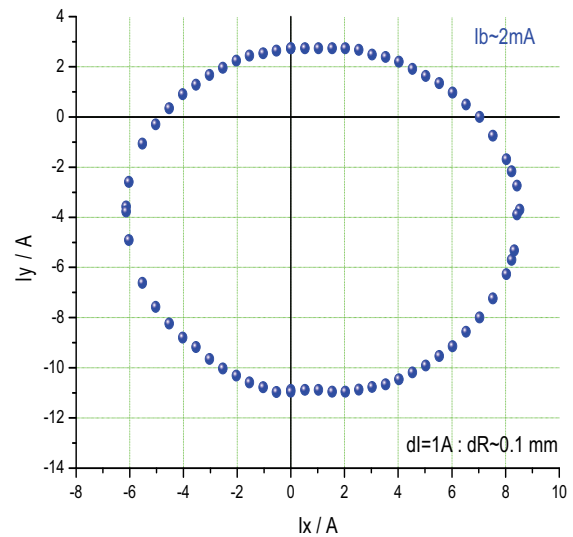
Current measurement using controlled beam displacement. The round structure of the beam positions with 2 mA current to the coaxial inner rod indicates homogeneous emission of the reconditioned 165 GHz gun emitter. The inner rod itself is not aligned in these measurements.

Since it was already obvious at the beginning of 2010 that the electron gun of the pre-prototype needed to be replaced, several activities for refurbishment and redesigns were started in parallel to the experiments. The aim was not just a replacement of worn-out components, it was also intended to gain flexibility and improve the relevance of the experiments for the long-pulse tests with the prototype at CRPP. Two basic decisions were made: The KIT Oxford Instruments magnet shall be directly equipped with a cooled normal conducting coil, suitable for CW operation. This reduces the warm bore hole of the magnet to a diameter of 220 mm, which in turn calls for a redesign of the pre-prototype tube to make it fit into this smaller hole. The other decision was to build a more modular electron gun, for easier design changes and also for easier repair. A condition for all those redesigns was to gain more similarity to the prototype, for easier comparisons and more relevant test cases. Under consideration of all these conditions, the redesigns were done, the corresponding hardware will in subsequent steps be purchased and build into the pre-prototype and the magnet. The changes were projected in a way that the tube can be operated at intermediate steps of redesign, so the first purchases aim at replacing the emitter, to be able to operate the gyrotron again as soon as possible.

Activities in support of the prototype refurbishment, future tests and for the gyrotron installation at ITER

The refurbishment of the industrial prototype for the ITER gyrotron was started in 2009 and aimed at delivery to CRPP Lausanne in summer 2010. Due to various delays, the delivery date now shifted to mid July 2011. The biggest problem was a cracking ceramic isolator during the final bake-out of the tube.

Through these delays, the activities in direct support of experiments with the refurbished prototype had to be postponed to 2011. Only one directly related measurement could be done, the new launcher of the refurbished gyrotron was measured at low power with an RF beam quality slightly worse than expected: 94.2 % Gaussian mode content at the RF window instead of 95.5 %, which was reached by the KIT system. The reason for this decline could not be determined, more information will be gained with the high power experiments. Another preparation for high power measurements was the test of a high power RF load, designed by CNR Milano. This load, a

cooled absorbing sphere, was designed for 2 MW CW operation. The concept was tested with a sphere that was covered by attenuating material only in half, so it would be suitable for 1 MW only and could be tested with the W7-X SN3 gyrotron (see next figure). The test validated the design as far as possible with this gyrotron.

Apart from that, work was done on simulating particle traps and understanding their relevance for magnetron injection electron gun designs. The results of these investigations were considered in the gun redesign. Finally, the design for a new magnet for the second industrial prototype was investigated through different design models and corresponding electron gun calculations, and intensively discussed among the contributing parties, which resulted in a design proposal which will be used in a call for tender by F4E.
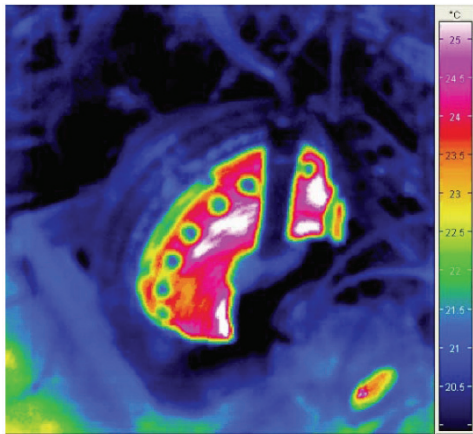

Thermal image of the spherical 1 MW CNR load (half coated, as model for the fully coated 2 MW load) at 700 kW / 140 GHz input power.

Independent of the delayed gyrotron test, a variety of activities were performed within the collaboration with CRPP to prepare the gyrotron procurement and installation at ITER. These activities range from investigations on the influence of stray magnetic fields and neighbouring gyrotrons over interface specifications to first estimations and observations on operation reliability. As an example, calculations on the influence of the tokamak field on the magnetic fields at the gyrotron collectors are shown in the figure below. Another example is the work on advanced collector sweeping schemes, as described in the section about the 1 MW backup gyrotron design (page 17). The goal of these different efforts is to define specifications and recommendations for the gyrotron installation at ITER for reliable nominal operation (F4E Grant GRT-034).
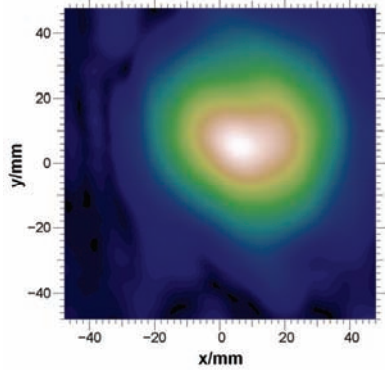
Simulation codes and designs for quasi-optical systems

The new TWL_DO code for launcher synthesis was further improved by a better optimisation routine, by inclusion of ohmic losses, transmission and reflection calculation, and by the calculation of the cross-polarized part of the output power. In addition, the launcher designs for the prototype refurbishment were further enhanced by adding phase correcting mirrors and optimizing them for improved transformation through a matching optics unit (MOU) into a HE_{11}-mode waveguide. The most relevant of these alternative designs will be manufactured and characterized by low- and high power measurements.
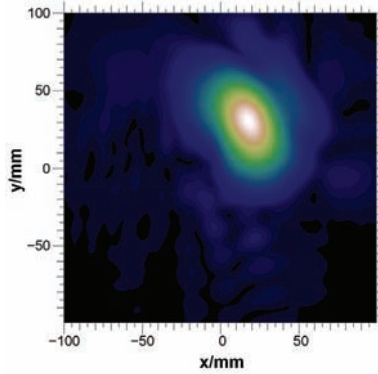
In addition, a complete mirror design for the MOU for the ITER gyrotron was accomplished. The purpose of this device is to match the gyrotron output beam to the transmission lines of the ITER ECRH system, and in particular compensate tolerances (two figures on next page). It turned out that the mirrors had to be designed by a new method for an optimal tolerance compensation without unacceptable coupling losses at high input beam misplacements.
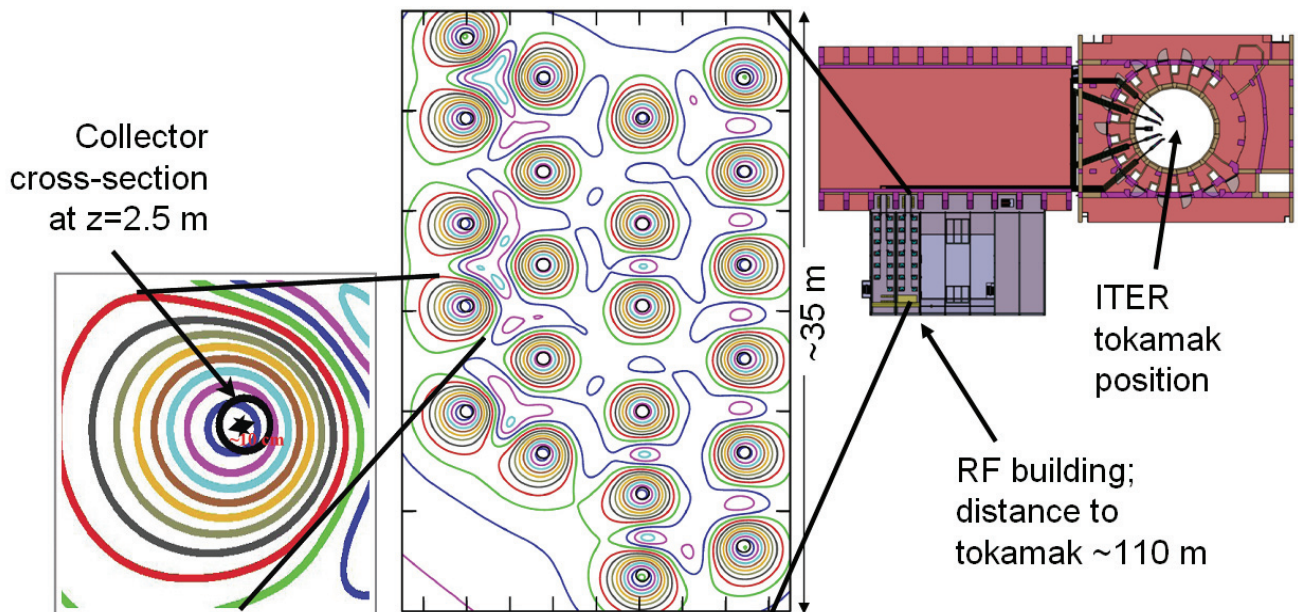
Magnetic field lines at the gyrotron collectors under influence of neighbouring gyrotrons and the ITER tokamak field. The misplacement of the circular collector fields indicate that compensation of stray fields will be required.
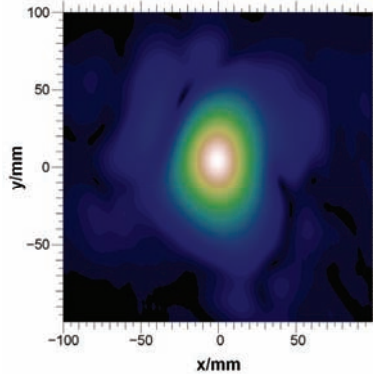
The 1st mirror: rotated by 5.9 and 6.5 degrees in x- and y-direction.

The 2nd mirror: rotated by 4.7 and 4.1 degrees in x- and y-direction.

Coupling efficiency: 96.66%

Power transmission: 95.24%

Amplitude distribution of the misaligned wave beam on the gyrotron window.

Amplitude distribution of the misaligned wave beam on the 1st mirror.

Amplitude distribution of the misaligned wave beam on the 2nd mirror.
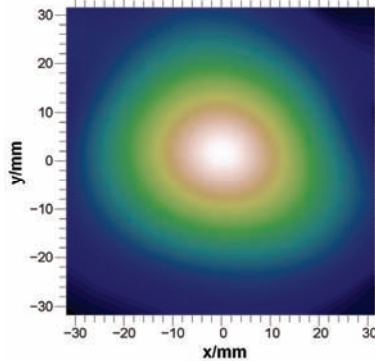
Amplitude distribution of the corrected RF beam at the entrance of the corrugated waveguide.

Example for the calculation of a misaligned RF input beam. The misalignment of 10 mm in both x and y direction is compensated by rotating the MOU mirrors.

In addition to the TWL_DO code, a new, faster analysis code LAUNCHER was successfully tested. Based on accelerated convolution techniques, this code calculates the wave propagation inside the launcher essentially faster than TWL_DO and can furthermore be extended for modelling tapered launchers.
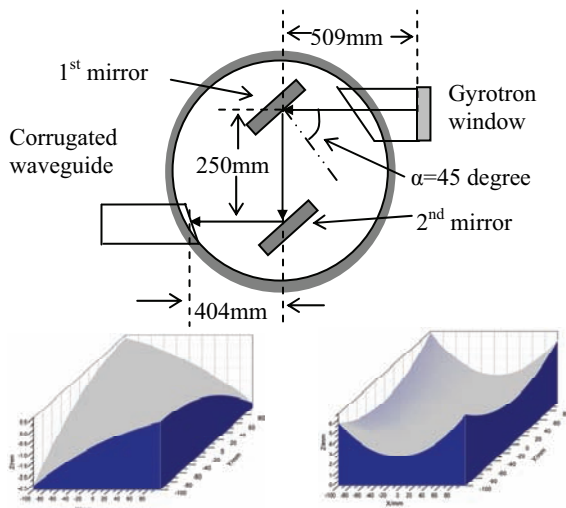
Profile of the 1st mirror. Profile of the 2nd mirror.

Sketch of the MOU box and the newly designed matching mirrors.

Gyrotron interaction codes: Investigations on dynamic after cavity interaction (ACI)

On the theoretical side, the investigations on dynamic ACI were further carried on. The hypothesis that the spent electron beam undergoes active interactions after the cavity, in the so called uptaper section, is still under discussion. Investigations with different KIT cavity designs indicated that this ACI actually manifests itself as an oscillation driven by the electron beam through its bunched structure that is created by the cavity interaction before. Such a behaviour, called dynamic ACI, could be demonstrated in several simulations, which seem to be supported by measurements of parasitic oscillations in the W7-X tube experiments and, in particular, in experiments with the step-tunable tube (see IHM Annual Report 2009). The latter had delivered only 600 kW output power, which was confirmed by simulations in which dynamic ACI caused the power limitation. The simulations also predicted that lifting the tube by 20 mm could remove this power limitation, which could actually be confirmed by the experiment. These investigations are ongoing (see page 23).

Since such observations indicate that dynamic ACI may be an important factor for gyrotron operation, a new method for a fast and simple prediction of dynamic ACI in an early design phase is under development. This method relies on an estimation of possible interaction frequencies along the gyrotron cavity and uptaper, to identify regions prone to dynamic ACI. The preliminary result is that extended regions with nearly constant interaction frequency have to be avoided. The easiest way to do that is to employ a steeply dropping magnetic field in the region after the cavity.

Progress on microwave measurement experiment

Through the implementation of a highly sensitive low noise amplifier, the high power millimetre source of the homemade D-band vector network analyzer could be replaced by a solid state multiplier source. This change was one important step in the process of modernizing this instrument for the measurement of quasi-optical components, since the high power source, based on a phase-locked backward wave oscillator tube, rapidly lost power and reliability.

The equipment for spectral measurement of the gyrotron output signal was further automated and prepared for integration into the test stand system. Now, a highly dynamic measurement system for finding parasitic oscillations and measuring their spectrum as well as the spectrum of the main frequency line is available which will be routinely employed for investigations on undesired oscillations and spectral purity in general. This system removes the ambiguity of harmonic mixer measurements through a multipath frequency measurement using different harmonics an a highly sensitive spectral analyzer. The measurement of a complete output spectrum over ranges of 40 GHz is now automatically possible, but needs of course long pulse lengths or repeated pulses.

Progress with the 1 MW backup gyrotron design

The 1 MW backup gyrotron design operated in the $TE_{32,9}$ cavity mode, projected as an alternative to the 2 MW coaxial ITER gyrotron, was finalized. In detail, a magnetron injection electron gun, a cavity with the appropriate uptaper, and a conventional output launcher with the appropriate mirror system were designed. Other components like the collector, RF window and beam tunnel were merely copied from existing designs for the W7-X gyrotron or the 2 MW ITER tube. All components were successfully tested for stability of operation and for fulfilling the ITER specification. In particular, the suitability of the W7-X gyrotron collector for power modulated gyrotron operation was investigated, with the result that the conventional longitudinal beam sweeping would need to be replaced by a transversal sweeping system for a 50 % power modulation – the way of modulation requested by ITER, using only the collector depression voltage for power modulation, increases the power load on the collector at lower RF output powers and requires a more efficient power distribution method over the collector surface.

For an actual realisation, the next step would be the technical layout, to be done by the manufacturer. This gyrotron will only be realised when the 2 MW tube development has to be replaced by a less ambitious project.

Conclusions and prospects

After the essential delays for all high power experiments during 2010, it remains the main goal to start again with long pulse prototype experiments at CRPP as well as with short pulse experiments with the pre-prototype at KIT. The central objective of the prototype experiments is, of course, the demonstration of a stable operation which fulfils the criteria for ITER gyrotrons. With this 1st prototype, the aim is to operate in pulses of 1 s, which is an important step towards CW operation. The main purpose of the pre-prototype is to support these experiments. This means that the plans for pre-prototype experiments will in case be aligned with the investigation needs of the prototype. Apart from that, there is a range of topics that will be investigated with varying priority. These are measurements of different output launchers and quasi-optical systems (currently, an alternative launcher antenna delivered by IAP Nizhny Novgorod is installed and will be tested for RF beam quality and stray radiation), in order to determine sources of stray radiation and to test the different concepts of further improved launchers that were proposed and designed during 2010. Then, different versions of beam tunnels will be employed for comparison. The experiments at different frequencies will be completed, and operation with depressed collector for energy recovery is foreseen, to demonstrate high efficiency operation and as first step towards longer pulses with the pre-prototype. It should be clear that not all of these tests can be done in 2011, so these works will be carried on over the next years.

In parallel to the experiments, the purchase of modular components for the pre-prototype will be continued. It is foreseen to operate a new modular electron gun at the end of 2011. In a later step, the body of the gyrotron will be replaced, in order to operate the pre-prototype inside the small bore hole which is left by the normal conducting CW coil – this coil must also be finally purchased. Furthermore, in preparation of a possible operation of the industrial prototype at KIT, this normal conducting coil needs to be amended by two smaller coils at the gun region (see figure on next page). After all these changes, a flexible modular pre-prototype gyrotron as a model for supporting the long pulse prototype will be available, suitable for better comparability of experiments and for easier design changes.

The activities for the design and procurement of a second long pulse prototype and a corresponding new magnet (the existing magnet at CRPP has a too high helium consumption) have to be continued in parallel. The need for compatibility with ITER requirements has to be taken into account in the specifications of the envisaged 10 MW gyrotron test stand at KIT as well.

On the theoretical and simulative side remains a clear need for improved modelling of non-idealized geometries. This will be approached on the one hand through removing some of the assumptions of the existing simulation codes, for example by extending the numerical models towards non-uniform magnetic fields, lossy materials and deviations from the azimuthal symmetry. With regard to quasi-optical output couplers, the efforts on faster simulations and inclusion of tapered launchers will be continued. On the other hand, the activities for using full-wave codes at least as verification tools will be intensified. In particular, the in-house full wave code PicLas will be equipped with suitable interfaces for gyrotron applications, and will be tested as complementary verification tool for all components of the gyrotron.

(a)　　　　　　　　　　(b)　　　　　　　　　　(c)
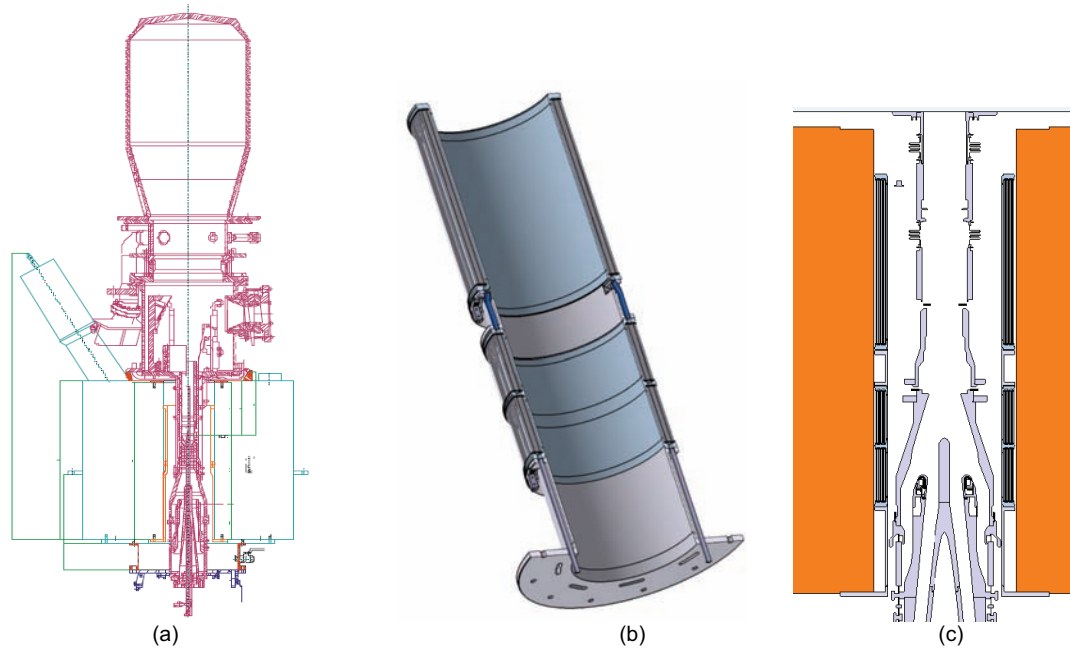
Cross section of the industrial prototype, installed in the KIT OI magnet (a). To adapt the OI magnet for operating this gyrotron, an additional normal conducting coil (b) has to be installed into the warm bore hole of the magnet, as detailed in (c).

Design Studies Towards a 170 GHz 4 MW Coaxial-Cavity Gyrotron

For future fusion devices it is desirable to develop gyrotrons with highest possible unit power to reduce the costs and space requirements for new ECRH systems. Currently the 2 MW coaxial-cavity gyrotron has reached prototype status so consequently a detailed design study for a 170 GHz 4 MW coaxial-cavity gyrotron was started in 2008. Within the EURATOM Fusion Training Scheme EC-TECH No. 042636 (FU06) this work is done as the main topic of a Ph.D. thesis. After physical and technical feasibility studies the designs for the major gyrotron components (electron gun, coaxial cavity, quasi-optical system for a two beams output and collector) have been developed. In addition, several thermo-mechanical studies were performed to identify long-pulse operation effects. The following table summarizes the major design parameters and goals.

Operating frequency f_0	170 GHz
RF output power P_{out}	4 MW
Total interaction efficiency η_{tot}	> 35 % (without depressed collector)
Peak ohmic wall loading (realistic) ρ_{wall}	< 2.0 kW/cm²
Loading coaxial insert (realistic) ρ_{coax}	< 0.2 kW/cm²
Emitter current density j_{beam}	< 5.0 A/cm²

*Design requirements for a 170 GHz 4 MW CW coaxial-cavity gyrotron.*

In a mode selection process one well qualified mode, namely $TE_{52,31}$, was found to deliver the desired output power and frequency. Extensive optimizations on the geometry of the interaction cavity have been performed to achieve highest efficiencies and acceptably low wall losses. All calculations have been done using self-consistent and instationary slow-variables code packages, which are available at KIT. In addition the tapers of the cavity have been designed using scattering matrix codes to guarantee lowest mode conversion towards the quasi-

optical output launcher and lowest backward power transmission towards the electron gun. Overall unwanted mode conversion of lower than 0.3% of the total power from the main mode is possible. A typical start-up simulation with linear voltage rise considering realistic gun parameters is shown in the next figure.
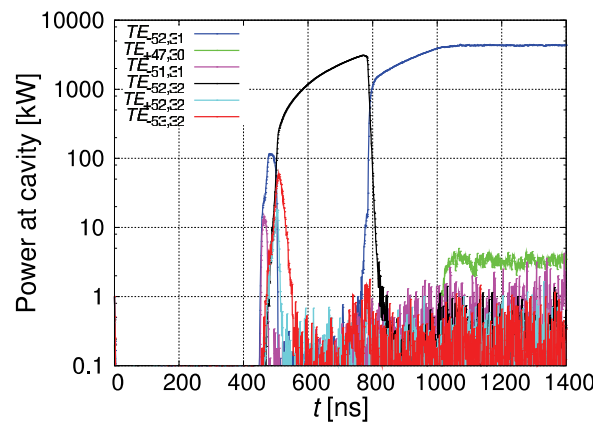

Self-consistent start-up simulation for the $TE_{-52,31}$ mode.

In a next step diode and triode-type magnetron injection gun designs have been developed. It was possible to find suitable designs using well-known script-based optimization algorithms. Automated optimization is necessary to determine results within a huge solution space of the electrical and geometrical parameters. Extensive parameter studies have been carried out to specify the adjustability and sensibility of the electron beam quality to the electrical and geometrical parameters. Within a triode-type magnetron injection gun the ratio α between perpendicular and the axial velocity components of the electron can be smoothly tuned using the voltage applied to the modulation anode. This can be seen in the following figure. In addition, considering the limitation imposed by the maximum allowable electric field, the required radial dimension of a triode-type gun at the axial position of its cathode is small, compared to the diode-type gun, due to the lower modulation voltage. The triode's additional modulation anode compensates the high electric field along the electrons' trajectories in the emitter region.
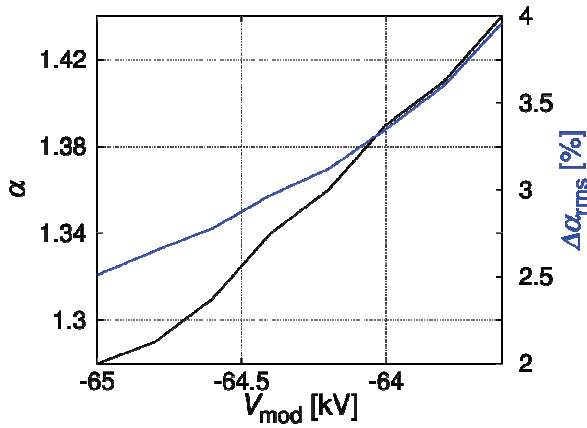
Velocity ratio α and its spread versus voltage applied to modulation anode.

Synthetic diamond discs, which are suitable for microwave beams of up to 2 MW, are used as output windows for gyrotrons. Consequently a gyrotron with an output power of 4 MW needs two windows, and its quasi-optical system should convert the high order volume mode into two Gaussian-like output beams. For this conversion a launcher antenna with two cuts was designed using a newly developed KIT in-house code. The beams are radiated with a very high Gaussian-mode content of 97% and 98% (vector correlation coefficient) and have an azimuthal separation of 144°. The field on the optimized launcher surface is shown in the next figure. In addition, two-dimensional filter techniques are introduced to simplify the launcher's surface perturbations in order to reduce the stray radiation level without lowering the beam quality. Reducing the perturbation depths allows a simplified fabrication process of the launcher and consequently reduces its overall costs.
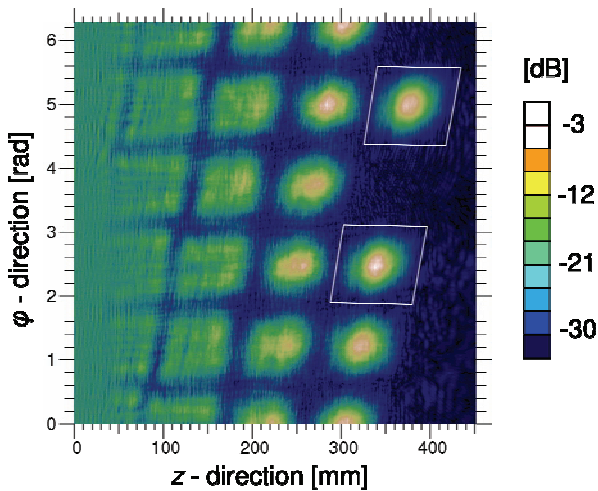
Field distribution on optimized two-beam launcher (irradiated beams in the white parallelograms).

Two collector layouts were optimized employing normal and dispersion strengthened copper as wall material which absorbs the electron beam. The designs were optimized using longitu-dinal magnetic sweeping systems with wobbled coil currents and optimized collector surface shapes. The admissible limit for the overall wall loading in the collector is only achievable with a high depression voltage, which requires in turn a high quality of the electron beam. The copper collector layout with an average wall loading of < 500 W/cm^2 has an inner radius of 400 mm and an absorbing length of approximately 1.0 m along the gyrotron axis. The higher admissible limit for dispersion strengthened copper (glidcop) of < 1000 W/cm^2 allows a more compact collector design with 300 mm radius and 0.8 m in length.

For the characterization of several long-pulse operation effects, various computing scripts were introduced to enable the data exchange between commercial finite-element approaches and corresponding KIT in-house codes. The expected surface temperature of the optimized coaxial 4 MW cavity is strongly sensitive to its surface roughness and the efficiency of the applied cooling technique. The figure below shows the deformed cavity in thermal steady state.
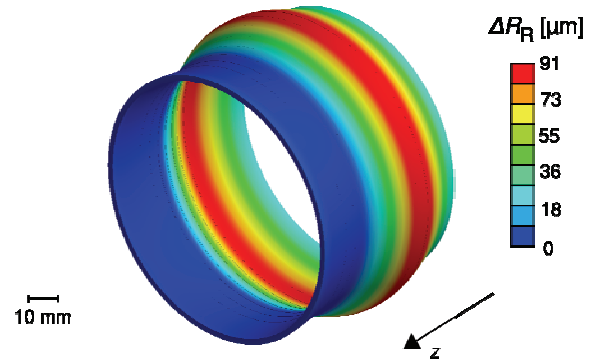
Deformed 4 MW cavity at thermal steady state.

The frequency shift due to thermal expansion of the cavity at nominal operating conditions with a peak wall loading of 1.7 kW/cm^2 for realistic dispersion strengthened copper is determined to be approximately -130 MHz. In addition, the resonator shows a strongly increasing quality factor for a reduced heat exchange coefficient at the cylindrical cavity section. In order to guarantee stable operation, the efficiency of the cavity cooling and the inner wall's surface roughness have to be controlled carefully. The utilized calculation techniques are verified with experimental data available for the 1 MW 140 GHz series tube SN1 for the stellarator Wendelstein 7-X and show satisfactory correlation.

During CW gyrotron operation, the coaxial insert and its impedance corrugation for advanced mode competition are heated and deformed. Based on two different models for the loading on the insert, the surface temperature was calculated and shows a strong dependence on the velocity of the cooling liquid in the insert's cooling channel. At nominal parameters the surface temperature reaches 120 °C and the corresponding deformation of the several grooves of the impedance corrugation is not critical.

The optimized inner surface structure of the quasi-optical output launcher consists of fine perturbations in the scale of several tens of millimeter. Towards the end of the launcher, both mm-wave beams are highly focused resulting in high local wall loading and a corresponding deformation of the optimized profile. The cooling channels with a rectangular cross-section are aligned as a double helix structure around the output coupler. The surface temperature at the launcher's focus points reaches 410 °C for nominal operating conditions. The vector correlation coefficient in relation to the ideal Gaussian distribution and therefore the quality of both beams decreases strongly with reduced efficiency of the cooling structure. As a consequence, adequate launcher cooling is necessary in order to guarantee efficient conversion of the high-order cavity mode into two Gaussian beams and to minimize the generated stray radiation. After application of a newly developed two-dimensional filter techniques, the smoothened launcher surface can operate more reliably at higher temperatures and smaller corresponding thermal deformations.

## Studies on advanced emitter and electron beam diagnostic systems

Today high power gyrotron oscillators for ECRH & CD in fusion devices have in principle proven their capability to deliver high millimetre wave power (for example 10 x 1 MW CW power at the W7-X ECRH system). Consequently, the scope now shifts towards improved reliability and efficiency of gyrotron devices. While gyrotrons today reach efficiencies of typically 50 % (up to 70 % at best) using a single stage depressed collector, an improved efficiency calls for multi-stage depressed collectors combined with optimized electron guns providing well controlled electron beam parameters, suitable for efficient millimetre wave generation. It can be expected that such advanced gyrotrons reach efficiencies in excess of 70 % typically. This will in return also improve the reliability through reduced thermal loading of the collector of the device, which today is the most critical component of a gyrotron. A second critical component is the emitter of the electron gun, which has by design a limited life time and which can deteriorate the millimetre wave generation through inhomogeneous emission. New emitter materials, developed by the company Calabazas Creek Research (CCR; see R.L. Ives et al., "Controlled Porosity Cathodes From Sintered Tungsten Wires", IEEE Trans. on Electron Devices, Vol. 52, No. 12, 2005), promise higher emission current densities and a better controlled and extended life time.

Status of work at the beginning of 2010 and achievements in 2010

The works were initiated at the beginning of 2010 by setting up a project and by building up the appropriate collaborations. The main part of the work in 2010 – 2012 will be within a dedicated dissertation for advanced concepts. It is foreseen to build a new low power gyrotron equipped with the new CCR emitter material, arranged as small and separated emitter ring segments. For comparison, a conventional emitter will also be ordered for the new gyrotron. With this device, the new emitter material will be qualified. Since such emitters must be segmented by design, the device also opens large fields for investigations on the influence of emission inhomogeneities on the gyrotron interaction and possibly related effects on parasitic oscillations.

These experiments are in addition complemented by the development of new electron beam diagnostic systems that allow for measurements during full operation of the gyrotron, in contrast to current electron beam testers which can only characterize the separated electron gun at scaled low power parameters. In a first approach, it is considered to calculate electron energy distributions from measurements of the electron's bremsstrahlung at the collector. Such measurements will give valuable insights into interaction mechanisms and electron beam parameters. In combination with the segmented emitter test gyrotron, it will be possible to qualify the measurement system, and on the other hand to use it both to investigate the properties of the new emitters as well as to support experiments on inhomogeneous emission.

The X-ray electron beam diagnostic is currently developed within a collaboration between KIT and the St. Petersburg State Polytechnical University (SPbSPU), Russia. In 2010, an extensive theoretical study on the calculation of electron energy distributions from bremsstrahlung was accomplished. The result is that a very good reconstruction of energy distributions is possible if the radiation is measured through materials and walls which do not absorb strongly, like the ceramic isolators on the gyrotron or additional windows, for example at the collector top (see next figure).
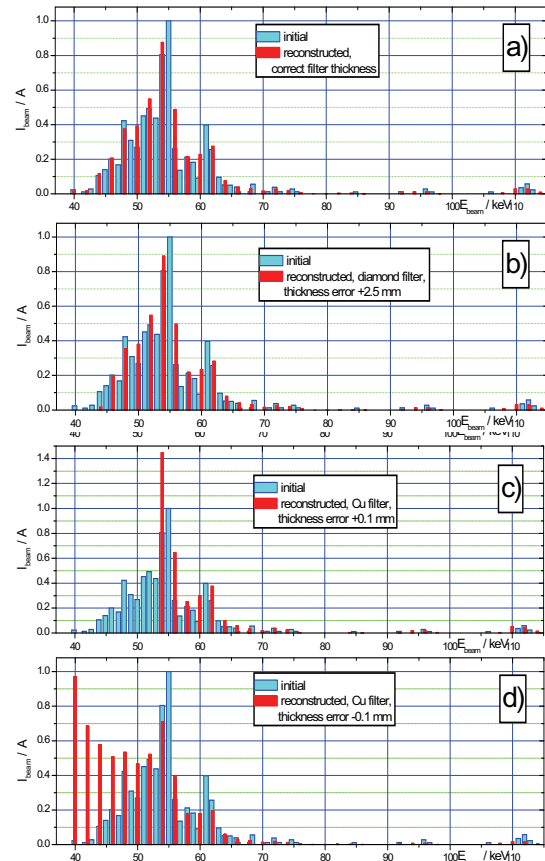

Influence of material parameter deviations on the reconstruction of electron beam energy spectra from X-ray measurements through different materials.

The construction of the test gyrotron was started. In order to begin the works quickly and at low costs, the first attempt was to re-use one of the available electron guns from former projects as conventional comparison test case. An old $TE_{10,4}$-mode gyrotron appeared suitable, but it was not possible to achieve any electron emission from it. It was therefore decided to order both a new emitter and a newly designed conventional emitter with the same overall shape from CCR. A first contract was given to CCR about investigations on a segmented sintered W-wire emitter construction.

To determine the beam parameters for the design of the new gun, it was necessary to first design the cavity of the low power test gyrotron. In addition, an available 0.5 T normal conducting magnet was checked and characterized for this project, to be independent from the highly loaded fusion test stands. The $TE_{3,1}$ mode was chosen as operating mode at the following parameters: frequency f = 28 GHz (second harmonic), cavity radius R_{cav} = 7.15 mm, optimum radius of the electron beam R_e = 3.13 mm and magnetic field in the cavity 0.516 T. The next table gives some of the most important parameters of the optimized triode-gun design. The next figure shows beam parameter simulations with different mod-anode voltages.

Beam current	2.2 A
Accelerating voltage	20 kV
Mod-anode voltage	15.6kV
Beam compression ratio	2.4
Beam radius (interaction region)	3.13 mm
Cathode radius	7.15 mm
Cathode angle	32.2 °
Axial width of the emitter	1.7 mm
Emitter current density	2.5 A/cm^2
Velocity ratio	1.56

Nominal triode-type electrongun parameters.
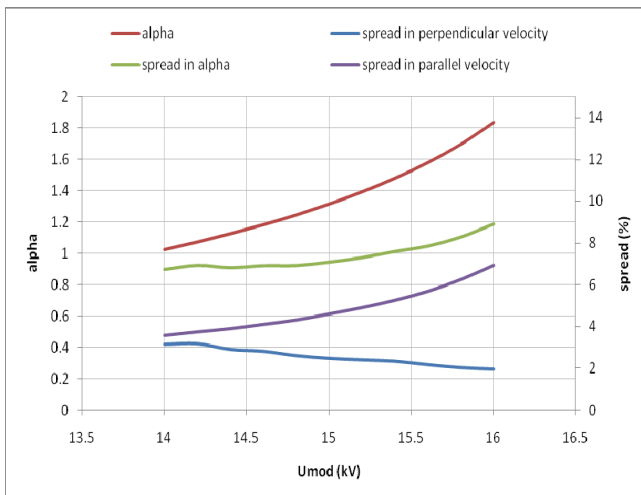
Velocity ratio (alpha), spread in alpha, as well as spread in parallel and perpendicular velocity components as a function of U_{mod}.

Conclusions and prospects

The first steps towards advanced gyrotron emitter materials, beam diagnostics and, in consequence, higher efficiency and reliability through better physical understanding and through the employment of multi-stage depressed collectors, were done by projecting and designing a test gyrotron with a novel, segmented emitter, and by starting investigations on an X-ray based beam diagnostic system. Within the next year, a first version of the new gyrotron should be assembled and tested. The X-ray diagnostic will also be tested in principle, to get the necessary experimental experience to build up a dedicated beam diagnostic system in subsequent steps during 2012.

ECR Heating and Current Drive – Step-Tunable Gyrotron Development

Introduction

In recent years electron cyclotron resonance heating and current drive (ECRH and ECCD) has been established as a successful instrument in magnetically confined fusion plasmas. Gyrotrons are the unique devices which meet the extraordinary requirements of those applications: output power in the MW range, 100 – 200 GHz output frequency, pulse length of several seconds up to continuous wave. Due to its excellent coupling to the plasma and the very good localization of the absorbed RF power, ECRH is applied in present day machines and is also foreseen in large forthcoming fusion project: it will be the main heating system for the stellarator W7-X which is currently under construction and it will play a major role in the ITER tokamak. In particular advanced tokamaks are operated in a plasma regime where MHD instabilities which may limit the performance are present. To a large extent the stability in a tokamak is influenced by the distribution of the internal plasma currents which can be manipulated by the injection of RF waves. The location of the absorption of RF waves with the angular frequency ω is dependent on the resonance condition $\omega - k_z v_z = \omega_c$ (k_z: z-component of the wave number, v_z: electron velocity along z-axis). Thus, by changing the wave frequency ω the absorption can be moved to any radial position where the local cyclotron frequency of the electrons ω_c holds for the expression above.

Industrial gyrotrons in the relevant frequency range with an output power of about 1 MW are usually designed for a fixed frequency. However, frequency tunable gyrotrons are not a standard product since these broadband tubes require additional optimization of major components of the gyrotron like the electron beam forming optics, cavity, quasi-optical mode converter and output window.

For experiments on plasma stabilisation at ASDEX Upgrade (IPP Garching) with advanced ECRH and ECCD, multi-frequency tunable (105 – 143 GHz) 1-MW long-pulse gyrotrons are highly needed.

Investigations on frequency spectrum and output power characteristics of a step-tunable gyrotron.

Measurements performed in 2008-2009 at KIT with a step-tunable gyrotron, made in short pulses of few milliseconds, have shown unexpected low efficiency of the device. The output power at 140 GHz employing the TE$_{22,8}$ mode was limited to 650 kW power at nominal operating parameters of cathode voltage and current. In addition, the appearance of parasitic oscillations having 4 GHz lower frequency than the main cavity mode with increase of the power was observed.
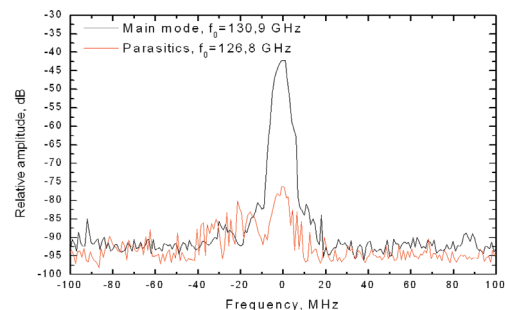

*Spectra of parasitic and main cavity mode (TE$_{22,7}$) oscillations.*

Spectrometric measurements revealed a broad spectrum of these unwanted oscillations shown in the figure. These measurements provide valuable information for theoretical investigation of this phenomenon. The suggestion was that the low efficiency of the gyrotron at working mode and parasitic oscillations are related to the so-called After Cavity Interaction (ACI) of the electron beam passing through the up-taper region with the propagating electromagnetic wave.

Several computer simulations with a multimode self consistent time domain model of the gyrotron interaction were performed. The simulations confirmed that combinations of the installed up-taper geometry and magnetic field in the up-taper, may lead to a significant effect of coupling between the electrons with transversal rest energy and RF wave. The interaction may initialize the complicated effects resulting in RF power reduction and its absorption by electrons in the region of the up-taper, auto modulation and instabilities of the output power.

As an example the simulated start up scenario for the TE$_{22.8}$ mode is shown in the next figure. In the simulation the geometry of the up-taper is included. As one can observe the generated power does not reach more than 600 kW in average, which is in agreement in with experimental measurements. In addition the axial structure of the field at time 1500 ns is shown in the second figure below. The field profile is not stable and varies very rapidly with time. The instantaneous efficiency deviates strongly from the time averaged efficiency demonstrating maximal value of the field in the up-taper region.
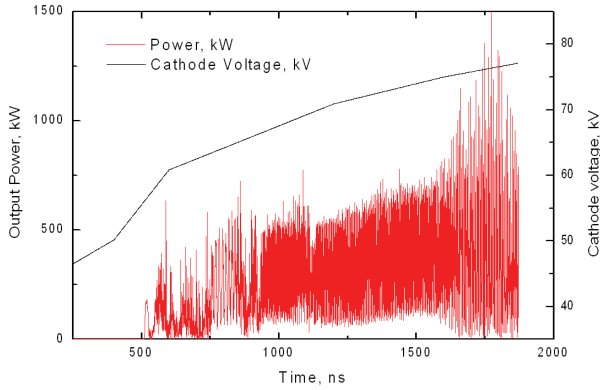

Start up scenario for the TE$_{22.8}$ mode.
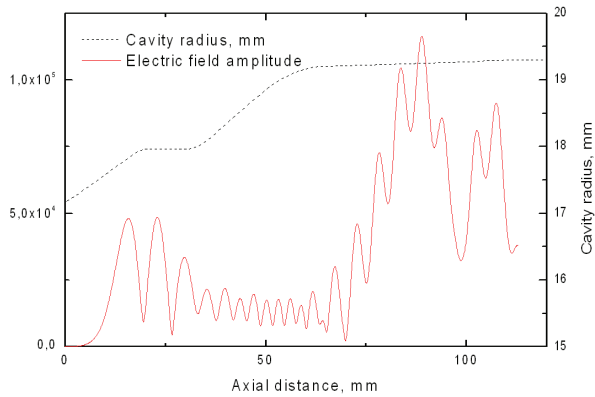
*Field profile of the TE$_{22,8}$ mode at t=1500 ns.*

In order to avoid gyro-resonance matching in the structure of the uptaper a stronger gradient of the magnetic field would improve the stability of the cavity oscillations. The magnetic field profile is determined by the arrangement of the super-conducting coils and is fixed. Since the axial gradient of the field is increasing with the distance from its maximum it is possible to affect the field amplitude of the electric field in the uptaper without significant influence of the field in cavity by moving the arrangement of cavity and up-taper in axial direction. Numerical simulations show that a shift of 20 mm would be an optimal value. The layout of the axial magnetic field distribution and cavity profile before and after shifting are given in the next figure.

Simulations with the cavity shifted by 20 mm, with respect to the maximum of the axial component of the magnetic field distribution were performed. All the other parameters in simulations remained the same. Simulated power and field profile are shown in the next two figures.
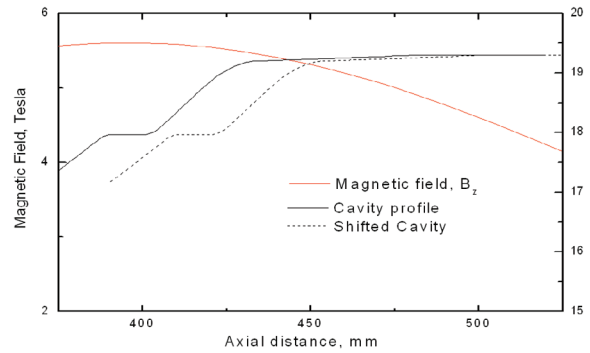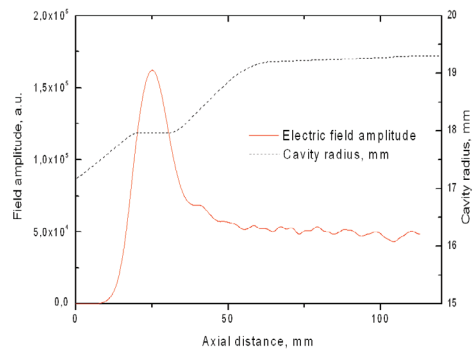

Magnetic field distribution and the cavity profiles.

As one can see the generated power is exceeding 1 MW at the same parameters, though it still demonstrates an unstable behavior with fluctuations of about 10 % from the averaged value.
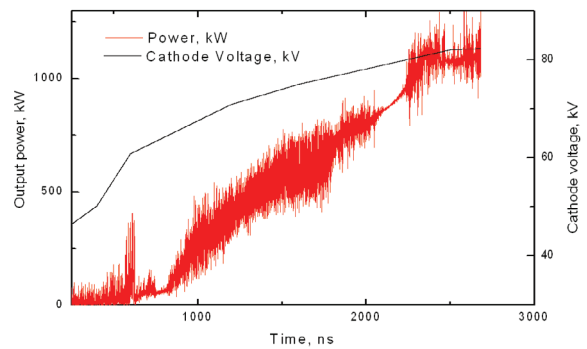
Start-up scenario for TE$_{22.8}$ mode with 20 mm shift of the cavity.

Field profile at t=2400 ns with 20 mm shift of the cavity.

The field profile in this case has one maxima located at the cavity's center, the distribution is close to the expected one, having the Gaussian shape. At the position of the up-taper starting from 60 mm, the field distribution still has instabilities (ripples) varying rapidly in time, but with lower amplitude compared to the one illustrated on the previous page. In all simulations the energy spread of electrons of 5 % was assumed to realize the simulation close to realistic conditions.

ESRAY calculations of the electron beam parameters for the case when the gyrotron is shifted by 20 mm have shown that the pitch factor and beam radius are very sensitive to the position of the emitter in the inhomogeneous field of the gun coil and deviate from nominal values significantly, so that no optimal operation is possible. Results of calculations are demonstrated in the next two figures. A strong increase of the pitch factor reaching the value of 2 with a very high variance as can be clearly observed.
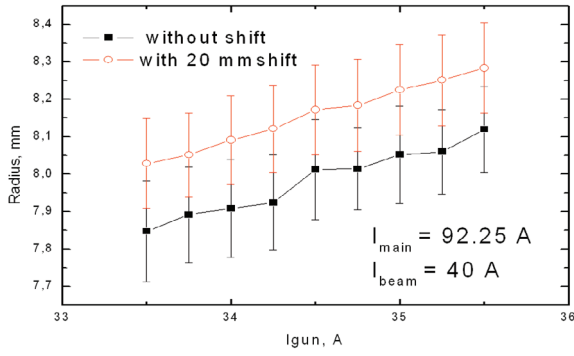
Radius of the electron beam in dependence of I_{gun}.
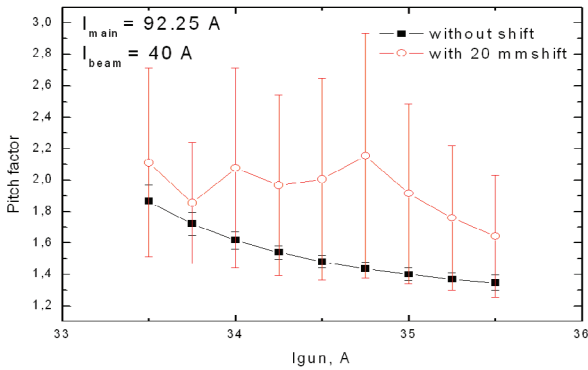
Pitch factor of the electron beam in dependence of I_{gun}.

Therefore, it was necessary to change the construction of the gyrotron in a way that the cathode remains at the same position. After modification of the experimental setup the measurements for a series of working modes were performed. In the next figure the curves for the $TE_{22,8}$ mode are shown. The beam currents are 43 and 45 A, for a measurement without shift and with 20 mm axial shift, respectively. After modification it was possible to obtain higher pow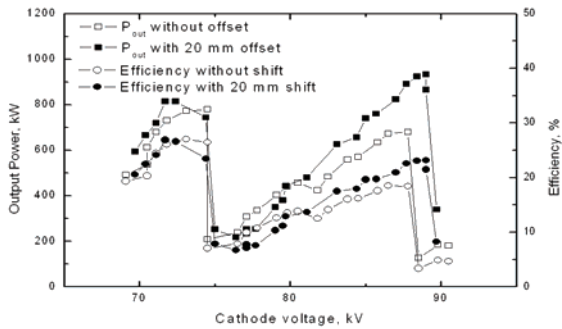er and better efficiency for the $TE_{22,8}$ mode at 140 GHz. The efficiency is calculated neglecting the effect of voltage depression which takes place in the regime of short pulses.

Power and efficiency of the $TE_{22,8}$ mode.

The highest efficiency up to 30% and output power of up to 950 kW was achieved for the modes $TE_{23,8}$ and $TE_{24,8}$ at reduced cathode voltage. As an example, the dependencies of power and efficiency as a function of cathode voltage are given in the next two figures. The RF efficiency of the $TE_{22,8}$ mode is lower in comparison with the modes $TE_{23,8}$ and $TE_{24,8}$ which both have larger caustic radii. The optimization for modes with lower value
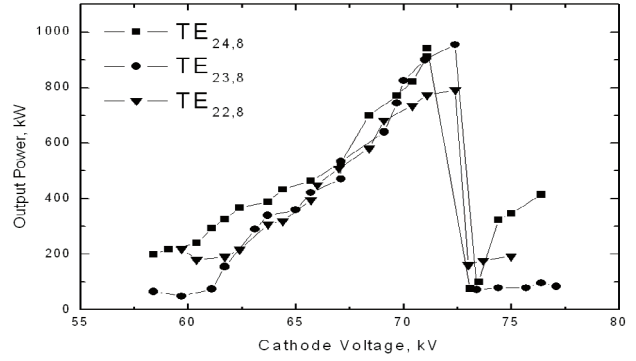
Generated power by the modes $TE_{24,8}$, $TE_{23,8}$ and $TE_{22,8}$ at reduced cathode voltage.
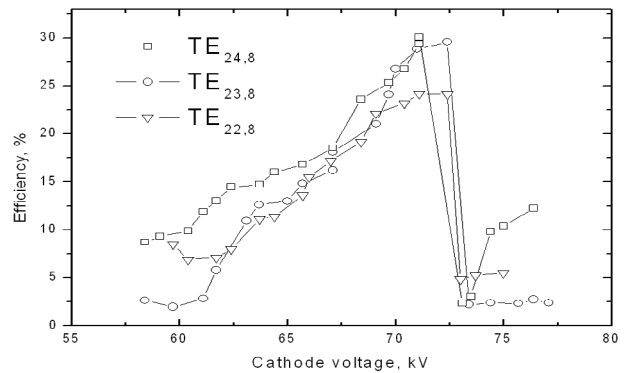
Efficiency for the modes $TE_{24,8}$, $TE_{23,8}$ and $TE_{22,8}$ at reduced cathode voltage.

of caustic radii may be performed by implementation of a triode type magnetron injection gun. This performance needs further investigations.

In summary, the next table shows the generated RF power and efficiencies for all measured modes in the frequency range from 130 to 146 GHz. In the last column the efficiency of modes corrected for the voltage depression effect calculated by ESRAY at working parameters of the electron beam is shown.

Mode	Frequency [GHz]]	U_{cath} [kV]	Power [kW]	Efficiency [%]	Efficiency Corrected [%]
$TE_{24,8}$	146.5	72.4	960	29.2	31.8
$TE_{23,8}$	143.5	88.4	1060	26.6	28.7
$TE_{23,8}$	143.5	72.4	960	29.5	32.3
$TE_{22,8}$	140.3	89	934	23.2	25
$TE_{22,8}$	140.3	71	773	24.2	26.5
$TE_{21,8}$	137	75	665	20.3	22.2
$TE_{22,7}$	130.9	89	1085	26.5	28.3
$TE_{22,7}$	130.9	73	820	25	26.7

Operating parameters, output power and efficiency of investigated cavity modes.

New quasi-optical mode converter

In 2010 measurements on the output beam pattern have been performed for several modes. The Gaussian mode content of the output beam is less then expected. It is assumed that ACI is the main reason for the poor beam quality.

A new type of quasi-optical mode converter for the step-tunable gyrotron was developed with the use of an advanced code for the launcher and mirrors synthesis. The launcher is optimized for nine modes, the Fundamental Gaussian Mode Content (FGMC) of the field calculated at the position of the output window (250 mm from gyrotron axis) for 9 Modes is as follows:

Mode	Frequency [GHz]	FGMC [%]
$TE_{17,6}$	104.9	96.4
$TE_{18,6}$	108.2	93.8
$TE_{19,6}$	111.5	90.3
$TE_{19,7}$	120.8	96.1
$TE_{20,7}$	124.1	97.0
$TE_{21,7}$	127.4	94.6
$TE_{21,8}$	136.7	91.0
$TE_{22,8}$	140.0	93.4
$TE_{23,8}$	143.3	94.3

Calculated Fundamental Gaussian Mode Content (FGMC) at the position of the output window for 9 modes.

The launcher will be used with quasi-elliptical mirror and new toroidal mirrors. The field propagation in the complete system consisting of launcher and mirrors is verified with the commercial code Surf3D for the $TE_{22,8}$ mode. The following figures show the field pattern and phase distribution, calculated at the position of Brewster window. The Gaussian fundamental mode content for $TE_{22,8}$ mode at the window is 93.5%.
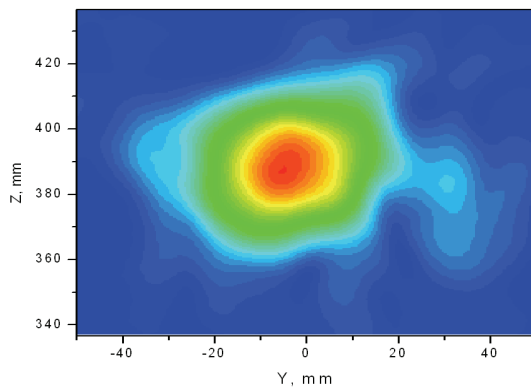
Amplitude distribution of the RF field in the window plane for $TE_{22,8}$ cavity mode.
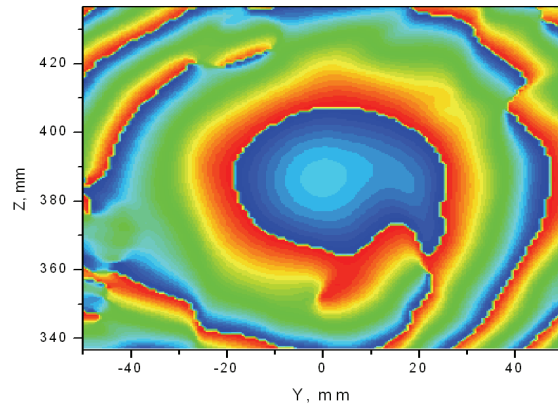
Phase distribution of the RF field in the window plane for the $TE_{22,8}$ cavity mode.

CVD-diamond Brewster window

Efficient operation for the large number of operating cavity modes at different frequencies is only possible by using a broadband synthetic diamond Brewster window fabricated by chemical vapor deposition (CVD). Due to the large Brewster angle of 67.2° deg, the diameter of the disk has also to be rather large in order to have sufficient aperture for the RF beam. One disk with a thickness of 1.7 mm and a diameter of 140 mm was developed by Element Six. This disk will be used for the elliptic shape of a gyrotron Brewster window with an effective aperture of 50 mm.

Because of the ellipticity, the stresses during the brazing procedure are different from circular disks. These stresses were calculated to be increased by a factor of 1.3. After successful preliminary brazing tests at TED with a quartz disk and a small diamond disk the brazing of the 140 mm diamond disk was ordered at TED.

Fast step-tunable magnet

A fast step tunable magnet which offers the possibility to change the magnetic field in the gyrotron cavity in the range 4.15 – 5.67 T has been ordered. With this magnet we will have the unique possibility to change the gyrotron frequency from 105 GHz to 143 GHz in steps of approximately 3 GHz within 0.5 s every 10 s. The maximum field will be 7.2 T which makes it suitable also for the investigation of 170 GHz gyrotrons for the ITER ECH&CD system.

In 2010 the complete magnet has been tested at the factory (Cryomagnetics, USA). It has been shown that the magnet fulfills important specifications, e.g. fast tunability, maximum magnetic field, Helium hold time and others. However, the required alignment of the mechanical and magnetic axis could not be realized. There is a large deviation of the axes of the

main magnet and the fast step tunable magnet, possible improvements and solutions are currently under discussion with the manufacturer.

ITER ECH Launcher Handling and Test Facility LHT

The ECRH Upper Launcher of ITER consists of different and partially complex components with individual design requirements (see figure). Therefore a Launcher Handling and Test facility (LHT) has been built up at KIT/IHM which provides an infrastructure for testing of different prototypes. It allows an experimental validation and a better knowledge of the significance of results obtained by design tools like numerical simulations. Strategies for acceptance testing can be developed and will be used as an input to procurement, manufacturing, testing and delivery to ITER. The LHT (next figure) provides a full scale experimental site with a water loop providing ITER blanket water parameters for normal operation (temperature from 100°C-150°C and a pressure up to 3 MPa), and bake out conditions (temperatures up to 240 °C and a pressure up to 4.4 MPa). Further components of the LHT are a rack to fix the prototypes and a control and Data Acquisition unit (CODAC). Additionally it offers a remote handling area to enable experimental testing of remote handling procedures. The construction of the prototype rack can be easily adapted to integrate new prototypes. A Blanket Shielding Module (BSM) flange prototype was manufactured which serves as mechanical interface to the test objects, e.g. to the BSM corner prototype.
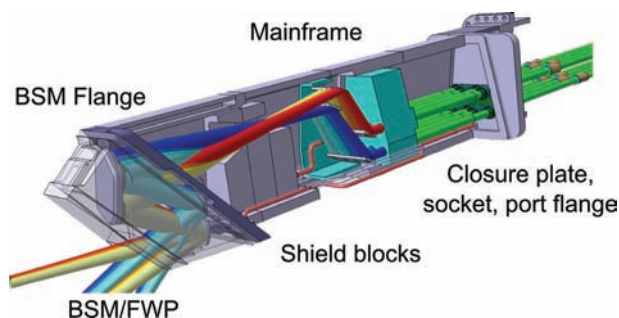
Sketch of the ITER ECRH upper launchers

LHT test facility with BSM corner prototype mock-up

The LHT facility will be fully developed and expanded to a testing facility for ITER launcher component acceptance tests. The planning of this work already will be started in 2011. New prototypes for the double wall structure of the launcher with different manufacturing routes were finished and can be tested. The technical supervision of the LHT facility is in the responsibility of IHM.

Involved Staff:

K. Baumann, Dr. B. Bazylev, DI M. Beringer, Dr. G. Dammertz, DI J. Flamm (IHE), **Dr. G. Gantenbein**, Dr. H. Hunger, Dr. Yu. Igitkhanov, **Dr. S. Illy**, Dr. J. Jin, **Dr. S. Kern**, **Dr. I. Landman**, R. Lang, DI W. Leonhardt, DI M. Losert, D. Mellein, S. Miksch, Dr. I. Pagonakis, A. Papenfuss, Dr. S. Peschanyi, Dr. B. Piosczyk, **Dr. T. Rzesnicki**, DI A. Schlaich (IHE), Dr. A. Samartsev, Dr. T. Scherer (IAM-AWP), DI M. Schmid, Dr. R. Schneider, W. Spiess, Dr. D. Strauss (IAM-AWP), J. Szczesny, Prof. M. Thumm, DI J. Weggen

External staff member „Sonderprojekt Mikrowellenheizung (PMW) für Wendelstein 7-X":

IPF Stuttgart:
M. Bohner, Dr. P. Brand, H. Dagostar, E. Filipovic, D. Hermann, H. Höhnle, **Dr. W. Kasparek**, Dr. Helga Kumric, Dr. C. Lechte, R. Munk, F. Müller, Dr. B. Plaum, S. Prets, M. Saliba, P. Salzmann, H. Schlüter

IPP Greifswald:
B. Berndt, Dr. H. Braune, **Dr. V. Erckmann**, F. Hollmann, L. Jonitz, Dr. H.-P. Laqua, Dr. G. Michel, F. Noke, F. Purps, T. Schulz, P. Uhren

IPP Garching:
DI M. Weißgerber

Program: NANOMIKRO

High temperature microwave processing

The investigations on in-situ Raman spectroscopy in collaboration with IFG were continued. The motivation for these studies is an experimental proof of selective microwave heating in composite materials. The basis for this is an adequate calibration that allows the conversion of Raman peak positions into a temperature. To improve accuracy in calibration a Linkam TS1500 hot stage has been acquired. This is a special device adapted to the Senterra Raman spectrometer that can go up to 1500°C by resistive heating For calibration measurements corresponding ceramic powder samples were filled into a tiny alumina crucible and placed into the Linkam hot stage. This was used to heat the powder samples to different temperature levels. Then Raman spectra were collected at constant temperatures and different levels of laser power in order to investigate if the laser power itself has an influence to the Raman spectra due to direct laser heating.

As a result, no significant difference between the Raman temperatures estimated for alumina and zirconia is obvious at temperature less than 500 °C. Nevertheless, although the sensitivity decreases, there above in statistical average a more pronounced heating of zirconia is indicated for samples including 10wt.% and 15wt.% of zirconia, respectively (see figure on next page).
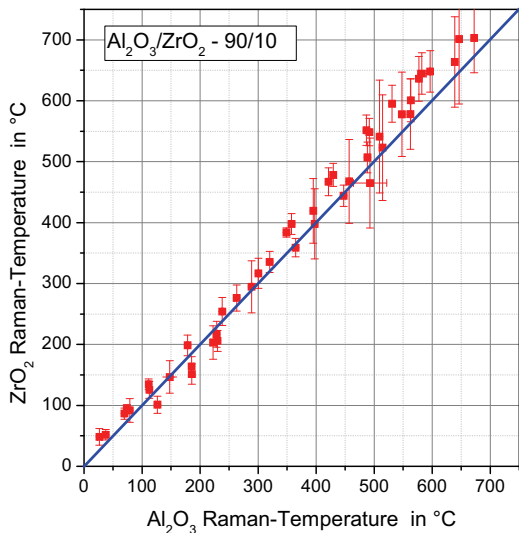
Comparison of ZrO_2- and Al_2O_3 temperatures estimated from Raman spectra.

In collaboration with the Federal University of Sao Carlos, Brazil detailed investigations on mm-wave sintering of Al_2O_3-SiC nanocomposites were performed. Systematic variation of process parameters and measurement in a mm-wave heated dilatometer were used to optimize the sintering process with respect to the achievable density, grain size and mechanical properties. As a result the sintering activity was significantly decreasing with increasing SiC content and with decreasing SiC particle size.

A project on microwave processing of metal powders, funded by the German Science Foundation DFG, has been started in close collaboration with the Indian Institute of Technology, Department of Electrical Engineering, Kanpur.

Involved Staff:

Dr. M. Ahmed (IHE), H. Brüsemeister, **Dr. G. Link**, Simone Miksch, C. Ott, K. Paulus, K.-T. Schäfer, Prof. M. Thumm

Programm NUCLEAR

Safety Research for Nuclear Reactors

Corrosion and wear protection for new reactor technologies

To guarantee security of future electricity supplies new types of nuclear reactors are investigated in the frame of GEN IV. The development of technologies required for the safety of fast heavy metal cooled reactors like the Lead Fast Reactor (LFR) is the core area of the work performed at KIT. Especially the development of advanced materials e.g. ODS steels and the investigation and improvements of their compatibility with the proposed coolants are in the focus of this work.

Aim of the institute's contribution is the development of corrosion barriers to improve the compatibility of new structural materials with liquid Pb or PbBi. Pulsed large area electron beams (GESA - process) are used to modify surfaces such that they satisfy the demands of their targeted environment. Corrosion test facilities for specimen exposure under relevant conditions and for combined loads like fretting or erosion together with corrosion are developed, built and used at the IHM. The conditioning and control of the required oxygen level in the liquid metal is an additional task of the work.

The entire activity is integrated in European and international projects and cooperation, e.g. ELSY, LEADER, GETMAT, ESFR.

In the frame of ELSY (lead fast reactor for transmutation) the development of effective corrosion barriers for fuel claddings using the GESA technology is investigated. In addition several candidate materials for heavy liquid metal pumps are tested with respect to their corrosion and erosion stability. The ELSY project was finished in 2010 and a follow-up project for the development of a Pb cooled fast demonstration reactor LEADER was started in the FP7 frame. The main tasks there are the transfer of the GESA FeCrAl process developed for fuel claddings to heat exchanger geometry, continuing the investigation of candidate pump materials and to develop oxygen control and purification strategies for a real reactor. In the ESFR project (development of a fast Na cooled European reactor) ideas to engineer Co-free wear resistant coatings were started and will be continued. In the GETMAT project four different tasks have to be fulfilled: corrosion stability of ODS, T91 and mixed welds in Pb; procurement of ODS 12 steel bought in Japan, improvement of GESA FeCrAlY process and fretting investigation of fuel clad materials in Pb environment.

The most important results obtained in 2010 are briefly presented here:

From previous research it is known that specimens of GESA modified FeCrAlY coated T91 steel having an Al content < 4 wt% form multilayered oxide scales like original T91. On the other hand, specimens with a higher Al content form thin Al_2O_3 scales that protect the steel against corrosion attack. The results of previous investigations indicate that the Al/Cr ratio seems to play an important role for the formation of this protective oxide scales. Most of the so far manufactured FeCrAlY specimens showed AlY oxides or Al oxide particles at the surface after GESA treatment. The role of Y in the formation of such oxides was under investigation too.

To determine the best suited Al/Cr ratio for Al-oxide formation and to evaluate the influence of Y specimens with different composition were prepared in the reporting period. Thin (up to 80 μm thick) FeCrAlY layers with different composition (Fe15Cr11.5Al0.5Y, Fe9Cr12Al0.5Y, Fe15Cr11.5Al) were deposed using Low Pressure Plasma Spraying on T91 steel specimens by Sulzer Metco. Remelting such specimens with GESA leads to incomplete melting of the layer and subsequent spallation (next figure). Simple mechanical grinding always generated gradients in the layer thickness. Therefore, a special grinding holder was developed that allows thinning the as sprayed layers homogeneously. A layer thickness of about 25μm was found to be most suitable for further processing using the GESA facility. Specimens of all three compositions were prepared first by thinning the FeCrAlY layer down to about 25μm and then followed by treatment using the GESA.
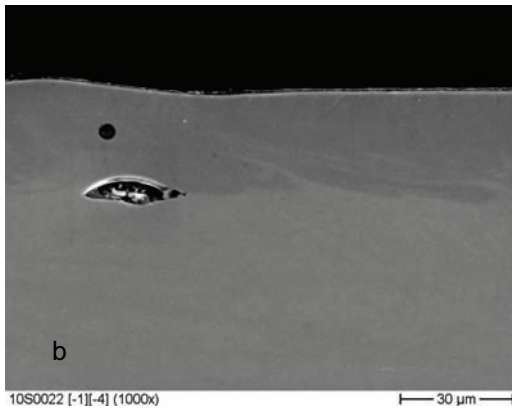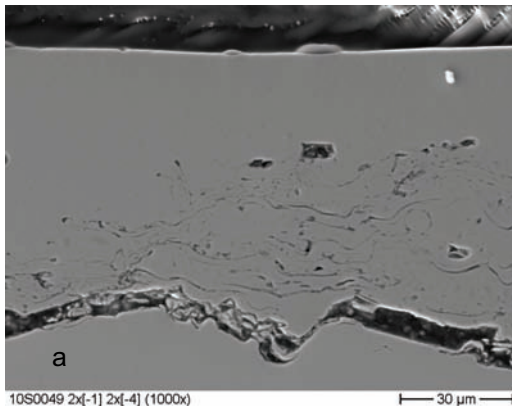
Remelted FeCrAlY-layer without (a) and with (b) prior grinding.

Such successfully remelted specimens were exposed in the COSTA facility in Pb with 10^{-6} and 10^{-8} wt% oxygen at 400, 450, 500 and 550 °C for about 1000h. Aim of the exposure was to identify the required Al content for the formation of Al-oxide scales in Pb alloy.

Specimens coated with FeCrAlY containing 15 wt% Cr, 11 wt% Al and 0.5 wt% Y show over the entire temperature range, even at 400°C, the formation of thin protective Al-oxide scales (next figure). Reducing the Cr content down to 9 wt% or omitting the Y resulted at some conditions in formation of multilayered oxide scales like on T91 original steel. This is depicted in the lower part of the figure where the specimens at 400 and 450°C show dark areas indicating the formation of Fe containing oxides. With reduced Cr content especially at lower temperatures the formation of Al-oxides cannot be assured. Using the Y-free coating the expected reduction in number or size of AlY oxides present at the surface after the GESA process did not occur. These oxides are mainly due to the oxidation during the plasma spray process. Therefore, spray processes resulting in significant smaller oxidation will be investigated in future.

Also in the frame of GETMAT a PhD work was started to perform fretting tests in liquid Pb. The test stand was developed and built (next figure). With first experiments in air literature data could be verified, which gives confidence that the facility itself provides reliable and also reproducible data. The dependence of the removed volume and the maximum groove depth are determined as a function of the number of cycles (following figure on next page). These data in air that were also obtained at increased temperature will be used to determine the influence of the Pb on the fretting corrosion.
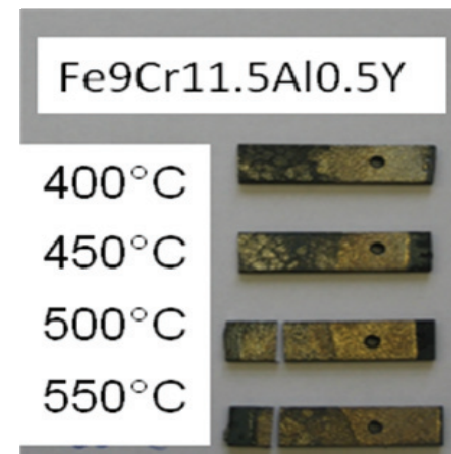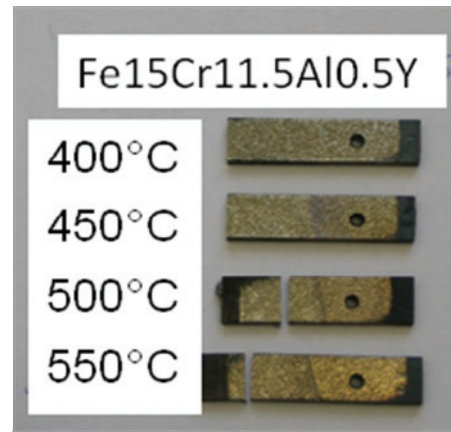
Photographs of specimens after exposure to Pb with 10^{-6} wt% at different temperatures: (15Cr) formation of thin scales at all temperatures (upper), (9 Cr) formation of thicker scales especially at lower temperatures (lower).

First experiments in Pb showed the influence of the coolant and the main parameters like load and amplitude. The formation and build-up of debris consisting of oxidized and still metallic particles on a T91 tube tested in the fretting facility in liquid Pb is one of the first results obtained (second figure on next page). A detailed parameter study also with different material combinations is now started to evaluate all related phenomena in detail.

Photo of fretting test-facility for tests in liquid lead alloy.
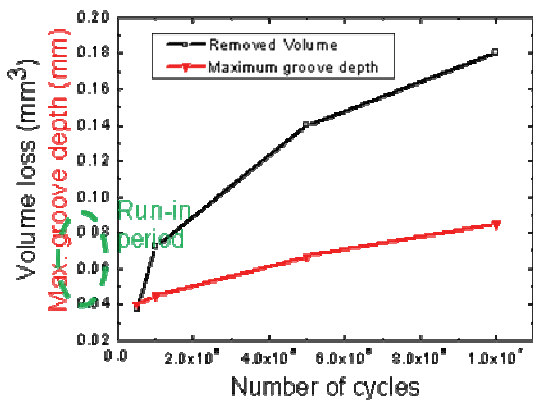
Loss of material and maximum groove depth as function of number of cycles.
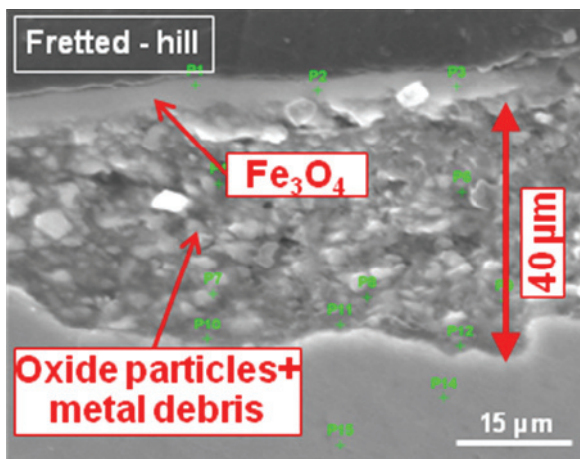
Scanning electron micrograph of cross- section at place of fretting wear in Pb.

The qualification of welds regarding their compatibility with liquid Pb is another task within the GETMAT project. Welds of T91 and ODS steels obtained using EB- and TIG - welding were exposed to lead with 10^{-6} and 10^{-8}wt% oxygen at 550°C for 2000h. This exposure was finished just at the end of 2010 and detailed results of post investigations are expected in 2011. At a first glance, the welded zones behave like the non-welded areas. Additional welds produced by different welding techniques and with different materials and material combinations will be tested in 2011.

The work for ELSY was finished with a final report and the LEADER project started. A first erosion test of candidate materials was performed with similar flow conditions like the ones used for the MEXT project where significant erosion was observed. This time the test temperature was reduced to 450°C compared to 650°C used in the MEXT (JAEA) test. Preliminary investigation of the specimens does not show severe wear of all tested specimens. Also in LEADER evaluation of heat conductivity of oxide layers formed in-situ is targeted. The thermal diffusivity of T91, FeCrAl bulk and a GESA surface modified FeCrAlY coated T91 were measured using laser flash calorimetry. Specimens of same kind are exposed to liquid Pb and their diffusivity will be measured after exposure to evaluate the influence of the formed oxide layers.

To establish an oxide map for FeCrAl alloys, bulk FeCrAl alloys with 9 different compositions were exposed to liquid Pb and PbBi at different temperatures. Detailed investigation of the exposed specimens will start in 2011.

The work for the ESFR (European Sodium cooled Fast Reactor) project mainly concerns the assessment of materials and surface treatment methods discussed and selected by the consortium. The development of Co-free wear resistant coatings is in the focus of this work. A commercially available alloy T700 (Ni base, Mo rich) was deposited by Sulzer Mecto and post treated using GESA. Fusing the coating to the 316 steel substrate was achieved in these first trials, but cracks are observed in the surface. Additional experiments including pre-heating to reduce the high thermal gradients will be performed.

One measure to obtain longer pulses with the GESA IV facility (so far prevented due to short circuiting as discussed last year) was applying a pre –pulse with reduced electron energy to clean the target surface prior to the "real" modification pulse. Therefore the Marx generator was adapted and changed. Such pre-pulses indeed reduce the number of early short circuits drastically. However, unfortunately short circuits in a later stage could not be prevented. Such short circuits might be overcome by optimizing the geometry and the dimension of the cathode. The ignition behavior of the cathode was investigated in air (figure) and clearly showed at ignition voltage of 15keV a very homogeneous behaviour.
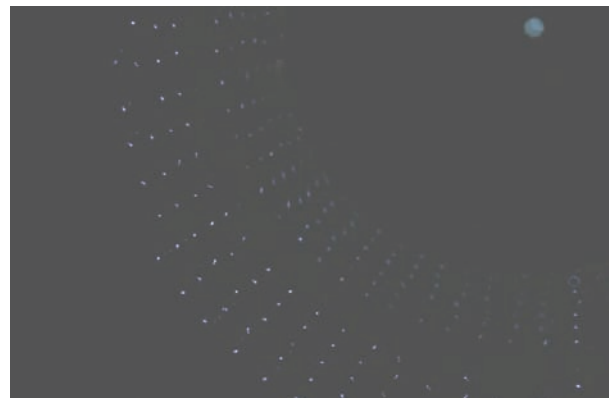
Ignition of GESA IV cathode in air at 15keV ignition voltage – all carbon fibres are ignited.

Reduction of Radiotoxicity

Corrosion protection in heavy liquid metal cooled sub-critical systems

Long-living high-level radioactive waste from existing nuclear power reactors should be transmuted in short-living radio nuclides using fast neutrons provided by a spallation target in an accelerator driven subcritical system or by a fast nuclear reactor. The objective is to reduce the final disposal time of high-level radioactive waste (plutonium, minor actinides) from some 10^{6} years down to about 1000 years. Liquid lead (Pb) and lead-bismuth (PbBi) are foreseen as spallation-target and coolant of such devices.

The aim of the IHM contribution in this field is the development of a suitable corrosion protection especially for parts under high loads like fuel claddings or pump materials in contact with liquid Pb or PbBi. Pulsed large area electron beams (GESA) are used to modify the surface of steels such that they fulfill the requirements of their surrounding environment. Corrosion test stands for exposure of specimens under relevant conditions are developed and operated. Test facilities for combined loads like erosion and corrosions were developed, built and operated. Conditioning the liquid lead with regard to its oxygen concentration are an additional focus of the work.

All tasks are embedded in European and international projects and cooperation e.g. DEMETRA, MEXT (JAEA), ISTC, ADRIANA.

The most relevant results obtained in the reporting period are briefly presented:

The DEMETRA project was finished in 2010 with a workshop where the most relevant results were presented. The IHM summarized the work performed within DEMETRA related to long term corrosion, corrosion modeling and corrosion barrier development. A first rough estimation concerning the required amount of Al to form Al_2O_3 at different temperatures could be given. While the Al content must be higher than ~6.2 wt% at 476°C, the required concentration decreases with increasing temperature, i.e. Al > ~5.6 wt% at 490°C and Al > ~5.2 wt% at 550°C.

Last year first preliminary evaluation of the creep behaviour of GESA treated T91 in liquid PbBi (LBE) and the determination of the lowest tolerable creep stress for T91 in PbBi were presented. More intensive investigations on these samples in 2010 lead to following results. At 550 °C the tests of original T91 in LBE at lower stress levels from 120 MPa down to 60 MPa showed a somehow unclear situation. The strain and 2nd strain rates are all at a similar level and remarkably lower than that of the 140 MPa experiment in LBE (next figure). However, they are all slightly higher than the strain and strain rates of the experiments performed at 140 MPa in air. Especially both tests at the lowest stress levels showed the highest strain and strain rate.

T91 creep 550°C 10-6 120MPa (1000x)   ⊢ 30 µm ⊣
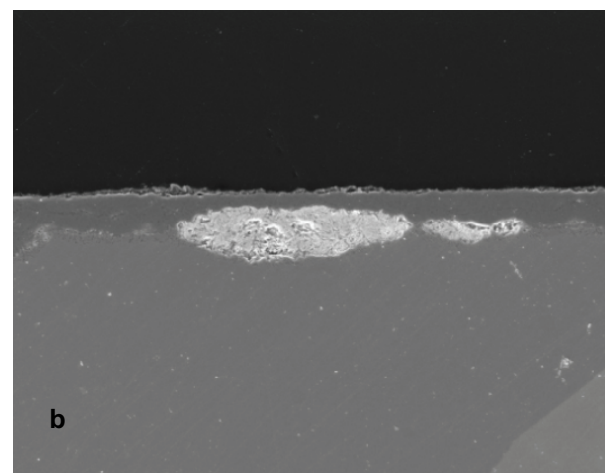
T91 creep 550°C 10-6 60MPa (550x)   ⊢ 50 µm ⊣

SEM image of cross section of T91 after creep test in LBE at a) 120 MPa with intact oxide scale and b) 60 MPa with magnetite layer penetrated by LBE.

The metallographic examination did not show cracking of the oxide scale, but penetration of LBE underneath the magnetite layer (figure above). Such penetration was also reported in corrosion tests of T91 not performed under stress.
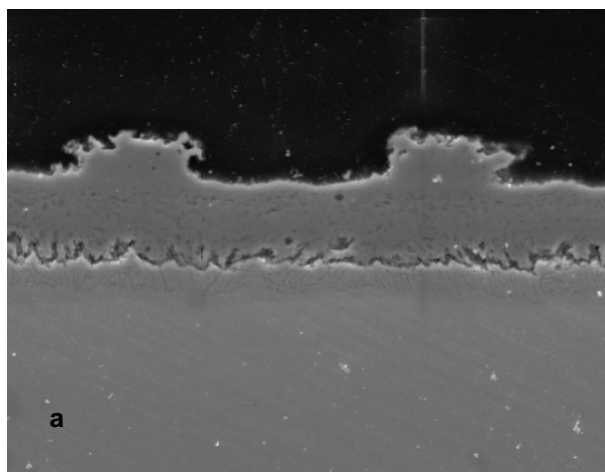
Naturally grown oxide scales on T91, magnetite and spinel, can crack already without additional external loading and are of course even more susceptible to cracking with external load. This leads to the conclusion that at temperatures above 550 °C improved corrosion barriers are required. Such a barrier produced by the Al surface alloying using the GESA process was tested in LBE and air. The tests in air show an increase in creep to rupture strength of the surface alloyed material, which might be a result of the increased hardness of the outer layer. The alloyed surface forms an alumina scale that is very thin (< 1µm) and seems to be more ductile. The strain tolerance of this coating was measured to be about 8 %. The tests in LBE clearly showed the improved behaviour of this surface modified T91. However, at 200 MPa up to a strain of about 3.5 % no difference compared to the original T91 tested in LBE was observed. The strain rates of the tests performed at lower stresses were only slightly higher compared to the strain rates obtained in tests with T91 in air at same stress and temperature levels (next figure).

Strain and strain rate versus time for low stress level test of original T91 in LBE at 550 °C.

exposure experiments. In stagnant PbBi Y and Ce have the most beneficial effect on corrosion resistance. Hf and Zr did only at some temperature and oxygen conditions improve the corrosion stability. Both elements did not deteriorate the corrosion resistance of the ODS under any condition. However, due to the influence of the minor elements on the creep strength, which was evaluated by our JAEA partners, Hf and Zr were selected as the most suitable minor alloying elements. Another clear conclusion for future work on Al alloyed ODS steels was to consider the influence of grain size on corrosion behavior of ODS steels. At high temperatures and under flowing conditions especially in turbulent flow conditions severe erosion/corrosion was observed. The exact reason for this phenomena and possible mitigation processes are not understood and defined.

Comparison of original T91 in air and LBE and surface alloyed T91 in LBE a) of secondary creep rates versus applied stress at 550 °C b) stress versus rupture times at 550 °C.

Considering the improved creep strength of surface alloyed T91 in air the results obtained in LBE at 550 °C were expected to be even better. Again the metallographic investigation of the tested specimens gave the answer. Due to imperfections in the surface coating and alloying process the Al content was not homogeneously high enough to guarantee the formation of a protective alumina scale. Parts of the specimens, up to 40 %, exhibit "normal" oxidation with the formation of Fe-Cr-Al spinel and magnetite. The cross section clearly showed the cracking of the magnetite layer and the penetration of the LBE. Regions with thin alumina scale do not crack at the lower strain regions and only in the necking region with the highest strain cracks could be observed. However, such cracks never were penetrated or filled with LBE. The Al-rich surface alloyed layer obtained after pulsed electron beam treatment showed strain and 2nd creep rates and creep to rupture times at 550 °C in LBE comparable to that of original T91 in air. The differences are mainly attributed to the non perfect surface alloyed specimens.

The MEXT project, a bilateral project with JAEA to qualify Al containing ODS steels for use in PbBi, was finished. The influence of minor alloying elements like Y, Ce, Zr und Hf on the compatibility with PbBi was evaluated on the basis of corrosion

SEM of cross section of Kanthal alloy after exposure and elemental linescan showing the formation of an Al-oxide scale.

To gain a deeper understanding of the corrosion behaviour of Al containing materials, four different commercially available alloys from Kanthal Company were exposed to Pb and PbBi at temperatures between 500 and 750 °C for 1000h. The exposed Kanthal alloys formed at most conditions thin Al – oxide scales that protected the steel (right figure on page 30).

At 500°C and 10^{-6} wt% oxygen the Kanthal alloy having the lowest Al and Cr content formed a multilayered oxide scale. An Al content of 4.3 wt% combined with 16wt% Cr is obviously not sufficient to ensure stable formation of Al-oxide layers at this condition. The Kanthal APM with 22 wt% Cr and ~5wt% Al, which is very similar to the alloys showing Al-oxide formation, formed at least partially a multilayered oxide scale. This might be a result of the larger grain size of this material. At 750 °C in PbBi with 10^{-8} wt% oxygen only the Kanthal alloy with the lowest Al and Cr concentration but with largest grains did not suffer from dissolution attack. A sound explanation for this unexpected behavior is not yet found. This again clearly shows the necessity to take a closer look on the additional influence of the microstructure on corrosion behaviour.

Optimisation of the GESA process

The remelting of metallic specimens using large area pulsed electron beams (GESA) results in a more or less pronounced waviness of the surface, which can have a negative impact on specific applications. To control this waviness or roughness basic understanding of the involved physical processes are required. The work performed in the reporting period in this area contained space and time resolved diagnostics of the processes taking place on a µs time scale. Streak camera photography and investigations of surface topography after solidification using high resolution confocal profilometry have been applied.

To quantify the phenomena of roughness formation statistically surface profiles are analyzed regarding their roughness and dominant undulation. A comparison of specimens remelted with different parameters shows that the structures grow in height and laterally the longer and more intensive the electron beam was. However, this rule is not valid for treatment with multiple pulses. In addition no correlation was found between different materials.

First the beam profile was determined from streak-exposures of the X-ray signal. In a following step the reflectivity of the target surface (stainless steel or aluminum) during the GESA treatment was measured (next figure). Evaluating these data the place and the onset of target movements could be determined. Starting time and duration of life of a melt on each recorded place were derived and compared with respective simulations.

The self glow of the vapour cloud that forms right ahead of the target (figure a) was recorded in addition. This gas cloud develops due to the evaporation of target material and is ionized by the electron beam at least partially. The ignition behaviour of this target plasma cloud and its plasma temperature and density are under investigation at time. The obtained results should allow predictions and conclusions about the interaction between plasma and target.

Involved staff:

DP. W. An, Robin Beckers (BA-Student), H. Brüsemeister, M. Eing, Mattia DelGiacco, Dr. Renate Fetzer, Dr. Annette Heinzel, Dr. A. Jianu, Prof. Y. Krasik (visiting scientist), DI (FH) F. Lang, **Dr. G. Müller**, Dr. H. Muscher, Dr. G. Schumacher (visiting scientist), A. Sivkovich, P. Spieler, Prof. M. Thumm, **Dr. A. Weisenburger**, DI (FH) F. Zimmermann
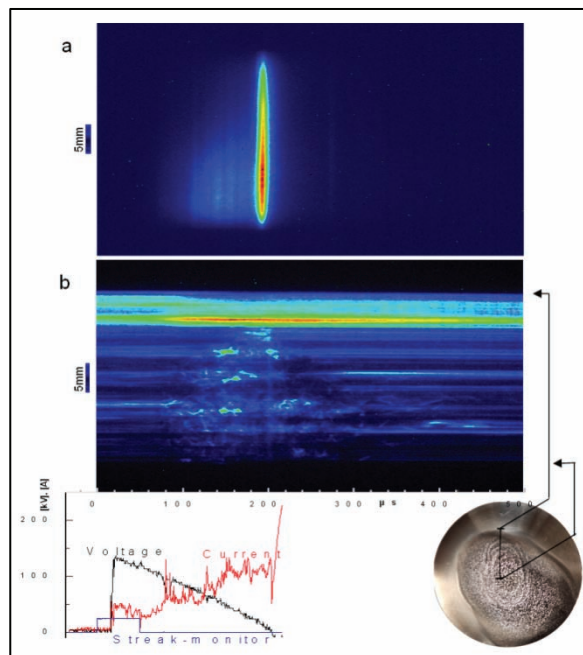
Stainless steel during pulsed electron beam treatment a) emitted light from target plasma, b) target surface reflected laser-light.

Program ENERGY:

Renewable Energies

Conditioning of Biomass by Pulsed Power Techniques

After completion of the photobioreactor for algae biomass production, work focussed on cultivation and monitoring of algae biomass. Contrary to expectations, the lipid droplets produced by microalgae could not be released into the extracellular aqueous medium by pulsed electric field treatment, whereas first experimental results indicate that solvent extraction can be improved by a factor of 2. Various diagnostic methods for cell ingredient monitoring were tested for applicability on algae biomass. The processing time of the diagnostics was found to be a crucial parameter, since algae digest or alter their cell content when being removed from controlled cultivation conditions. First experiments on the extraction of proteins or dissolved carbon compounds by pulsed electric field (PEF) treatment indicate an increase of a factor of 2 – 4.

Pulsed electric field (PEF) assisted extraction of lipids from microalgae (GC-MS-diagnostics)

Up to now, the extraction of lipids from microalgae is predominantly accomplished by organic solvent admixture. Subject of this work was, to elucidate processing benefits contributed by PEF-treatment.

The organisms used in the extraction experiments were Auxenochlorella protothecoides (a.p.), a green algae with an adequate lipid inventory, when properly cultivated. The applied pulse parameters for algae treatment were: Pulse length t_{Imp}=10-1000ns, specific treatment energy W=10-400kJ/kg and electric field strength E=40-70kV/cm. In the past year, the result of PEF assisted lipid extraction was qualitatively examined by means of Nile Red staining and fluorescence imaging (c.v. JB 2009). For the acquisition of quantitative results, in 2010, the processed samples were analysed by gas chromatography and mass spectrometry (GC-MS). The investigation was conducted in cooperation with the Institute of Functional Interfaces (IFG). The
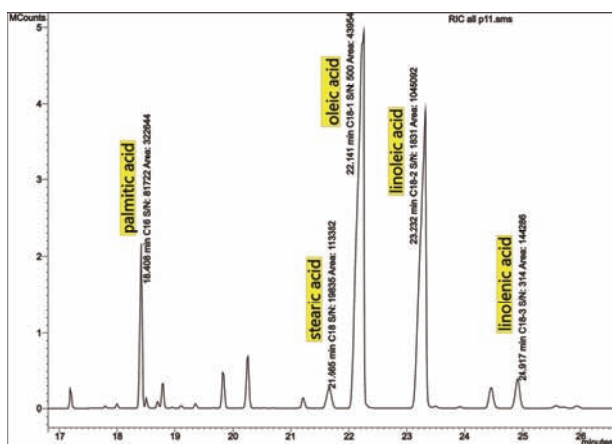
Gaschromatogram of the green algae Auxenochlorella protothecoides (A.p.).

evaluation of the lipid extraction was performed by diagnosis of the free long chain fatty acids (LCFAs) in the examined samples (figure above). Palmitic acid, stearic acid, oleic acid, linoleic acid and linolenic acid were chosen as reference, since they represent the main part of the lipid inventory of the examined microalgae. For each experiment the algae samples were separated by centrifugation into algae pellet and supernatant, consisting of culture medium and potentially extracted lipids. The LCFA- recovery occurred in a two step extraction. In the first step, the aqueous phase was removed by methanol/chloroform (50/50) and in a second step, LCFAs were extracted with tert-buthylmethylether. Alternatively, acetic ether and 2-propanol were tested for aqueous phase removal, but showed no advantage compared to methanol/chloroform.

In numerous experiments with PEF, no LCFAs could be found in the supernatant of the centrifuged algae suspension. Hence, the following statements concerning the lipid extraction refer solely to the algae pellet. Initially, an increase of the lipid recovery with E=40kV/cm and t_{Imp}=400ns, according to an increase of the applied energy could be observed. This appeared particularly in the fractions of the dominant LCFAs: oleic acid, linoleic acid and palmitic acid. In later PEF- experiments with increased pulse length (t_{Imp}=1000ns), this tendency was not reproducible. The search for reasons for these differing results delivered the insights, that a quick performance of the PEF- experiments and even more important, the instantaneous performance of the following GC-MS- analysis play a decisive role. Further investigation on this subject showed, that the composition of algae samples is not stable. Untreated algae pellets, stored at 4-8°C, digest their lipid inventory up to 60%, within 24h. In some samples linolenic acid and stearic acid were completely decomposed. Extracted LCFAs stored in Methanol at ambient temperature for 24h, were more stable, but showed a reduction of the lipid inventory by 20%, too. By keeping in mind, that each sample analyses takes 45 minutes, it is obvious, that the analysis of samples from large experimental campaigns and the associated results, need to be considered critically. Due to the different temporal decomposing behaviour of LCFAs arbitrary fluctuations of the LCFA composition are supposable. Hence, the application of a time depending correction is impossible.

Fluorescence diagnostics for microalgae lipid status monitoring

In order to satisfy the worldwide demand for oil and fuel in future, alternative oil-resources gain more and more importance. Algae-based bio-fuel could be a promising alternative fuel-source. To guarantee a rich harvest and an efficient extraction of triglycerides from the microalgae cells, a fast and simple lipid status detection method is required.

Nile red is a fluorescent dye which is used to localize and to quantify lipids, particularly neutral intracellular lipid droplets. We investigated the suitability of nile red for rapid quantitative detection of neutral lipids in algae, cultured in a photo-bioreactor, without preliminary algae lyophilization. The *Auxenochlorella protothecoides* algae, which accumulates triglycerides as an energy reservoir when starving for nitrogen, was selected for the evaluation. Algal biomass was collected during the growing phase and was immediately used for fluorescence diagnostics. To ensure that the difference in the fluorescence signal is caused by the oil droplets only, the cell suspension samples were diluted to an equal optical density, which was determined by photometric measurement.

The quantitative relation between relative fluorescence intensity and oil content was determined by using milk suspension with different oil concentration as standard. The effect of nile red concentration on lipid quantification was tested by different final concentrations in the range between 0.01 and 0.50 % oil. At least 6 µg/ml nile red is required to cover the specified oil concentration. It was demonstrated that living cells from medium have no negative effect on the fluorescence. Using this fluorescence method it was possible to identify the point of oil-production and to measure the accumulation of oil within a growing microalgae culture.
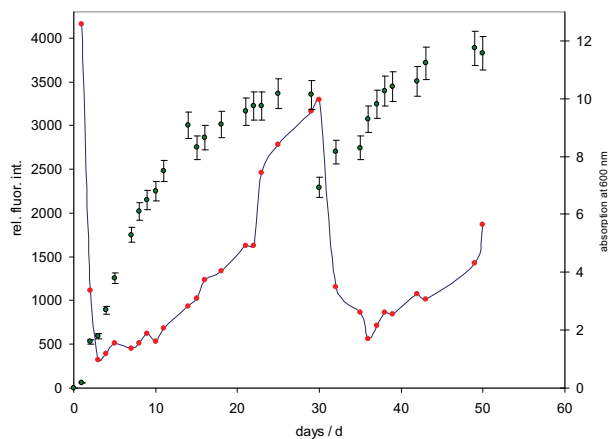
Relative fluorescence intensity of nile red stained microalgae culture during growth in a photo bioreactor (solid curve) indicating the lipid content. Growth curve of the microalgae culture measured by absorption right scale (dots, SE bars). The algae were partially harvested after 30 days.

The figure above compares cell density and relative lipid content of the algae biomass. During the first 30 days of cultivation the lipid content slowly increases at the beginning of the cultivation and increases faster, when the cell density approaches the stationary phase. At day 30 half of the algae suspension of the photobioreactor was harvested and replaced by medium. Wheras cell density recovers fast, lipid content significantly rises before day 50. This demonstrates that cell density and lipid content are not related directly. An easy-to-use lipid diagnostic is essential for algal lipid production.

Fast diagnostics for cell ingredient extraction from microalgae

The permeabilization of the plasma membrane of microalgae by pulsed electric field (PEF) treatment is expected to improve the extraction of cellular substances. A PEF treatment usually increases the concentration of various solutes in the extra-cellular medium. The main classes of extractable substances are 1) lipids, 2) peptides and proteins and 3) sugars and poly-saccharides.

Regarding the diverse chemical nature of the substances, the monitoring of these three classes of bio-products subsequent to pulse application requires three different approaches. Furthermore, the methods have to be rapid, simple, of reasonable precision and easy to integrate into the daily laboratory routine.

1) Lipids

First introduced in 1937, the Sulfo-Phospho-Vanillin-Reaction has been improved several times, resulting in a standard routine for estimating of total lipid content in human cerebrospinal fluid. The chemical basis of this colorimetric reaction is the formation of a charged coloured complex of vanillin and fatty acids in strong acidic milieu that absorbs maximally at 525 nm. The increase of absorbance at 525 nm is proportional to the amount of the formed complex, and thus to the amount of lipid present in the extract. For evaluation, the measured absorbance of the sample is compared to a calibration curve, obtained from the analysis of a suitable lipid standard. This method has been adapted to extracted algal lipids. Olive oil was used as standard (next figure). The results show a good accuracy in the range of 0.1 to 20 g lipids per litre. The extraction of algal lipids was accomplished by admixing of ethanol at different concentrations to freeze-dried *Auxenochlorella protothecoides* grown in the photobioreactor.

Sulfo-Phospho-Vanillin-Reaction
Calibration curve

$y = 0{,}253x + 0{,}0016$
$R^2 = 0{,}9995$
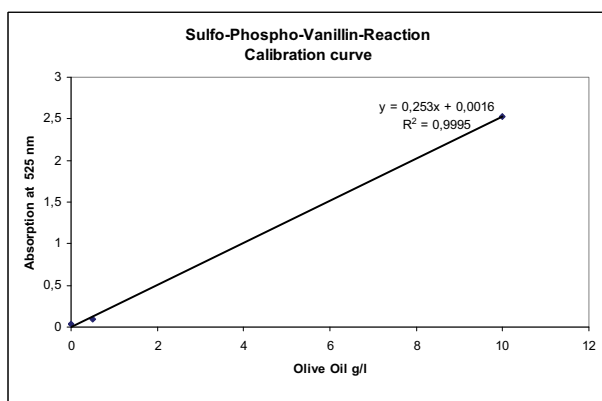
Calibration curve obtained with the Sulfo-Phospho-Vanillin-Reaction using olive oil as standard.

Our experiments reveal, that the total lipid content of dry algae biomass is in the range of 30% of dry mass. An extraction with 100% ethanol led to an efficiency of about 10% of the totally stored lipids. First experiments with pulsed electric field treated algae (179 J/kg specific energy input) prior to freeze-drying yielded in a 2 to 3 fold increase in lipid extraction efficiency, when using ethanol as solvent. A further investigation of the improving effect of PEF treatment in combination with solvent-mediated lipid extraction will be subject of future work.

2) Proteins

The quantitative detection of proteins and peptides in the super-natant of algae cultures is done via photometric analysis following a method commonly known as "Bradford-Test". The principle of the Bradford assay is based on an absorbance shift of the dye Coomassie Brilliant Blue G-250. For acidic medium conditions the red derivate of the dye is converted into the blue derivate, which binds to the targeted protein. The increase of absorbance at 595 nm is proportional to the amount of bound dye, and thus to the amount (concentration) of protein being

present in the sample. This method exhibits reasonable precision for protein concentrations in the range between 1 µg/ml and 200 µg/ml. BSA (Bovine serum albumin) is used as standard for calibration. As already obtained from our experiments on lipid extraction, we observe an increase in protein concentration in algae supernatant after treatment with pulsed electric fields (197 J/kg specific energy) of a factor of 2 to 3.

3) Polysaccharides and sugars

The colorimetric assays for lipid and protein diagnostic are established in laboratory routine and perform. For sugar and polysaccharide diagnostics an adequate photometric method would be desirable. As a possible candidate, the reaction of sugar with the organic reagent anthrone will be analysed for adaptability to quantify algal saccharid extraction.

Stimulation of growth and fruiting body yield of fungi by ns pulsed electric field (nsPEF) exposure

The stimulating effect of ultrashort electric fields on the mycelium growth of the basidiomycete *Hypsizygus ulmaris* has been shown in former experiments. To verify these results, the statistics of the experiments have been increased. Spores of the basidiomycete *Hypsizygus ulmaris* (elm oyster mushroom) were exposed to pulsed electric fields of 5 - 50 kV/cm. The rectangular pulses were generated by a transmission line pulse generator and delivered to a standard electroporation cuvette (electrode distance: 4 mm) containing the immersed spores. The pulse duration (25 ns and 100 ns) and the number of pulses (10-100) were adapted for a certain specific energy delivery to the load.

Typical specific energies used for the treatments were in the range between 100 mJ/ml and 10000 mJ/ml. After pulsed electric field treatment, 100 µl of the treated spore suspension was used to inoculate an agar plate and incubate it for 12 days at 25°C in the dark. Mycelium growth was documented by daily images of the agar plates. The mycelium-covered areas were evaluated by the ImageJ software.

The results confirm the findings of the first experimental campaign. An increase of the mycelium covered area up to a factor of 2.75 compared to the control has been observed. The growth stimulating effect exhibits a temporal maximum at day 6 and day 7 after pulsed electric field exposure and finally adapts to the growth velocity of the control (next figure).
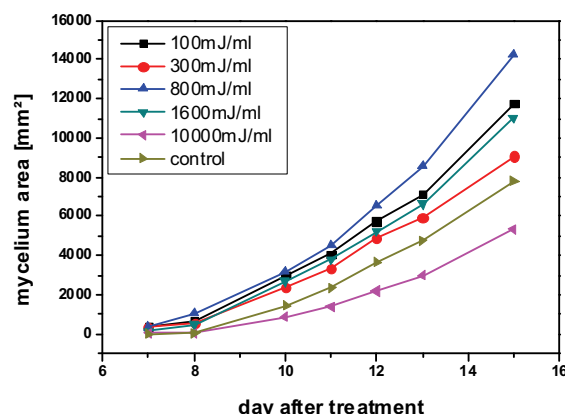
Mycelium area in mm^2 for different treatment energies 7-15 days after pulsed electric field exposure.

100 mJ/ml   control

Growth of *Chlamydomonas rheinhardtii*

Development of the optical density during growth of the microalgae Chlamydomonas rheinhardtii.

Experiments on this topic will be started in March 2011. This work will be funded by the Baden-Wuerttemberg foundation.

Mycelium area in mm² for a treatment energy of 100 mJ/ml and the resulting yield after the first fruiting phase (left) compared to the control (right).

Interestingly, nsPEF-treatment also improves the development of rhizomorphic mycelium, which is responsible for the formation of fruiting bodies. To determine the effect of the treatment on mushroom yield, the treated mycelia were used to inoculate sterile substrate bags each filled with 2,5 kg of grain. For every sample, treated with a certain energy and for the control two representative agar plates had been used. The bags had been incubated for three weeks at 25 °C in the dark. For primordia formation the funghi need a temperature stimulus. During the experiment the stimulation was accomplished by incubating the mycelium bags for 1 week at 10 °C in the dark. Afterwards, each bag has been used to inoculate 1,5 kg sterile beech wood chips in a green house. For fruiting, the mycelium bricks have been incubated at 18°C with a 14 h light-cycle per day. First results indicate an increase of the mushroom yield by a factor of 2 compared to the control (figure above).

The statistics of the experiments have to be increased to verify the yield increase for basidiomycetes. Additional experiments will be performed to determine whether the growth stimulating effect of nsPEF can be reproduced for other genera.

Growth stimulation of microalgae by ns pulsed electric field (PEF) treatment

Encouraged by the promising results of growth stimulation on plant seedlings and fungi, experimental preparations were started to apply PEF-stimulation to microalgae. A MOSFET-switched 25 Ohm Blumlein pulse generator was completed. The pulse duration can be adjusted between 10 ns and 100 ns. A continuous-flow treatment chamber was designed and built, allowing a continuous pulsed electric field treatment of pumpable algae suspensions. After passing the PEF treatment chamber, the algae suspension flows through the measurement cuvette of a spectrometer. The optical density values were acquired and stored digitally. The set-up records growth curves of high reproducibility (next figure).
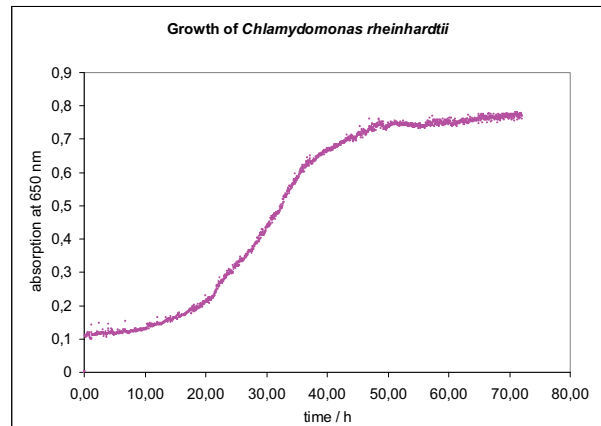
Shared Research Group (SRG 60-1)

Supra-physiological voltages induce a highly conductive, K⁺ selective state of the plasma membrane in BY-2 cells.

Experiments with the patch clamp technique on protoplasts derived from the tobacco culture cell line BY-2 had revealed previously, that the cellular membrane undergoes transition from a low-conductance to a high-conductance state upon hyper- or depolarization beyond certain threshold potentials that are far outside the physiological voltage range. More recently, we tested the ion selectivity of the electro-permeabilized state of the membrane by imposing an electrolyte concentration gradient across the membrane and applying fast voltage ramp protocols.

After establishing the whole cell configuration, the membrane was clamped for 10 ms at potentials eliciting either the low-conductance or the high-conductance state (here, -110 and -320 mV, respectively). Following this prepulse the voltage was rapidly changed at a rate of ~40 mV/ms (the slope was somewhat lower when the actual voltage drop at the membrane was considered rather than the clamped voltage). When the intermediate voltage range was scanned, the shape of the IV curve strongly depended on the prepulse potential, indicating that the high-conductance state of the membrane was retained. Both curves intersect at a voltage of -26 mV (figure on next page); this corresponds to the reversal potential, $E_{rev.}$, of the currents elicited by electro-permeabiliziation. By applying the Goldman equation ("i" = inside; "o" = outside):

$$E_{rev.} = 59mV * \log \frac{P_{K+}/P_{gluconate}[K^+]_o + [gluconate]_i}{P_{K+}/P_{gluconate}[K^+]_i + [gluconate]_o} \quad (1)$$

a relative permeability for K⁺ *versus* gluconate of 8.0 was estimated form these data (ignoring the possible contribution of other ions). A similar K⁺ selectivity was found when a positive prepulse potential was chosen, with the slope of the voltage ramp being negative (data not shown). For outside-out patches we arrived at the same conclusion.
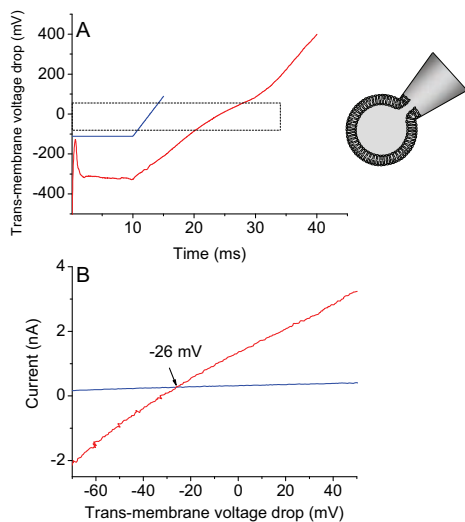
Current-voltage relations of a protoplast clamped in the whole cell configuration (B) obtained from rapid voltage ramps (A; dotted box: voltage range shown in B). Following a prepulse to -110 mV (blue) and about -320 mV (red), a rapid voltage ramp at a rate of 40 mV/ms (blue) and about 24 mV/ms (red) was imposed. IV curves intersect at -26 mV. Solutions were: Pipette (concentrations in mM)) 120 K-gluconate, 10 EGTA, 2.68 $MgCl_2$ (free Mg^{2+} 2), 3.91 $CaCl_2$ (free Ca^{2+} 10^{-4}) 2.13 Mg-ATP, 2 Mes. Bath 30 K-gluconate, 5 $CaCl_2$, 2 $MgCl_2$, 10 Mes/BTP pH 5.8. A relative permeability $P_{K+}/P_{Gluconate}$ of 8.0 was calculated by applying the Goldman equation (see text, equation 1).

The striking observation that the electro-permeabilized membrane was K+ selective prompted us to test whether this could have been due to K+ channels being artificially activated by the strong electric field gradient generated in the membrane during supra-physiological voltage pulses. However, two observations are at variance with this hypothesis:
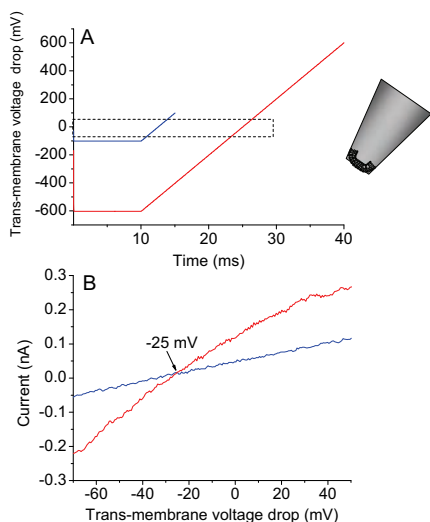
Same type of experiment as shown in the previous figure, but on an outside out patch (A; voltage protocol; B, current-voltage curve). The relative permeability $P_{K+}/P_{gluconate}$ for this experiment calculated from the reversal potential of -25 mV was 7.1.
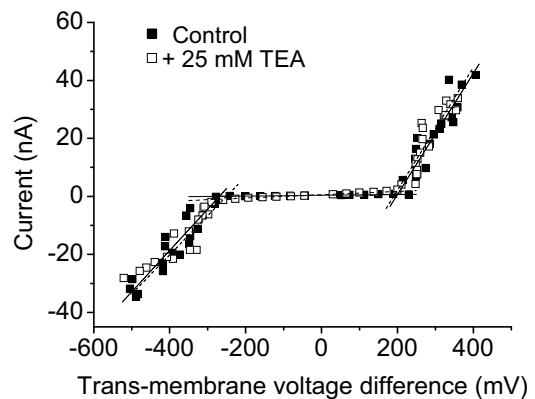
Almost identical whole-cell current-voltage curves were obtained from 10-ms rectangular voltage pulses before and after the addition of 25 mM TEA-nitrate to the bath. Three segments of the IV curve could be identified; linear fits (straight lines) were applied separately. Slope values were (control/TEA$^+$; in nS): 143/135 (hyperpolarization); 1.3/5 (intermediate range); 209/211 (depolarization). Threshold potentials were -268/-258 mV (hyperpolarization); 200/198 mV (depolarization).

(I) The K$^+$ channel blocker Tetraethylammonium (TEA) did not affect the current-voltage relation of BY-2 protoplasts. This inhibitor is known to block K$^+$ channels in various cell types, including BY-2 cells.

(II) When BY-2 protoplasts were screened for K$^+$ channel activity using long (1.5 s) moderately depolarizing voltage pulses, delayed outward currents were elicited that could be assigned to the K$^+$ outward rectifier previously characterized for this cell type. Interestingly, the amplitude of these currents *decreased* after 10-ms rectangular pulses to about +250 mV had been applied, suggesting that K$^+$ channel activity was actually partly inhibited by extreme voltages instead of being enhanced. A quantitative analysis of the gating properties of these currents based on tail currents revealed that the voltage dependence of the channel as indicated by the "midpoint potential" ($V_{1/2}$) was shifted to more positive voltages by supra-physiological depolarizing prepulses.

Control

+140 mV
+120 mV
+100 mV
+ 80 mV
+ 60 mV
+ 60 mV
+ 40 mV
+ 20 mV

-80 mV
-100 mV

After pulse exposure
(n = 5, length 10 ms, amplitude ~250 mV)

0.25 nA

+140 mV
+120 mV
+100 mV
+ 80 mV
+ 60 mV
+ 40 mV
+ 20 mV
+ 0 mV
- 20 mV
- 40 mV

-80 mV
-60 mV
-80 mV   -100 mV

500 ms

■ Control
□ After pulse exposure

Current (nA) vs Trans-membrane voltage difference (mV)
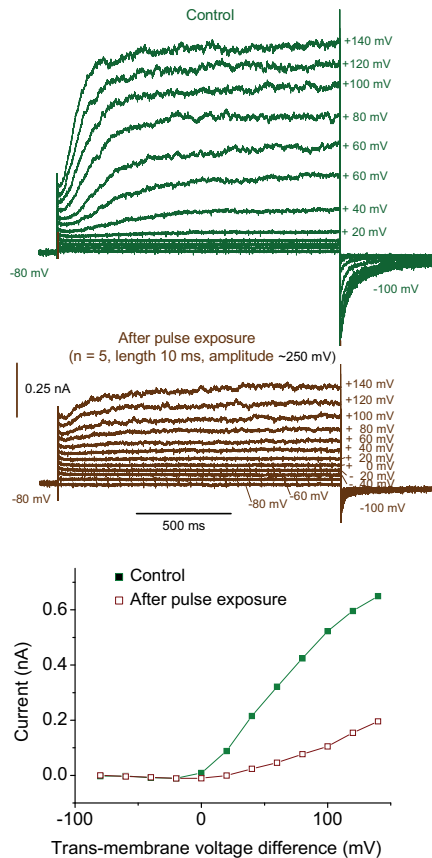
Whole cell K⁺ currents elicited by 1.5-s depolarizing voltage pulses as indicated at each trace under control conditions (top) and after stepping the membrane potential 5 times to about 250 mV for 10 ms (center). Bottom: steady state IV curves derived from these data.

Rather, these observations indicated that formation of liquid pores in the membrane (as implied by the term 'electroporation') describes the molecular processes induced by strong electric fields more accurately than the artificial activation of ion channels.

$$I_{tail} = \frac{I_{tail,max}}{1 + \exp\{(V_{1/2} - V) * \partial * F / RT\}}$$

tail current amplitude (nA) vs Trans-membrane voltage difference (mV)

Voltage dependence of K⁺ channels inferred from tail current amplitudes (Fig. 4). Data were fitted by a Boltzmann equation given in the figure, with
$I_{tail,max}$ = *maximum current amplitude,* $V_{1/2}$ = *midpoint potential,* δ = *apparent minimum gating charge. R, F and T have their usual meaning.*
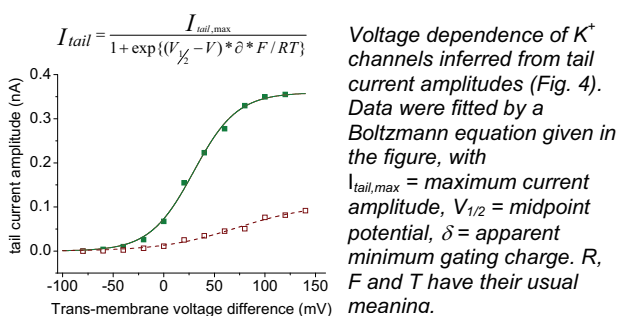
A more detailed analysis of membrane permeability of the electro-permeabilized state is currently under way, using various ionic substrates. This approach will also be useful to obtain more detailed information on the size of the pores generated by strong electric fields.

The NIMEP project – The Non Invasive Microfluidic Electrophysiology Platform

The project started in 2010 with the establishment of the required model organisms and the optimization of the culturing conditions. Besides the large unicellular green alga *Eremosphaera viridis* that has frequently been used in electro-physiological studies, protoplasts derived from the tobacco cell line *Nicotiana tabacum* Virginia Bright Italian-0 (VBI-0) were

chosen for initial experiments; VBI-0 protoplasts are well suited because of their large diameter up to 150 µm. Cell culture could be established on solid medium and as a suspension culture, and protocols for the formation and purification of protoplasts were optimized with respect to large size and high yield. For both cell lines staining protocols for the voltage sensitive fluorescence dyes ANNINE-6 and ANNINE-6plus have been developed.
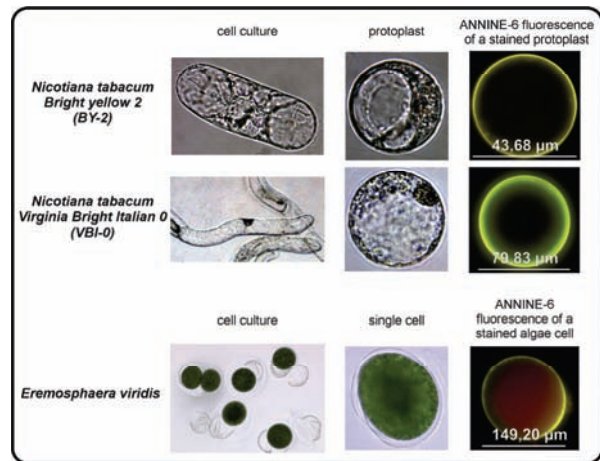
Microscopic images of cells (left) and protoplasts (center) of the tobacco cell lines BY-2 and VBI-0 as well as of the alga Eremosphaera viridis. The right column shows fluorescence images of ANNINE-6 stained protoplasts and algal cells, respectively.

After cell wall regeneration of VBI-0 protoplasts, these spherical cells can by impaled with fine-tipped microelectrodes. First experiments showed promising results. For protoplasts immobilized in agarose the regeneration of the cell wall could be observed with time. To verify the development of the cell wall structures, an essay using the fluorescent dye „Calcofluor White" was developed. Further efforts are required to optimize the staining protocol for immobilized cells, especially to reduce the high fluorescence background in the agarose layer.

current density [pA/pF] — BY-2 unstained, BY-2 stained with ANNINE-6
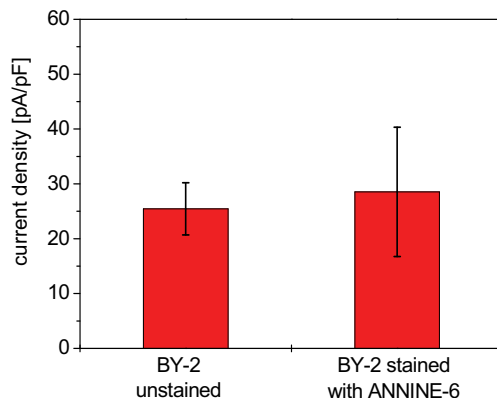
Comparison of currents recorded on ANNINE-6 stained BY-2 protoplasts and unstained protoplasts in the whole cell configuration at a command voltage of 120 mV (4 measurements each, mean ± SE).

Using the patch clamp technique first measurements with unstained and ANNINE-6-stained *Nicotiana tabacum* BY-2 protoplasts have been performed. Whole cell currents in response to voltage pulses with variable amplitude have been recorded in the whole cell configuration. A comparison of current

densities at a command voltage of 120 mV suggests, that the insertion of ANNINE-6 molecules in the plasma membrane has no effect on the activity of voltage-gated potassium channels. This result is an important prerequisite for the use of ANNINE-6 in the NIMEP project.

Membrane-charging measurements on plant cells

As already reported in the annual report of 2009, the cytoskeleton of plant cells seems to play a non-negligible role in the plasma-membrane permeabilization process caused by an external electric field pulse, at least in the regime of seconds to minutes after pulse exposure. We also observed a significant drop of the membrane voltage at the hyperpolarized hemisphere of BY-2 protoplasts 500 ns after the onset of an external electric field pulse of 1 kV/cm.

To examine the influence of actin on this transient plasma membrane permeabilization, a transgenic cell line, YFP-Talin, where the microfilaments are constitutively bundled due to talin overexpression, has been used. Stained cells were exposed to a pulsed electric field of a field strength of 1 kV/cm and the relative fluorescence intensity change F/F_0 of the voltage-sensitive dye ANNINE-6, being proportional to the membrane voltage, was recorded 500 ns after onset of the field pulse. Equal measurements had been performed on BY-2 wild-type (WT) cells. A comparison of both measurements is shown in the figure below.
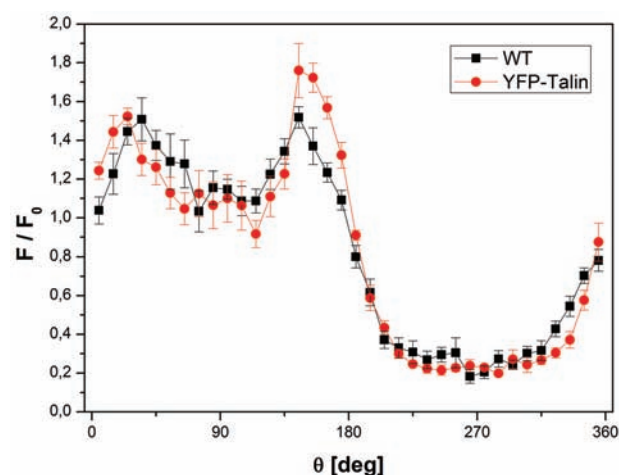

Azimuthal distribution of the relative fluorescence intensity change F/F_0 500 ns after the onset of a 1 kV/cm field pulse, depicted for BY-2 wild-type (WT) cells and the transgenic cell line YFP-Talin.

Both cell lines exhibit a comparable drop of the fluorescence intensity at the hyperpolarized hemisphere. Therefore, a stabilizing influence of actin microfilaments on the plasma membrane integrity can be neglected in the nanosecond time regime.

Giant Unilamellar Vesicles (GUVs) as a supplementary tool to examine membrane-specific processes

GUVs, artificial, spherical liposomes exhibiting diameters up to tens of μm, provide an almost ideal model of a cell without internal structures. Therefore, they allow for measurements of membrane charging and membrane transport processes avoiding influences of membrane-attached or integrated constituents as for example the cytoskeleton, voltage-gated channels or membrane-anchored proteins. GUVs usually are formed using an electro-swelling process in non-ionic aqueous media from multilamellar deposits of phospholipids on conductive-coated glass slides. To ensure realistic membrane charging time constants in the order of several 100 ns, GUVs

have to be formed under physiological conditions, i.e. ionic strengths of the formation buffer solution up to 150 mM NaCl equivalent. Adjusting the formation parameters, GUVs could be formed in physiological buffer solutions exhibiting electric conductivities comparable to those of the cytoplasm. The liposomes have been stained by addition of 1 mol% of headgroup-labeled lipids to allow a direct visualization of their growth using fluorescence microscopy (figure).
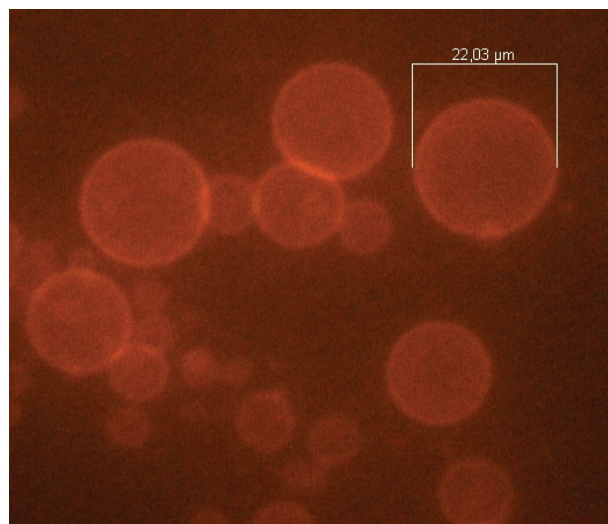
Fluorescence microscopic image of fluorescently labeled GUVs formed from pure phosphatidylcholine. The largest GUVs exhibit diameters in the order of 20 μm, comparable to biological cells. The liposomes have been formed in a PBS buffer solution with an electric conductivity of 16 mS/cm, similar to the cytoplasm conductivity.

This kind of vesicles can be used as model cells to examine properties of voltage-sensitive dyes, e.g the membrane-specific integration of dyes by variation of the GUVs lipid composition, as well as membrane permeabilization or membrane transport processes. Since they exhibit a negligible resting potential, unlike non-artificial biological cells, they are used in ongoing experiments to examine the influence of the resting potential on the permeabilization process of the membrane.

Bacterial decontamination of highly contaminated waste water by means of Pulsed Electric Fields

A major part of the objectives, concerning the sustainable protection of water resources, was accomplished during a 3-years joint project, supported by BMBF, involving Karlsruhe Institute of Technology (IHM, IFG), the University of Mainz and Eisenmann AG. In the framework of this research project it was demonstrated, that pulsed electric field treatment is an alternative and sustainable decontamination method for hospital wastewater, which is increasingly contaminated by antibiotic-resistant human pathogens. In laboratory it was shown, that the decontamination efficiency of PEF treatment was more than 4 log-rates when the wastewater was pre-heated to 50 °C. These results were obtained from experiments on the gram-positive bacterium *E. faecium*, found to be difficult to inactivate by PEFs. Combined PEF and thermal treatment experiments revealed a synergistic effect on inactivation rate.

Based on these results, the pilot plant was modified to facilitate a combination between thermal and PEF treatment. Furthermore, a thermal energy recovery should be tested with a heat circulation system mainly consisting of heat exchangers. In particular, the laboratory results, obtained from batch experiments, should be confirmed at the pilot plant, which operates under continuous flow conditions. For this purpose a heat exchanger system was built, which allows pre-heating,

post-heating and a holding time on high temperature level for 30 s and 60 s, respectively. Basis for the design of heat management system was the following parameter set for experiments to be performed with the pilot plant. The proposed set of experiments includes three basic procedures:

(i) A reference experiment without heat management;
(ii) The determination of decontamination and energy efficiency of the simultaneous application of heat and PEFs. For this mode of operation the inlet wastewater temperature was chosen to be 40 °C and 50 °C. The specific electric treatment energy input is 40 J/ml and 80 J/ml.
(iii) Determination of the decontamination and energy efficiency of a sequential procedure: Post-heating to 55 °C and 60 °C subsequent to PEF treatment at 40 J/ml and 80 J/ml.

The heating circulation system, consisting of three heat exchangers and a water heater, was built by Eisenmann AG at the beginning of the year. The first operating test of the modified pilot plant using a new treatment reactor was performed at University of Mainz in spring. The wastewater circulation through the different treatment procedures is shown in the schematic flow diagram. The heating circulation system consists of two loops. The pre-heating and energy recovery loop is plotted in red while the loop for post-heating is displayed in blue.
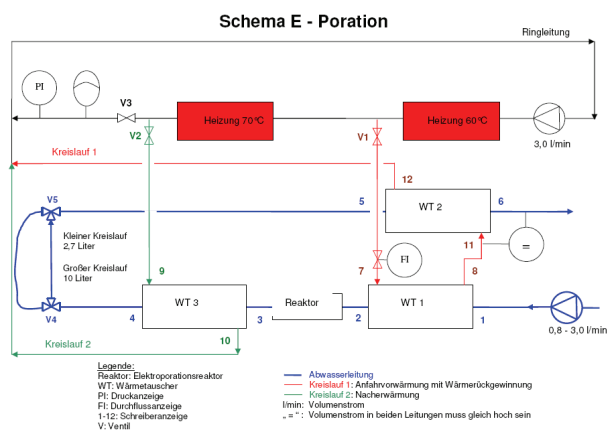
Schematic diagram of the wastewater flow through the heat management system of the pilot plant.

To clarify the decontamination kinetics of the combined treatment, two pathogenic bacterial strains (isolates from patients) were selected by University Hospital in Mainz. The effect of simultaneous treatment with heating (50 °C and 60 °C respectively) and PEF treatment was studied on these selected bacteria strains. The reference numbers of the experiments are listed in the table. The decontamination efficiency for both bacterial strains and different treatment procedures showed a behavior comparable to the results of the laboratory experiments. However, the efficiency of the pilot plant in all cases was 1 log lower (next figure). Particularly, the combined treatment with PEF and heating to 60 °C had the same efficiency as obtained from batch experiments. The magnitude of the synergistic effect depends on the sensitivity of bacterial strain to thermal treatment at temperatures below 55 °C. Thermal heating to temperatures above 60 °C was not considered, because the natural digestion of free DNA by nucleases in the wastewater would be inhibited.

The high energy consumption was a limiting factor for an industrial application of this method so far. A combined treatment of wastewater with PEF and heat could reduce electric energy demand for bacterial decontamination at least by a factor of 3. In that case inactivation efficiency is still higher than obtained with conventional decontamination methods.
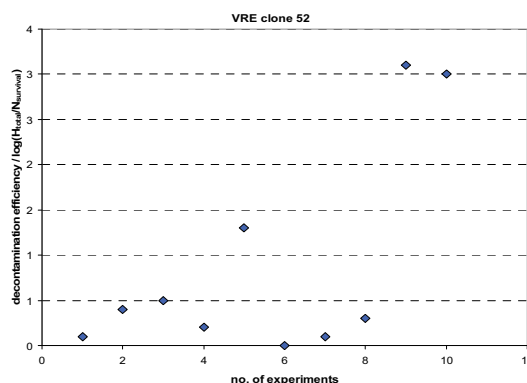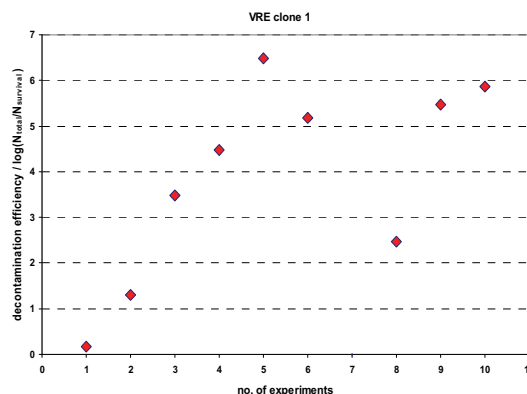
The decontamination efficiency of two pathogenic bacterial strains exposed to different treatments (conforming to the set of experiments) in the pilot plant.

no. of experiment	experimental procedure	electric energy	energy recovery	post-heating
	conductivity: 1380 µS/cm			
1	only PEF	40 J/ml		
2	only PEF	80 J/ml		
3	only PEF	120 J/ml		
4	sequential treatment: PEF and subsequent heating (60 °C)	40 J/ml	10 J/ml	60 °C
5	sequential treatment: PEF and subsequent heating (60 °C)	80 J/ml	20 J/ml	60 °C
6	thermal treatment at 60 °C	-	-	-
7	thermal treatment at 60 °C for 30 s	-	-	-
8	simultaneous treatment: PEF and thermal treatment	40 J/ml	10 J/ml	50 °C
9	simultaneous treatment: PEF and thermal treatment	80 J/ml	20 J/ml	60 °C
10	simultaneous treatment: PEF and thermal treatment	40 J/ml	10 J/ml	60 °C

Set of different experimental procedures performed at the pilot plant to verify the decontamination efficiency.

PEF-treatment of grape mash

The experiments on the PEF-treatment of grape mash in co-operation with the State Institute for Viticulture and Oenology Freiburg have been performed with the grape varieties Müller-Thurgau, Trollinger, and Pinot Noir. The experiments took place at the cooperative of wine-makers in Kappelrodeck, and at the State Research Institute for Viticulture and Pomiculture in Weinsberg. The experiments in Weinsberg have been performed in the frame of a Certified Engineer's Thesis.

By PEF treatment with the electroporation device KEA-WEIN a good opening of the cells could be achieved. The following figure shows the wines made from the grape variety Trollinger without maceration (Blanc-de-Noir), after only pumping through the device, and PEF-treatment (next figure).

Trollinger (from left to right: Blanc-de-Noir, pumped, PEF-treated).
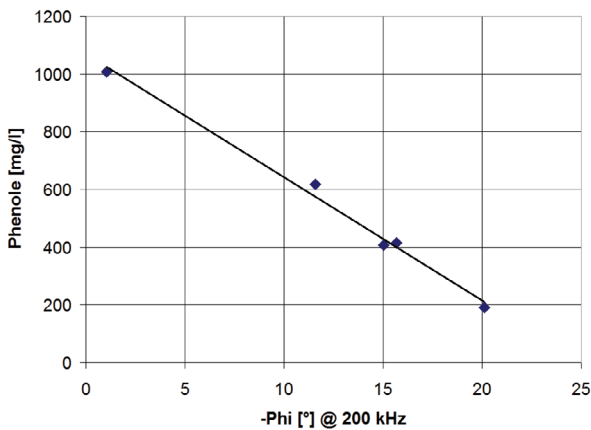
Total phenolic content in the must (Müller-Thurgau) after 4 h extraction in dependence on the phase angle of the complex impedance at 200 kHz.

The experiments on PEF-treatment have been accompanied by impedance measurements in order to evaluate the degree of cell opening. According to the figure above, which shows as an example the results for the grape variety Müller-Thurgau, there is a good linear dependence between the electric measurements, and the chemical analysis of the content of tanning substances after the 4 hours lasting extraction phase. So the impedance measurement seems to be suitable to determine the degree of cell opening in a simple way in order to adapt succeeding processing steps if required.

PEF-treatment of sugar beets

In the frame of the co-operation with SÜDZUCKER on the PEF-treatment of sugar beets, in this year the research and development activities towards an industrial-scale electroporation device have been continued.

Design of pulsed-power components

Contribution to the design of spark gaps

For the design of spark gaps for long-term operation it is helpful to know about the dependence of the wear from the pulse parameters. Estimations of the wear based on the extrapolation of data published in literature turned out to be inaccurate. Therefore, experiments on the wear of electrodes made from tungsten-copper alloy have been performed for different pulse parameters usual for PEF-treatment devices. The table shows

the considered parameter range. The next figure shows the measured wear in dependence of the load integral of the pulse current. According to the next figure there is a good agreement of the wear and the load integral in the considered parameter range.

experiment no.	1 ◆	2 ✳	3 ▲	4 ■	5 ●	6 +	7 ✕
Î [kA]	0.8	1.1	2.7	3.4	3.0	2.8	2.1
transferred charge [mC]	5.7	7.3	6.0	7.8	6.8	6.2	5.8
load integral [A²s]	2.4	4.2	10.6	17.6	13.7	11.4	7.4

Table 1: Range of parameters for experiments on the wear of electrodes.
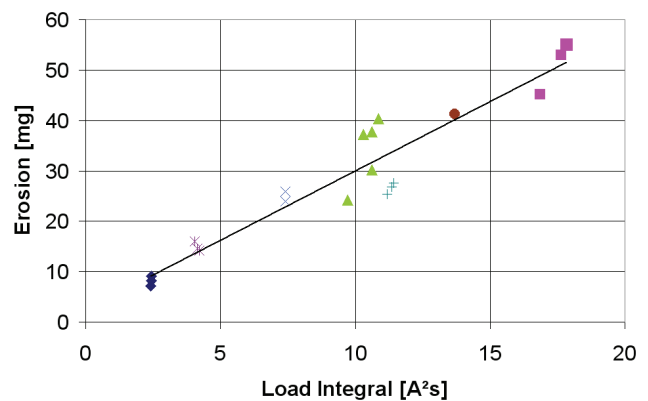
Dependence of the wear of electrodes on the load integral.

Measurement of the thermal losses at the electrodes of a switching spark gap.

For the design of the heat sink the thermal losses at the electrodes of a switching spark gap are of interest. In order to measure the thermal power fed into the electrode's shaft, a circuitry has been designed, which measures the temperature difference along the cylindrical shaft and determines based on the thermal resistivity the thermal power during operation of the spark gap.

The following figure shows the test setup. The temperature sensors (NTC) are situated inside the shaft (1). It is fixed to the base plate (2), which is kept on nearly constant temperature by means of a chiller and cooling water circuit. The electronic circuitry is shielded by its metallic housing (3). The measurement data are transferred to a computer on ground potential via a fibre-optic cable. The electrode (4) serves for grading the electric field. The next figure shows the measurement results of an experimental run. The measured temperature difference NTC1-NTC2 of in average 12.1 K corresponds to a transferred thermal power of 8.7 W. NTC3 measures the temperature of the base plate. For both spark gap electrodes in the frame of the measurement accuracy the same measurement results have been obtained.
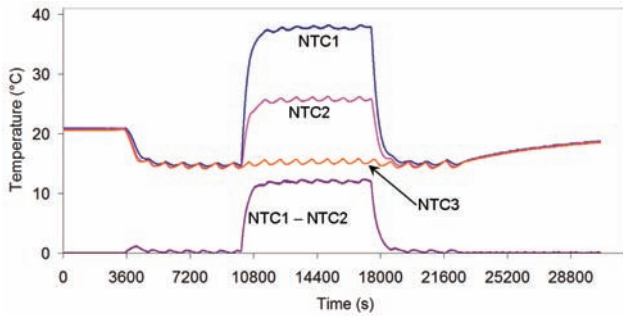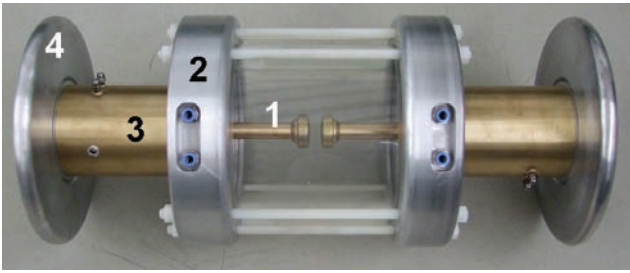
Test set-up for measuring the thermal losses of a spark gap and measured temperatures.

Simplified design of an electroporation reactor

For a new design of an electroporation reactor usually the electrode geometry and the parameters of the pulse circuit are adapted stepwise by means of field calculations in order to achieve the desired field distribution and pulse shape. But often only an adaptation of a known electrode geometry to another flow rate is required. If by this change of scale the properties of the flow are not influenced significantly, the design adaptation can be performed by scaling only without new field calculations. In the case of a substantially homogeneous electric field distribution the electroporation reactor can be divided into the centre section with a nearly homogeneous field distribution, and the inlet- and outlet sections with an inhomogeneous field distribution. The diameter of the reactor determines the scaling of the lengths of the outer sections only. The centre section can be additionally stretched according to the requirements. As an example the next figure shows the dependence of the reactor's ohmic resistance and length of the treatment area on the inner diameter d_i for a collinear design.

Resistance of middle section R_C

$$R_C = \frac{l}{\kappa \cdot 0.25\pi \cdot d_t^{\,2}}$$

Resistance of inlet- and outlet section R_{IO}

$$R_{IO} = \frac{0.32}{\kappa \cdot d_t}$$

Total resistance R

$$R = 2R_{IO} + R_C$$

Length of treatment area l_t

$$l_t = l + 1.7 \cdot d_t$$
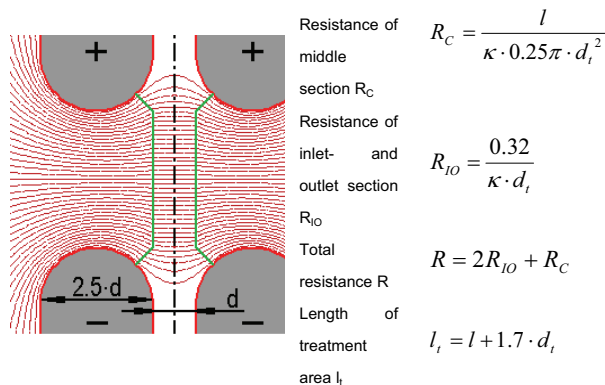
Scaling of resistance and length of the treatment area depending on the diameter for a collinear geometry.

Involved Staff:

DI F. Attmann, DP Th. Berghöfer, H. Brüsemeister, Dr. Ch. Eing, Fr. Dr. B. Flickinger, **Dr. W. Frey**, DP H. Giese (Gast), Fr. DI M. Göttel, Dr. Chr. Gusbeth, Fr. Dr. P. Hohenberger (Uni KA), DI (FH) F. Lang, K. Leber, E. Menesklou, **Dr. G. Müller**, K. Paulus, Fr. S Rocke, **Dr. M. Sack**, K.-D. Schorb, DI (FH) J. Singer, R. Stängle, DI R. Sträßner, A. Wolf, Dr. L. Wegner (Uni KA), R. Wüstner, H. Zimmermann.

Program: Efficient Energy Use and Conversion (REUN)

Energieeffiziente Mikrowellentechnik

As part of the BMBF project "innovative, modular microwave technology for production of fibre composite structures" microwave integrated tools could be improved so that first mentionable results were achieved.

With an improved pultrusion tool for the first time a total length of 10 m of a circular profile with 9 mm diameter made of carbon fibre reinforced plastic (CFRP) could be produced in collaboration with the Institute of Textile Technology (ITV) in Denkendorf (figure).
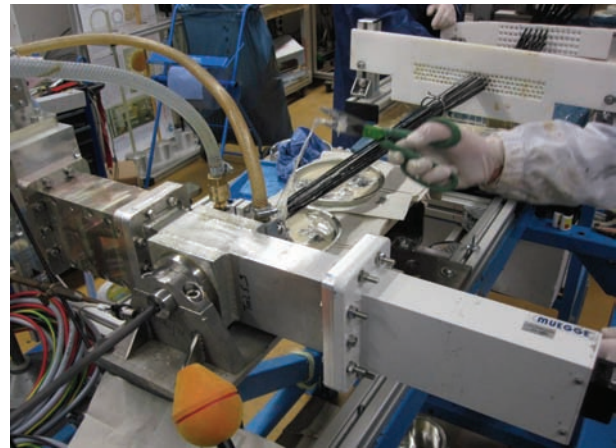
Experiment on microwave pultrusion of CFRP.

The tool for the fabrication of cast blanks for the manufacture of ceramic brake discs has been optimized in its thermal and electromagnetic behaviour and provided with suitable temperature measuring points, so that now a fully automated process control is possible. Thus for the first time, systematic parametric studies for further process optimization are feasible.

An application for a subsequent joint BMBF research project for microwave processing of CFRP materials called FLAME was approved, with few changes required. So that now KIT who will be the project coordinator has to complete the required application forms and project plans.

Another BMBF project called MACOS has started in April 2010. This project will allow the development of a microwave equipment for the ablation of contaminated surfaces in nuclear power plants in collaboration with IMB of CS. First principle concepts have been developed and a test set for dielectric characterization of concrete materials was set up.

The kick-off meeting of a joint project on "Recovery of CO2 as a carbon brick by use of mainly renewable energy sources" was taking place in November 2010. This project is coordinated by Bayer Technology Services.

Involved Staff:

Fr. J. Dittrich, **Dr. L. Feher**, S. Layer, **Dr. G. Link**, Dr. A. Melcher, V. Nuß, MSc D. Prastiyanto, T. Seitz, Dr. S. Stanculovic, Fr. C. Zöller

List of Publications

FUSION: Program Nuclear Fusion

Publications at cross-referenced journals:

Bongers, W.A., Graswinckel, M.F., Goede, A.P.H., Kasparek, W., Danilov, I., Fernandez Curto, A., deBaar, M.R., van den Berg, M.A., Donne, A.J.H., Elzendoorn, B.S.Q., Heidinger, R., Ivanov, P., Kruijt, O.G., Lamers, B., Meier, A., Piosczyk, B., Plaum, B., Ronden, D.M.S., Thoen, D.J., Schmid, M., Verhoeven, A.G.A.
A remotely steered millimetre wave launcher for electron cyclotron heating and current drive on ITER.
Fusion Engineering and Design, 85(2010) S.69-86
DOI:10.1016/j.fusengdes.2009.07.001

Bruschi, A., Erckmann, V., Kasparek, W., Petelin, M.I., Thumm, M., Bin, W., Cirant, S., D'Arcangelo, O., Hollmann, F., Lubyako, L., Noke, F., Plaum, B., Purps, F., Zohm, H., ECRH Team at IPP Greifswald
Diplexers for power combination and switching in high power ECRH systems.
IEEE Transactions on Plasma Science, 38(2010) S.1427-38
DOI:10.1109/TPS.2010.2047658

D'Andrea, D., Munz, C.D., Schneider, R.
Modeling of long-range intra- and inter-species charged particle collisions for PIC simulations.
Communications in Computational Physics, 7(2010) 877-903
DOI:10.4208/cicp.2009.09.094

Gantenbein, G., Dammertz, G., Flamm, J., Illy, S., Kern, S., Latsas, G., Piosczyk, B., Rzesnicki, R., Samartsev, A., Schlaich, A., Thumm, M.
Experimental investigations and analysis of parasitic RF oscillations in high-power gyrotrons.
IEEE Transactions on Plasma Science, 38(2010) S. 1167-77
DOI:10.1109/TPS.2010.2041366

Garkusha, I.E., Arkhipov, N.I., Klimov, N.S., Makhlaj, V.A., Safronov, V.M., Landman, I., Tereshin, V.I.
The latest results from ELM-simulation experiments in plasma accelerators.
Physica Scripta, T138(2009) S.014054/1-6
DOI:10.1088/0031-8949/2009/T138/014054

Landman, I.S., Pestchanyi, S.E., Igitkhanov, Y., Pitts, R.
Modelling of wall and SOL processes and contamination of ITER plasma after impurity injection with the Tokamak code TOKES.
Fusion Engineering and Design, 85(2010), S. 1366-70
DOI:10.1016/j.fusengdes.2010.03.044

Li, G., Jin, J.,Rzesnicki, T., Kern, S., Thumm, M.
Analysis of a quasi-optical launcher toward a step-tunable 2-MW coaxial-cavity gyrotron.
IEEE Transactions on Plasma Science, 38(2010) S. 1361-68
DOI:10.1109/TPS.2010.2043267

Makhlaj, V.A., Garkusha, I.E., Malykhin, S.V., Pugachov, A.T., Landman, I., Linke, J., Pestchanyi, S., Chebotarev, V.V., Tereshin, V.I.
Residual stresses in tungsten under exposure with ITER ELM-like plasma loads.
Physica Scripta, T138(2009) S. 014060/1-5
DOI:10.1088.0081-8949/T138/014060

Pestchanyi, S., Garkusha, I., Landman, I.
Simulation of tungsten armour cracking due to small ELMs in ITER.
Fusion Engineering and Design, 85(2010) S. 1697-1701
DOI:10.1016/j.fusengdes.2010.05.005

Rzesnicki, T., Piosczyk, B., Kern, S., Illy, S., Jin, J., Samartsev, A., Schlaich, A., Thumm, M.
2.2-MW record power of the 170-GHz European preprototype coaxial-cavity gyrotron for ITER.
IEEE Transactions on Plasma Science, 38(2010) S.1141-49
DOI:10.1109/TPS.2010.2040842

Thumm, M., Rzesnicki, T., Piosczyk, B., Flamm, J., Gantenbein, G., Illy, S., Jin, J., Kern, S., Samartsev, A., Schlaich, A.
2.2 MW record power of the 0.17 THz European pre-prototype coaxial-cavity gyrotron for ITER.
Terahertz Science and Technology, 3(2010) Nr. 1, S. 1-20

Thumm, M., Brand, P., Braune, H., Dammertz, G., Erckmann, V., Gantenbein, G., Illy, S., Kasparek, W., Kern, S., Laqua, H.P., Lechte, C., Leonhardt, W., Marushchenko, N.B., Michel, G., Piosczyk, B., Schmid, M., Turkin, Y., Weissgerber, M.
Status and high power performance of the 10-MW 140-GHz ECH system for the stellarator Wendelstein 7-X.
Plasma and Fusion Research, 5(2010) S. 1006/1-8

Other printed publications:

Avramides, K.A., Dumbrajs, O., Vomvoridis, J.L., Kern, S.
Gyrotron interaction simulations with tapered magnetostatic field.
35th Int. Conf. on Infrared, Millimeter and Terahertz Waves (IRMMW-THz-2010), Roma, I, Sept 5-10, 2010, Proc. on USB-Stick.

Beringer, M., Illy, S., Jin, J., Kern, S., Thumm, M., Lievin, C.
A 4 MW 170 GHz coaxial-cavity gyrotron – design of the major components.
22nd Joint Russian-German Meeting on ECRH and Gyrotrons, Nizhny-Novgorod, Russia, June 29 – July 5, 2010. Folien auf CD-ROM.

Beringer, M., Illy, S., Jin, J., Kern, S., Lievin, C., Thumm, M.
Design of major components for a 4 MW 170 GHz coaxial-cavity gyrotron.
11th Int. Vacuum Electronics Conf. (IVEC 2010), Monterey, CA, May 18-20, 2010. Proc. S. 35-36, Piscataway, N.J.: IEEE, 2010

Braune, H., Erckmann, V., Illy, S., Michel, G., Noke, F., Purps, F., W7-X ECRH teams at IPP, IPF and KIT
Collector loading during high frequency power modulation.
35th Int. Conf. on Infrared, Millimeter and Terahertz Waves (IRMMW-THz 2010), Roma, I, September 5-10, 2010
Proc. on USB-Stick

Bruschi, A., Bin, W., Cirant, S., Dell'Era, F., Gantenbein, G., Leonhardt, W., Muzzini, V., Samartsev, A., Schmid, M.
Progress and test of the spherical matched load designed for 2 MW-CW.
Workshop on RF Heating Technology of Fusion Plasmas, Como, I, September 13-15, 2010, Folien auf CD-ROM

D'Andrea, D., Maschek, W., Schneider, R.
Simulation of Coulomb collisions in plasma accelerators for space applications.
Int.Top.Meeting on Nuclear Applications and Utilization of Accelerators (AccApp'09), Wien, A, May 4-8, 2009. Folien auf CD-ROM. Wien: IAEA, 2010, IAEA-I3-CN-173

Darbos, C., ITER EC International Design Team
Status of the ITER electron cyclotron H&CD system.
35th Int. Conf. on Infrared, Millimeter and Terahertz Waves
(IRMMW-THz 2010), Roma, I, September 5-10, 2010
Proc. on USB-Stick

Flamm, J., Jin, J., Neudorfer, J., Roller, S., Thumm, M.
Investigations on wave propagation in launchers of advanced
gyrotron output couplers.
35th Int. Conf. on Infrared, Millimeter and Terahertz Waves
(IRMMW-THz 2010), Roma, I, September 5-10, 2020, Proc. on
USB-Stick

Gantenbein, G., Dammertz, G., Erckmann, V., Kasparek, W.,
Kern, S., Latsas, G., Lechte, C., Piosczyk, B., Rzesnicki, T.,
Samartsev, A., Schlaich, A., Thumm, M., Tigelis, I., Vaccaro, A.
Progress in stable operation of high power gyrotrons for ECRH.
22nd Joint Russian-German Meeting on ECRH and Gyrotrons,
Nizhny Novgorod, Russia, June 29 – July 5, 2010. Folien auf
CD-ROM

Gantenbein, G., Erckmann, V., Illy, S., Kern, S., Kasparek, W.,
Lechte, C., Leonhardt, W., Lievin, C., Samartsev, A., Schlaich,
A., Schmid, M., Thumm, M.
Status and recent results of the 140 GHz, 1 MW CW gyrotron
development for the stellarator W7-X.
Workshop on RF Heating Technology of Fusion Plasmas,
Como, I, September 13-15, 2010; Folien auf CD-ROM

Igitkhanov, Yu., Landman, I., Wobig, H., Sagara, A.
Burning plasma control in stellarator fusion reactor.
9th Int. Symp. on Fusion Nuclear Technology (ISFNT-9), Dalian,
China, October 11-16, 2009. Abstract on USB-Stick

Illy, S., Beringer, M., Kern, S., Thumm, M.
Collector design studies for a 1 MW cyclindrical-cavity and a 4
MW coaxial-cavity gyrotron.
35th Int. Conf. on Infrared, Millimeter and Terahertz Waves
(IRMMW-THz 2010), Roma, I, September 5-10, 2010, Proc. on
USB-Stick

Ioannidis, Z., Kern, S., Avramides, K., Latsas, G., Tigelis, I.
The contribution of higher-order spatial harmonics in
eigenvalues and ohmic losses calculations in coaxial corrugated
cavities.
35th Int. Conf. on Infrared, Millimeter and Terahertz Waves
(IRMMW-THz 2010), Roma, I, September 5-10, 2010, Proc. on
USB-Stick

Jin, J., Flamm, J., Kern, S., Rzesnicki, T., Thumm, M.
Design of phase correcting mirror system for coaxial-cavity
ITER gyrotron.
11th Int. Vacuum Electronics Conf. (IVEC 2010), Monterey, CA,
May 18-20, 2010. Proc. S. 29-30, Piscataway, M.J.: IEEE, 2010

Kasparek, W., Erckmann, V., Petelin, M., Bruschi, A., Research
Groups at IPF, IPP, IAP, IFP, KIT, TNO and FOM
High-power diplexers for plasma heating and diagnostic
systems: developments, epxeriments, and prospects.
3rd Int. Workshop on Far-Infrared Technologies (IW-FIRT 2010),
Fukui, J, March 15-17, 2010, Book of Abstracts S.20-21, Proc.
on CD-ROM, University of Fukui

Kasparek, W., Erckmann, V., Hollmann, F., Michel, G., Noke,
F., Purps, F., Plaum, B., Brand, P., Lechte, C., Filipovic, E.,
Saliba, M., Wang, Y., Petelin, M., Koposova, E., Lubyako, L.,
Doelman, N., van den Braber, R., Bruschi, A., Bongers ,W.,
Krijger, B., Stober, J., Wagner, D., Groups at IPF Stuttgart, IPP
Greifswald, IAP N.Novgorod, IFP Milano, KIT Karlsruhe, TNO
Delft, FOM Rijnhuizen
Recent results in the development of compact resonant
diplexers.
22nd Joint Russian-German Meeting on ECRH and Gyrotrons,
Nizhny Novgorod, Russia, June 29 – July 5, 2010, Folien auf
CD-ROM

Kasparek, W., Lechte, C., Plaum, B., Erckmann, V., Laqua, H.,
Michel, G., Gantenbein, G., Thumm, M.
Transmission system for ECRH on Wendelstein 7-X.
Institut für Plasmaforschung Universität Stuttgart, Annual
Report 2010, S. 40-41

Kasparek, W., Plaum, B., Lechte, C., Erckmann, V., Michel, G.,
Zohm, H., Petelin, M., Bruschi, A., Thumm, M., Bongers, W.,
Doelman, N.
A diplexer for power combination and fast switching.
Institut für Plasmaforschung Universität Stuttgart, Annual
Report 2010, S. 44

Kasparek, W., Erckmann, V., Hollmann, F., Michel, G., Noke,
F., Purps, F., Plaum, B., Brand, P., Lechte, C., Filipovic, E.,
Saliba, M., Doelman, N., van den Braber, R., Bongers, W.,
Krijger, B., Petelin, M., Koposova, E., Lubyako, L., Bruschi, A.,
Stober, J., Wagner, D., Groups at IPF Stuttgart, IPP Greifswald,
IAP N.Novgorod, IFP Milano, KIT Karlsruhe, TNO Delft, and
FOM Rijnhuisen
Compact resonant diplexers for advanced ECRH: design, low-
and high-power tests and plans.
Workshop on RF Heating Technology of Fusion Plasmas,
Como, I, September 13-15, 2010, Folien auf CD-ROM

Kern, S., Avramides, K.A., Roy Choudhury, A., Dumbrajs, O.,
Gantenbein, G., Illy, S., Samartsev, A., Schlaich, A., Thumm, M.
Simulation and experimental investigations on dynamic after
cavity interaction (ACI).
35th Int. Conf. on Infrared, Millimeter and Terahertz Waves
(IRMMW-THz 2010), Roma, I, September 5-10, 2010, Proc. on
USB-Stick

Kern, S., Avramides, K.A., Roy Choudhury, A., Borie, E.,
Gantenbein, G., Illy, S., Samartsev, A., Schlaich, A.,
Thumm, M.
Different types of afeter cavity interaction in gyrotrons.
Workshop on RF Heating Technology of Fusion Plasmas,
Como, I, September 13-15, 2010, Folien auf CD-ROM

Latsas, G.P., Tigelis, I.G., Moraitou, M.D., Kern, S., Vomvoridis,
J.L., Ioannidis, Z.C.
Parametric study on the effet of the dielectric and geometric
propertis on the parasitics in gyrotron beam tunnels.
35th Int. Conf. on Infrared, Millimeter and Terahertz Waves
(IRMMW-THz 2010), Roma, I, September 5-10, 2010, Proc. on
USB-Stick

Omori, T., Albajar, F., Alberti, S., Baruch, U., Beckett, B., Bigelow, T., Bonicelli, T., Bruschi, A., Caughman, J., Chavan, R., Cox, D., Darbos, C., deBaar, M., Denisov, G., Gandini, F., Gassman, T., Goodman, T.P., Henderson, M., Hotte, J.P., Jean, O., Kajiwara, K., Kasparek, W., Kasugai, A., Kern, S., Kobayashi, N., Kushwah, M., Moro, A., Nazare, C., Oda, J., Purohit, D., Ramponi, G., Rao, S.L., Rasmussen, D., Ronden, D., Saibene, G., Sakamoto, K., Scherer, T., Shapiro, M., Singh, N.P., Strauss, D., Takahashi, K., Temkin, R.
Status of the ITER EC H&CD system.
Workshop on RF Heating Technology of Fusion Plasmas, Como, I, September 13-15, 2010, Folien auf CD-ROM

Pagonakis, I.G., Hogge, J.P., Alberti, S., Illy, S., Piosczyk, B., Kern, S., Lievin, C., Tran, M.Q.
Status of the EU 170 GHz / 2 MW / CW coaxial cavity gyrotron for ITER: the dummy gun experiments.
35th Int. Conf. on Infrared, Millimeter and Terahertz Waves (IRMMW-THz 2010), Roma, I, September 5-10, 2010, Proc. on USB-Stick

Rzesnicki, T., Piosczyk, B., Kern, S., Illy, S., Jin, J., Samartsev, A., Schlaich, A., Thumm, M.
Experiments with the European 2 MW coaxial-cavity pre-prototype gyrotron for ITER.
11th Int.Vacuum Electronics Conf. (IVEC 2010), Monterey, CA, May 18-20, 2010. Proc. S. 27-28. Piscataway, N.J.: IEEE, 2010

Rzesnicki, T., Piosczyk, B., Roy Choudhury, A., Illy, S., Jin, J., Kern, S., Samartsev, A., Schlaich, A., Thumm, M.
Recent results with the European 2 MW coaxial-cavity pre-prototype gyrotron for ITER.
35th Int.Conf. on Infrared, Millimeter and Terahertz Waves (IRMMW-THz 2010), Roma, I, September 5-10, 2010, Proc. on USB-Stick

Scherer, T., Strauß, D., Schreck, S., Gantenbein, G., Kleefeldt, K., Leonhardt, W., Meier, A., Mellein, D., Serikov, A., Späh, P., Vaccaro, A., Aiello, G.
Design validation of the structural components and CVD diamond torus windows in the ITER ECH upper launcher.
Workshop on RF Heating Technology of Fusion Plasmas, Como, I, September 13-15, 2010, Folien auf CD-ROM

Schlaich, A.
Aufbau und Anwendung eines Systems zur Spektralanalyse von Gyrotronpulsen im Millimeterwellenbereich.
Diplomarbeit, Karlsruher Institut für Technologie 2009; KIT Scientific Reports, KIT-SR 7541 (Juli 2010)

Schlaich, A., Flamm, J., Gantenbein, G., Kern, S., Latsas, G., Rzesnicki, T., Samartsev, A., Thumm, M., Tigelis, I.
Investigations on parasitic oscillations in megawatt gyrotrons.
11th Int. Vacuum Electronics Conf. (IVEC 2010), Monterey, CA, May 18-20, 2010. Proc. S. 33-34. Piscataway, N.J.: IEEE, 2010

Thumm, M., Rzesnicki, T., Piosczyk, B., Flamm, J., Gantenbein, G., Illy, S., Jin, J., Kern, S., Samartsev, A., Schlaich, A.
Recent results of the 2 MW-0.17 THz European pre-prototype coaxial-cavity gyrotron for ITER.
3rd Int. Workshop on Far-Infrared Technologies (IW-FIRT 2010), Fukui, J, March 15-17, 2010. Abstracts S. 12-13. Proc. of CD-ROM. University of Fukui

Thumm, M.
State-of-the-art of high power gyro-devices and free electron masers. Update 2009.
KIT Scientific Reports KIT-SR 7540 (April 2010)

Thumm, M., Rzesnicki, T., Piosczyk, B., Flamm, J., Gantenbein, G., Illy, S., Jin, J., Kern, S., Samartsev, A., Schlaich, A.
Status of the 2 MW, 170 GHz pre-prototype coaxial-cavity gyrotron for ITER.
22nd Joint Russian-German Meeting on ECRH and Gyrotrons, Nizhny Novgorod, Russia, June 29-July 5, 2010. Folien auf CD-ROM

Thumm, M., Rzesnicki, T., Piosczyk, B., Flamm, J., Gantenbein, G., Illy, S., Jin, J., Kern, S., Samartsev, A., Schlaich, A.
Status of the European 2 MW, 170 GHz pre-prototype coaxial-cavity gyrotron for ITER.
Workshop on RF Heating Technology of Fusion Plasmas, Como, I, September 13-15, 2010, Folien auf CD-ROM

Wagner, D., Stober, J., Leuterer, F., Monaco, F., Münich, M., Schmid-Lorch, D., Schütz, H., Zohm, H., Thumm, M., Scherer, T., Meier, A., Gantenbein, G., Flamm, J., Kasparek, W., Höhnle, H., Lechte, C., Litvak, A.G., Denisov, G.G., Chirkov, A., Popov, L.G., Nichiporenko, V.O., Myasnikov, V.E., Tai, E.M., Solyanova, E.A., Malygin, S.A.
Multi-frequency ECRH as ASDEX upgrade, status and plans.
35th Int. Conf. on Infrared, Millimeter and Terahertz Waves (IRMMW-THz 2010), Roma, I, September 5-10, 2010. Proc. on USB-Stick

Wagner, D., Stober, J., Franke, T., Leuterer, F., Monaco, F., Münich, M., Reich, M., Schütz, H., Zohm, H., Thumm, M., Scherer, T., Meier, A., Gantenbein, A., Flamm, G., Kasparek, W., Lechte, C., Litvak, A.G., Denisov, G.G., Chirkov, A.V., Popov, L.G., Nichiporenko, V.O., Myasnikov, V.E., Tai, E.M., Solyanova, E.A., Maligyn, S.A.
Multi-frequency ECRH system at ASDEX upgrade.
22nd Joint Russian-German Meeting on ECRH and Gyrotrons, Nizhny Novgorod, Russia, June 29 – July 5, 2010. Folien auf CD-ROM

Wagner, D., Stober, J., Leuterer, F., Monaco, F., Münich, M., Reich, M., Schmid-Lorch, D., Schütz, H., Zohm, H., Thumm, M., Scherer, T., Meier, A., Gantenbein, G., Flamm, J., Kasparek, W., Höhnle, H., Lechte, C., Litvak, A.G., Denisov, G.G., Chirkov, A., Popov, L.G., Nichiporenko, V.O., Myasnikov, V.E., Tai, E.M., Solyanova, E.A. Malygin, S.A.
Status of the multi-frequency ECRH system at ASDEX upgrade.
Workshop on RF Heating Technology of Fusion Plasmas, Como, I, September 13-15, 2010, Folien auf CD-ROM

Zaginaylov, G.I., Kern, S.
Simplified analytic model for improved field calculation inside the coaxial gyrotron cavity.
European Microwave Week, Paris, F, September 26 – October 1, 2010

Papers or lectures, which are not available in printed form:

Albajar, F., Alberti, S., Avramides, K.A., Benin, P., Bonicelli, T., Cirant, S., Darbos, C., Gantenbein, G., Gassmann, T., Goodman, T.P., Henderson, M., Illy, S., Ionnidis, Z., Hogge, J.P., Jin, J., Kern, S., Latsas, G., Lievin, C., Pagonakis, I.G., Piosczyk, B., Rzesnicki, T., Thumm, M., Tigelis, I., Tran, M.Q., Vomvoridis, J.
The European 2 MW gyrotron for ITER.
16th Joint Workshop on Electron Cyclotron Emission and Electron Cyclotron Resonance Heating, Sanya, China, April 12-15, 2010. Book of Abstracts.

Arnoux, G., Bazylev, B., Lehnen, M., Loarte, A., Riccardo, V., Bozhenko, S., Devaux, S., Eich, T., Fundamenski, W., Jachmich, S., Thomsen, H., JET EFDA Contributors
Heat load measurement on the JET first wall during disruptions.
19th Int.Symp. on Plasma Surface Interactions in Controlled Fusion Devices (PSI-19), San Diego, CA, May 24-28, 2010.
Book of Abstracts S. 95.

Bazylev, B., Arnoux, G., Fundamenski, W., Lehnen, M., JET EFDA Contributors
Modeling of runaway electron beams for JET and ITER.
19th Int. Symp. on Plasma Surface Interactions in Controlled Fusion Devices (PSI-19), San Diego, CA, May 24-28, 2010.
Book of Abstracts S. 198

Bazylev, B., Landman, I., Pestchanyi, S., Igitkhanov, Yu., Loarte, A., Pitts, R., Lehnen, M., Safronov, V., Podkovyrov, V., Klimov, N., Garkusha, I., Makhlay, W.
Simulations of material damage and high energy fluxes to ITER divertor and first wall during transients and runaway electron loads.
23rd IAEA Fusion Energy Conference, Daejeon, Korea, October 11-16, 2010

Beringer, M.H., Illy, S., Jin, J., Kern, S., Thumm, M.
Physical component designs and thermo-mechanical studies towards a 4 MW 170 GHz coaxial-cavity gyrotron:
ITG Vacuum Electronics Workshop, Bad Honnef, November 15-16, 2010

Coenen, J.W., Philipps, V., Brezinsek, S., Bazylev, B., Kreter, A., Hirai, T., Laengner, M., Tanabe, T., Ueda, Y., Samm, U., TEXTOR Team
Analysis of tungsten melt layer motion and splashing under Tokamak conditions at TEXTOR.
23rd IAEA Fusion Energy Conference, Daejeon, Korea, October 11-16, 2010

Coenen, J.W., Bazylev, B., Preszinsek, S., Philipps, V., Hirai, T., Kreter, A., Sergienko, G., Pospiesczyk, A., Tanabe, T., Ueda, Y., Samm, U., TEXTOR-Team
Tungsten melt layer motion and splashing on castellated surfaces at the Tokamak TEXTOR.
19th Int. Symp. on Plasma Surface Interactions in Controlled Fusion Devices (PSI-19), San Diego, CA, May 24-28, 2010.
Book of Abstracts S. 65

Damyanova, M., Kern, S., Illy, S., Thumm, M., Sabchevski, S., Zhelyazkov, I., Vasileva, E.
Modelling and simulation of gyrotrons for ITER.
Int. Workshop and Summer School on Plasma Physics, Kiten, BG, July 5-10, 2010

Flamm, J., Jin, J., Thumm, M.
An FFTF based spectral method for analysis of launchers in advanced gyrotron output couplers.
ITG Vacuum Electronics Workshop, Bad Honnef, November 15-16, 2010

Flamm, J.
Analysis of cylindrical waveguides with specifically perturbed inner wall using an FFTF based spectral method.
KIT PhD symp., Karlsruhe, 30. September 2010

Gantenbein, G., Rzesnicki, T., Piosczyk, B., Kern, S., Illy, S., Jin, J., Samartsev, A., Schlaich, A., Thumm, M.
2.2 MW operation of the European coaxial-cavity pre-prototype gyrotron for ITER.
23rd IAEA Fusion Energy Conference, Daejeon, Korea, October 11-16, 2010

Gantenbein, G., Dammertz, G., Kern, S., Latsas, G., Piosczyk, B. Rzesnicki, T., Samartsev, A., Schlaich, A., Thumm, M., Tigelis, I.
Progress in stable operation of high power gyrotrons.
16th Joint Workshop on Electron Cyclotron Emission and Electron Cyclotron Resonance Heating, Sanya, China, April 12-15, 2010. Book of Abstracts

Garkusha, I.E., Landman, I., Linke, J., Makhlaj, V.A., Medvedev, A.V., Malykhin, S.V., Pestchanyi, S., Pugachev, A.T., Sadowski, M.J., Skladnik-Sadowska, E., Tereshin, V.I.
Experimental simulation of ITER ELMs impacts to the tungsten surfaces with QSPA Kh-50.
23rd IAEA Fusion Energy Conference, Daejeon, Korea, October 11-16, 2010

Henderson, M., Albajar, F., Alberti, S., Baruch, U., Bigelow, T., Becket, B., Bertizzolo, R., Bonicelli, T., Bruschi, A., Caughman, J., Chavan, R., Cirant, S., Collazos, A., Cox, C., Darbos, C., deBaar, M., Denisov, G., Farina, D., Gandini, F., Gassman, T., Goodman, T.P., Heidinger, R., Hogge, J.P., Illy, S., Jean, O., Jin, J., Kajiwara, K., Kasparek, W., Kasugai, A., Kern, S., Kobayashi, N., Kumric, H., Landis, J.D., Moro, A., Nazare, C., Oda, J., Omori, T., Pagonakis, I., Piosczyk, B., Platania, P., Plaum, B., Poli, E., Porte, L., Saibene, G., Sakamoto, K., Snachez, F., Scherer, T., Shapiro, M., Sozzi, C., Spaeh, P., Strauss, D., Sauter, O., Takahashi, K., Tanga, A., Temkin, R., Thumm, M., Tran, M.Q., Udintsev, V., Zohm, H., Zucca,. C.
An overview of the ITER EC H&CD system and functional capabilities.
23rd IAEA Fusion Energy Conference, Daejeon, Korea, October 11-16, 2010

Henderson, M., Albajar, F., Alberti, S., Baruch, U., Bigelow, T., Becker, B., Bertizzolo, R., Bonicelli, T., Bruschi, A., Caughman, J., Chavan, R., Cirant, S., Collazos, A., Cox, C., Darbis, C., deBaar, M., Denisov, G., Farina, D., Gandini, F., Gassman, T., Goodman, T.P., Heidinger, R., Hogge, J.P., Illy, S., Jean, O., Jin, J., Kajwara, K., Kasparek, W., Kasugai, A., Kern, S., Kobayashi, N., Kumric, H., Landis, J.D., Moro, A., Nazare, C., Oda, J., Omori, T., Pagonakis, I., Piosczyk, B., Platania, P., Plaum, B., Poli, E., Porte, L., Saibene, G., Sakamoto, K., Sanchez, F., Scherer, T., Shapiro, M., Sozzi, C., Spaeh, P., Strauss, D., Sauter, O., Takahashi, K., Tanga, A., Temkin, R., Thumm, M., Tran, M.Q., Udintsev, V., Zohm, H., Zucca, C.
EC H&CD system for ITER.
16th Joint Workshop on Electron Cyclotron Emission and Electron Cyclotron Resonance Heating, Sanya, China, April 12-15, 2010. Book of Abstracts

Igithkanov, Yu., Bazylev, B., Landman, I.
Calculation of runaway electron stopping power in ITER.
19th Int. Symp. on Plasma Surface Interactions in Controlled Fusion Devices (PSI-19), San Diego, CA, May 24-28, 2010.
Book of Abstracts S. 199

Igitkhanov, Yu., Bazylev, B.
Electric field and hot spots formation.
26th Symp. on Fusion Technology (SOFT 2010), Porto, P., September 27 – October 1, 2010

Illy, S., Flamm, J., Gantenbein, G., Jin, J., Kern, S., Piosczyk, B., Rzesnicki, T., Samartsev, A., Schlaich A., Thumm, M.
Recent experimental results of the 2 MW, 170 GHz European pre-prototype coaxial-cavity gyrotron for ITER.
37th IEEE Int. Conf. on Plasma Science (ICOPS 2010), Norfolk, VA, June 20-24, 2010. Book of Abstracts S. 234

Jin, J., Kern, S., Rzesnicki, T., Thumm, M.
Improved design of a quasi-optical mode converter for the coaxial-cavity ITER gyrotron.
16th Joint Workshop on Electron Cyclotron Emission and Electron Cyclotron Resonance Heating, Sanya, China, April 12-15, 2010. Book of Abstracts

Jin, J., Flamm, J., Kern, S., Rzesnicki, T., Thumm, M.
Theoretical and experimental investigation of a quasi-optical mode converter for a coaxial-cavity gyrotron.
ITG Vacuum Electronics Workshop, Bad Honnef, November 15-16, 2010

Klimov, N., Podkovyrov, V., Zhitlukhin, A., Kovalenko, D., Landman, I., Pestchanyi, S., Bazylev, B., Janeschitz, G., Loarte, A., Merola, M., Hirai, T., Linke, J., Compan, J., Federici, G., Riccardi, B., Mazul, I., Giniyatulin, R., Khimchenki, L.
Experimental study of PFCs erosion and eroded material deposition under ITER-like transient loads at plasma gun facility QSPA.
19th Int. Symp. on Plasma Surface Interactions in Controlled Fusion Devices (PSI-19), San Diego, CA, May 24-28, 2010. Book of Abstracts S. 51

Landman, I.S.
Tokamak code TOKES. Models and implementation.
4th Alushta Int. Conf. on Plasma Physics, Alushta, UA, September 13-19, 2010

Landman, I.S., Pestchanyi, S.E., Igitkhanov, Y., Pitts, R.
Two-dimensional modelling of disruption mitigation by massive gas injection.
26th Symp. on Fusion Technology (SOFT 2010), Porto, P., September 27 – October 1, 2010

Lehnen, M., Alonso, A., Arnoux, G., Baumgarten, N., Bozhenkov, S.A., Brezinsek, S., Brix, M., Eich, T., Huber, A., Jachmich, S., Kruezi, U., Morgan, P.D., Plyusnin, V.V., Reux, C., Riccardo, V., Sergienko, G., Stamp, M.F., Thornton, A., Koltunov, M., Tokar, M., Bazylev, B., Landman, I., Pestchanyi, S., JET EFDA Contributors
Disruption mitigation by massive gas injection in JET.
23rd IAEA Fusion Energy Conference, Daejeon, Korea, October 11-16, 2010

Litnovsky, A., Philipps, V., Wienhold, P., Kreter, A., Kirschner, A., Matveev, D., Brezinsek, S., Sergienko, G., Pospieszczyk, A., Schweer, B., Schulz, C., Schmitz, O., Coenen, J.W., Samm, U., Krieger, K., Hirai, T., Emmoth, B., Rubel, M., Bazylev, B., Breuer, U., Stärk, A., Richter, S., Komm, M., TEXTOR Team
Overview of material migration and mixing, melting, fuel retention and cleaning of ITER-like castellated structures in TEXTOR.
19th Int. Symp. on Plasma Surface Interactions in Controlled Fusion Devices (PSI-19), San Diego, CA, May 24-28, 2010. Book of Abstracts S. 73

Loarte, A., Campbell, D., Gribov, Y., Pitts, R.A., Klimov, N., Podkovyrov, V., Zhitlukhin, A., Landman, I., Pestchanyi, S., Bazylev, B., Linke, J., Loewenhoff, T., Pintsuk, G., Schmitz, O., Liang, Y., Evans, T.E. Schaffer, M., Fenstermacher, M.E., Becoulet, M., Huysmans, G., Nardon, E., Baylor, L., Canik, J., Maingi, R., Ahn, J.W., Riccardi, B., Saibene, G., Sartori, R., Cavinato, M., Eich, T., Jakubowski, M., Lang, P.T., Thomson, H., Suttrop, W., Da la Luna, E., Wilson, H., Kirk, A.
ITER-ELM control requirements, ELM control schemes and required R&D.
23rd IAEA Fusion Energy Conference, Daejeon, Korea, October 11-16, 2010

Neudorfer, J., Stindl, T., Stock, A., Schneider, R., Petkow, D., Roller, S., Munz, C.D., Auweter-Kurtz, M.
Three-dimensional simulation of rarefied plasma flows using a high order particle in cell method.
13th Results and Review Workshop of the HLRS, Stuttgart, October 4-5, 2010

Omori, T., Henderson, M.A., Albajar, F., Alberti, S., Baruah, U., Bigelow, T., Beckett, B., Bertizzolo, R., Bonicelli, T., Bruschi, A., Caughman, J., Chaven, R., Cirant, S., Collazos, A., Cox, C., Darbos, C., deBaar, M., Denisov, G., Farina, D., Gandini, F., Gassmann, T., Goodman, T.P., Heidinger, R., Hogge, J.P., Illy, S., Jean, O., Jin, J., Kajiwara, K., Kasparek, W., Kasugai, A., Kern, S., Kobayashi, N., Kumric, H., Landis, J.D., Moro, A., Nazare, C., Oda, J., Pagonakis, I., Piosczyk, B., Platania, P., Plaum, B., Poli, E., Porte, L., Purohit, D., Ramponi, G., Rao, S.L., Rasmussen, D., Ronden, D., Rzesnicki, T., Saibene, G., Sakamoto, K., Sanchez, F., Scherer, T., Shapiro, M., Sozzi, C., Spaeh, P., Strauss, D., Sauter, O., Takahashi, K., Temkin, R., Thumm, M., Tran, M.Q., Udintsev, V., Zohm, H.
Overview of the ITER EC H&CD system and its capabilities.
26th Symp. on Fusion Technology (SOFT 2010), Porto, P, September 27-October 1, 2010

Pagonakis, I.G., Hogge, J.P., Alberti, S., Piosczyk, B., Illy, S., Kern, S., Lievin, C.
An additional criterion for gyrotron gun design.
37th IEEE Int. Conf. on Plasma Science (ICOPS 2010), Norfolk, VA, June 20-24, 2010. Book of Abstracts S. 236

Pestchanyi, S.
Modeling of brittle destruction of W surfaces under repetitive loads.
ITPA Technical Group Meeting, Seoul, Korea, October 16-21, 2010

Pestchanyi, S.
Modeling of brittle destruction of ITER armour under repetitive loads.
ITPA Technical Group Meeting, Seoul, Korea, October 16-21, 2010

Pestchanyi, S., Garkusha, I., Landman, I.
Simulation of residual thermostress in tungsten after repetitive.
26th Symp. on Fusion Technology (SOFT 2010), Porto, P, September 27 – October 1, 2010

Rzesnicki, T., Piosczyk, B., Roy Choudhury, A., Illy, S., Jin, J., Kern, S., Samartsev, A., Schlaich, A., Thumm, M.
Recent improvements on the 2 MW, 170 GHz coaxial-cavity pre-prototype gyrotron.
ITG Vacuum Electronics Workshop, Bad Honnef, November 15-16, 2010

Schlaich, A., Flamm, J., Gantenbein, G., Kern, S., Samartsev, A., Thumm, M.
Characterization of undesired RF oscillations in megawatt gyrotrons.
ITG Vacuum Electronics Workshop, Bad Honnef, November 15-16, 2010

Schlaich, A., Flamm, J., Gantenbein, G., Kern, S., Latsas, G., Rzesnicki, T., Samartsev, A., Thumm, M., Tigelis, I., Zwick, T.
Erweiterung der Gyrotron-Frequenzmesstechnik.
Treffen des Kompetenzbereichs Systeme und Prozess, KIT, Karlsruhe, 24.-25. März 2010

Schlaich, A.
Investigations on parasitic oscillations in megawatt gyrotrons.
KIT PhD Symp., Karlsruhe, 30. September 2010

Schmid, M., Erckmann, V., Gantenbein, G., Illy, S., Kern, S., Lievin, Ch., Samartsev, A., Schlaich, A., Rzesnicki, T., Thumm, M.
Technical developments at the KIT gyrotron test facility.
26th Symp. on Fusion Technology (SOFT 2010), Porto, P, September 27 – October 1, 2010

Schreck, S., Aiello, G., Gantenbein, G., Meier, A., Scherer, T.A. Spaeh, P., Strauss, D., Vaccaro, A.
Prototype manufacturing and testing of components of the ECH upper launcher for ITER.
23rd IAEA Fusion Energy Conference, Daejeon, Korea, October 11-16, 2010

Stober, J., Wagner, D., Gianone, L., Leuterer, F., Monaco, F., Maraschek, M., Mlynek, A., Mszanowski, U., Münich, M., Poli, E., Reich, M., Schmid-Lorch, D., Schütz, H., Schwinzer, J., Treutterer, W., Zohm, H., ASDEX Upgrade Team, Meier, A., Scherer, T., Flamm, J., Thumm, M., Höhnle, H., Kasparek, W., Stroth, U., Litvak, A., Denisov, G.G., Chirkov, A.V., Tai, E.M., Popov, I.G., Nichiporenko, V.O., Myasnikov, V.E., Soluyanova, E.M., Malygin, S.A.
ECRH on ASDEX upgrade. System extension, new modes of operation, plasma physics results.
16th Joint Workshop on Electron Cyclotron Emission and Electron Cyclotron Resonance Heating, Sanya, China, April 12-15, 2010. Book of Abstracts

Thumm, M.
Progress on gyrotrons for ITER and future thermonuclear fusion reactors.
37th IEEE Int. Conf. on Plasma Science (ICOPS 2010), Norfolk, VA, June 20-24, 2010. Book of Abstracts S. 333

Vaccaro, A., Aiello, G., Gantenbein, G., Meier, A., Scherer, T., Schreck, S., Spaeh, P., Strauss, D.
Silicon oil DC200(R)5cSt as an alternative coolant for CVD diamond windows.
16th Joint Workshop on Electron Cyclotron Emission and Electron Cyclotron Resonance Heating, Sanya, China, April 12-15, 2010. Book of Abstracts

Patents:

Dammertz, G., Erckmann, V., Schmid, M.
Method and apparatus for collector sweeping control of an electron beam.
JP-OS 2010 526 417 (2010.07.29)

Program: NANOMIKRO

Books, book chapters

Link, G., Thumm, M., Faubel, W., Heissler, St., Weidler, P.G.
Investigation of selective microwave heating by use of Raman spectroscopy.
Bansal, N.P. [Hrsg.], Processing and Properties of Advanced Ceramics and Composites II; Hoboken, N.J.: Wiley, 2010
S. 27-34 (Ceramic Transactions; 2010)

Publications at cross-referenced journals:

Arzhannikov, A.V., Burdakov, A.V., Kalinin, P.V., Kuznetsov, S.A., Makarov, M.A., Mekler, K.I., Polosatkin, S.V., Postupaev, V.V., Rovenskikh, A.F., Sinitsky, S.L., Sklyarov, V.F., Stepanov, V.D., Sulyaev, Yu.S., Thumm, M.K.A., Vyacheslavov, L.H.
Subterahertz generation by strong Langmuir turbulence at two-stream instability of high current 1 MeV REBs.
Terahertz Quasi-Optics, 5(2010) Nr. 4, S. 44-49

Kesari, V., Purohit, N., Thumm, M.
Analysis of ohmic quality factor of circumferentially corrugated circular cavities.
Journal of Infrared Millimeter and Terahertz Waves, 31(2010) S. 510-20
DOI:10.1007/s10762-009 - 9604-5

Konoplev, I.V., Fisher, L., Cross, A.W., Phelps, A.D.R., Ronald, K., Thumm, M.
Excitation of surface field cavity and coherence of electro-magnetic field scattering on two-dimensional cylindrical lattice.
Applied Physics Letters, 97(2010) S.261102/1-3

Konoplev, I.V., Fisher, L., Ronald, K., Cross, A.W., Phelps, A.D.R., Robertson, C.W., Thumm, M.
Suface-field cavity based on a two-dimensional cylindrical lattice.
Applied Physics Letters, 96(2010) S.231111/1-3
DOI:10.1063/1.3428776

Kühn, J., van Raay, F., Quay, R., Kiefer, R., Mikulla, M., Seelmann-Eggebert, M., Bronner, W., Schlechtweg, M., Ambacher, O., Thumm, M.
Device and design optimization for AlGaN/GaN X-band-power-amplifiers with high efficiency.
Journal of Infrared Millimeter and Terahertz Waves, 31(2010) S.367-79
DOI:10.1007/s10762-009-9583-6

Kuznetsov, S.A., Arzhannikov, A.V., Gelfand, A.V., Kubarev, V.V., Navarro-Cia, M., Beruete, M., Falcone, F., Sorolla,M., Thumm, M.
Microstructured quasi-optical selective components for subterahertz and terahertz applications.
Terahertz Quasi-Optics, 5(2010) Nr. 4, S.79-90

Thumm, M.
High power microwave and millimeter-wave technology.
160th ISIJ Meeting, Sapporo, J., Sepember 25-27, 2010
Current Advances in Materials and Processes, 23(2010) S.838-41 (CD-ROM)

Zhang, S.C., Thumm, M.
Terahertz transverse-magnetic-wave cyclotron auto-resonance maser with a large-orbit relativistic electron beam.
Physics Letters A, 374(2010) S.1745-48
DOI:10.1016/j.physleta.2010.02.019

Other printed publications:

Kosuga, K., Idehara, T., Ikeda, R., Tatematsu, Y., Ogawa, I., Misudo, S., Saito, T., Agusu, L., Mudiganti, J.C., Thumm, M.
Development of THz gyrotron FU CW III using a 20 T superconducting magnet.
35th Int. Conf. on Infrared, Millimeter and Terahertz Waves (IRMMW-THz 2010), Roma, I, September 5-10, 2010. Proc on USB-Stick

Kosuga, K., Idehara, T., Ikeda, R., Ogawa, I., Mitsudo, S., Saito, T., Agusu, L., Thumm, M.
Development of THz gyrotron using a 20 T superconducting magnet.
3rd Int. Workshop on Far-Infrared Technologies (IW-FIRT 2010), Fukui, J, March 15-17, 2010. Abstracts S. 73. Proc. on CD-ROM

Kühn, J., van Raay, F., Quay, R., Kiefer, R., Maier, T., Stibal, R., Mikulla, M., Seelmann-Eggebert, M., Bronner, W., Schlechtweg, M., Ambacher, O., Thumm, M.
Design of highly-efficient GaN X-band-power-amplifier MMICs.
2009 IEEE MTT-S Int. Microwave Symp. (IMS 1009), Boston, Mass., June 7-12, 2009. Piscataway, N.J.: IEEE, 2009
S. 661-64; also publ. online

Kuznetsov, S.A., Arzhannikov, A.V., Gelfand, A.V., Kubarev, V.V., Navarro-Cia, M., Beruete, M., Falcone, F., Sorolla, M., Thumm, M.
Microstructured quasi-optical selective components for subterahertz and terahertz applications.
Terahertz Quasi-Optics, 5(2010) Nr. 4, S.79-90

Link, G., Thumm, M., Faubel, W., Heissler, St., Weidler, P.G.
Raman spectroscopy for experimental investigation of microscale selective microwave heating.
Materials Science and Technology Conf. and Exhibition (MS&T 2010), Houston, Tex., October 17-21, 2010
Proc. on CD-ROM S. 2936

Phelps, A.D.R., Konoplev, I.V., Fisher, L., Cross, A.W., Ronald, K., Robertson, C.W., Thumm, M.
Surface field cavity based on a two-dimensional cylindrical lattice.
35th Int. Conf. on Infrared, Millimeter and Terahertz Waves (IRMMW-THz 2010), Roma, I, September 5-10, 2010.
Proc. on USB-Stick

Singh, U., Kumar, N., Alaria, M.K., Purohit, L.P., Sinha, A.K., Piosczyk, B., Thumm, M., Gantenbein, G.
Effect of beam tunnel geometry on electron beam parameters for 42 GHz gyrotron.
11th Int. Vacuum Electronics Conf. (IVEC 2010), Monterey, CA, May 18-20, 2010, Proc. S.357-58, Piscataway, N.J.: IEEE, 2010

Papers or lectures, which are not available in printed form:

Krishna, P.V., Kartikeyan, M.V., Thumm, M.
Mode selection and launcher design for a 95 GHz, 100 kW, CW gyrotron.
Int. Conf. on Microwave Antenna, Propagation and Remote Sensing (ICMARS-2010), Jodhpur, IND, December 14-17, 2010

Link, G.
A review on microwave processing activities at the Karlsruhe Institute of Technology
Vortr.: Universidade Federal de Sao Carlos, Sao Paulo, BR, 5. Oktober 2010

Link, G.
Basics in microwave processing (eingeladen)
Vortr.: Universidade Federal de Sao Carlos, Sao Paulo, BR, 18. September 2010

Thumm, M.
Historische deutsche Beiträge zur Theorie und Anwendung von elektromagnetischen Oszillationen und Wellen.
Vortr.: VDE Bezirksverein Mittelbaden, Karlsruhe, 19. Oktober 2010

Program: NUKLEAR

Publications at cross-referenced journals:

Rineiski, A., Kessler, G.
Proliferation-resistant fuel options for thermal and fast reactors avoiding neptunium production.
Nuclear Engineering and Design, 240(2010) S.500-510
DOI:10.1016/j.nucengdes.2009.11.003

Other printed publications:

An, W., Fetzer, R., Müller, G., Weisenburger, A., Engelko, V.
Origin and development of surface waviness due to intense pulsed electron beam treatment.
3rd Euro-Asia Pulsed Power Conf. / 18th Int. Conf. on High-Power Particle Beams (EAPPC-BEAMS 2010), Jeju, Korea, October 10-14, 2010. Book of Abstracts S.284. Proc. on USB-Stick

D'Andrea, D., Maschek, W., Schneider, R.
Charged particle collisions for particle simulation methods.
Int. Topical Meetg. on Nuclear Applications and Utilization of Accelerators (AccApp'09), Wien, A, May 4-8, 2009
Proc. on CD-ROM Paper AT/RD-05. Wien:IAEA, 2010 (Proceedings Series) IAEA-I3-CN-173

DelGiacco, M., Jianu, A., Spieler, P., Weisenburger, A., Müller, G.
Fretting tests in liquid lead alloy – concept and test facility.
1st Int. Conf. on Materials for Energy, Karlsruhe, July 4-8, 2010.
Extended Abstracts Book A S. 278-80
Frankfurt a.M.: Dechema, 2010

Fazio, C., Rieth, M., Linday, R., Aktaa, J., Schneider, H.C., Konys, J., Yurechko, M., Müller, G., Weisenburger, A., Knebel, J.U.
Structural and cladding materials development and characterisation for innovative nuclear waste transmutation systems.
1st Int. Conf. on Materials for Energy, Karlsruhe, July 4-8, 2010.
Extended Abstracts Book A S. 193-95
Frankfurt a.M.: Dechema, 2010

Kieser, M.
Untersuchung der Korrosionseigenschaften von Strukturwerkstoffen für Pumpen in mit flüssigem Blei gekühlten Transmutationsanlagen und Aufbau eines Erosionsprüfstandes.
Dissertation, Universität Karlsruhe 2009

Müller, G., Engelko, V., Rusanov, A.
Increasing corrosion resistance of 1.4970 and T-91 steels exposed to heavy liquid metal with the help of microsecond-pulsed intense electron beam.
10th Int. Conf. on Modification of Materials with Particle Beams, Tomsk, Russia, September 19-24, 2010. Proc. on CD-ROM.
Tomsk : Publishing House of the IAO SB RAS, 2010, pp. 261-264

Müller, G., An, W., Berghöfer, T., DelGiacco, M., Eing, Ch., Fetzer, R., Flickinger, B., Frey, W., Giese, H., Göttel, M., Gusbeth, C., Heinzel, A., Sträßner, R., Wegner, L., Weisenburger, A., Zimmermann, F., Engelko, V.
Progress in high power-particle beams and pulsed power applications at Karlsruhe Institute of Technology.
3rd Euro-Asian Pulsed Power Conf. / 18th Int. Conf. on High-Power Particle Beams (EAPPC-BEAMS 2010), Jeju, Korea, October 10-14, 2010. Book of Abstracts S. 305. Proc. on USB-Stick

Muscher, H., Kieser, M., Weisenburger, A., Müller, G.
Untersuchung der Ursachen des steilen Abfalls der Geschwindigkeit von Blei im Ringspalt eines ADS-Erosionsprüfstandes.
Jahrestagung Kerntechnik 2010, Berlin, 4.-6. Mai 2010
Berlin: INFORUM GmbH, 2010, CD-ROM Paper 1211

Weisenburger, A., Jianu, A., Heinzel, A., DelGiacco, M., Müller, G.
Pulsed E-beams to improve corrosion barriers for lead alloy cooled reactors: Overview and dedicated mechanical tests.
1st Int. Conf. on Materials for Energy, Karlsruhe, July 4-8, 2010.
Extended Abstracts Book A S.227-29. Frankfurt a.M.: Dechema, 2010

Papers or lectures, which are not available in printed form:

DelGiacco, M., Jianu, A., Spieler, P., Weisenburger, A., Müller, G.
Fretting corrosion tests in liquid lead alloy – concept and test facility.
The Nuclear Materials Conf. (NuMat 2010), Karlsruhe, October 4-7, 2010

Engelko, V., Müller, G.
Multi-arc source of intense large area microsecond electron beams.
3rd Euro-Asian Pulsed Power Conf. (EAPPC 2010) and 18th Int. Conf. on High-Power Beams (BEAMS 2010), Jeju Island, Korea, October 11-15, 2010. Book of Abstracts S. 270

Fazio, C., Rieth, M., Linday, R., Aktaa, J., Schneider, H.C., Konys, J., Yurechko, M., Müller, G., Weisenburger, A.
Activities performed within the program of nuclear safety research on structural and cladding materials for innovative reactor system able to transmute nuclear waste.
Joint EC-IAEA Topical Meeting on Development of New Structural Materials for Advanced Fission and Fusion Reactor Systems, Barcelona, E, October 5-9, 2009

Fazio, C., Van den Bosch, J., Munoz, F.J.M., Henry, J., Roelofs, F., Turroni, P., Mansani, L., Weisenburger, A., Gorse, D., Abella, J., Brissonneau, L., Dai, Y., Magielsen, L., Neuhasen, J., Vladimirov, P., Class, A., Jeanmart, H., Ciampichetti, A., Gerbeth, G., Wetzel, T., Karbojian, A., Litfin, K., Tarantino, M., Zanini, L.
Development and assessment of structural materials and heavy liquid metal technologies for transmutation systems (DEMETRA): highlights on major results.
Technology and Components of Accelerator-Driven Systems (TCADS 2010), Karlsruhe, March 15-17, 2010. Book of Abstracts S.24

Heinzel, A., Hartmann, C.
Schwerpunkte der nuklearen Sicherheitsforschung am Karlsruher Institut für Technologie (KIT).
DAtF-Kolloquium zur Berufsorientierung, Frankfurt, 14.-17. März 2010

Kessler, G.
The future development of fission reactors and their fuel cycles.
Vortrag Max-Planck-Institut für Physik, München, 4. Mai 2010

Müller, G., Weisenburger, A., Jianu, A., Heinzel, A.
FeCrAl based corrosion barriers for HLM cooled systems.
11th Information Exchange Meeting on Actinide and Fission Product Partitioning and Transmutation, San Francisco, CA, November 1-5, 2010

Müller, G., Weisenburger, A., An, W., Jianu, A., Markov, V.G., Kashtanov, A.D.
Improving the creep resistance of steels exposed to heavy liquid metals by surface modification/alloying using intense pulsed electron beams.
The Nuclear Materials Conf. (NuMat 2010), Karlsruhe, October 4-7, 2010

Weisenburger, A., DelGiacco, M., Jianu, A., Müller, G.
Compatibility of different steels and alloys with lead up to 750 °C.
1st Int. Workshop on Technology and Components of Accelerator-driven Systems (ADS), Karlsruhe, March 15-17, 2010. Book of Abstracts S.40

Weisenburger, A., Jianu, A., Heinzel, A., DelGiacco, M., Müller, G., Markov, V.D., Kastanov, A.D.
Corrosion barrier development using electron beams for application in lead alloys with focus on recent creep to rupture tests.
2nd Int. Workshop on Structural Materials for Innovative Nuclear Systems, Daejeon, Korea, August 31 – September 3, 2010

Weisenburger, A., Schroer, C., Heinzel, A., Konys, J., Steiner, H., Müller, G., Fazio, C., Gessi, A., Babayan, S., Kobzova, A., Martinelli, L., Ginestar, K., Martin-Munoz, F.J., Soler Crespo, L.
Long-term corrosion on T91 and AISI 316L steel in flowing lead alloy and corrosion protection barrier: experiments and models.
Int. DEMETRA Workshop on Development and Assessment of Structural Materials and Heavy Liquid Metal Technologies for Transmutation Systems, Berlin, March 2-4, 2010

Weisenburger, A., Jianu, A., Heinzel, A., DelGiacco, M., Müller, G.
Pulsed E-beams to improve corrosion barriers for lead alloy cooled reactors: overview and dedicated mechanical tests.
18th Int. Conf. on Nuclear Engineering (ICONE-18), Xi'an, China, May 17-21, 2010.
10th Int. Workshop on Spallation Materials Technology (IWSMT), Beijing, China, October 18-22, 2010

Patents:

Bluhm, H.J., Fütterer, M., Hoppe, P., Singer, J.
A head-end process for the reprocessing of reactor core material.
EP-OS 1 849 164 (2007.10.31)
EP-PS 1 849 164 (2008.07.09)
CN-OS 101 138 051 (2008.03.05)
UA-PS 88680 (2009.08.05)
CN-PS 101 138 051 (2010.09.29)
RU-PS 2 395 127 (2010.02.02)

Program ENERGY (EE)

Books, book chapters

Wegner, L.H.
Oxygen transport in waterlogged plants.
Mancuso, S. [Hrsg.] Waterlogging Signalling and Tolerance in Plants
Part I: Whole-Plant Regulation
Berlin [u.a.]: Springer, 2010, S. 3-22

Publications at cross-referenced journals:

Flickinger, B., Berghöfer, T., Hohenberger, P., Eing, C., Frey, W.
Transmembrane potential measurements on plant cells using the voltage-sensitivity dye ANNINE-6.
Protoplasma, 247(2010) S.3-12
DOI:10.1007/s00709-010-0131-y

Sack, M., Sigler, J., Eing, C., Stukenbrock, L., Stängle, R., Wolf, A., Müller, G.
Operation of an electroporation device for grape mash.
IEEE Transactions on Plasma Science, 38(2010) S.1928-34
DOI:10.1109/TPS.2010.2050073

Sack, M., Sigler, J., Frenzel, S., Eing, Chr., Arnold, J., Michelberger, Th., Frey, W., Attmann, F., Stukenbrock, L., Müller, G.
Research on industrial-scale electroporation devices fostering the extraction of substances from biological tissue.
Food Engineering Reviews, 2(2010) S.147-56
DOI:10.1007/s12393-010-9017-1

Shabala, Se., Shabala, Sv., Cuin, T.A., Pang, J., Percey, W., Chen, Z., Conn, S., Eing, C., Wenger, L.H.
xylem ionic relations and salinity tolerance in barley.
The Plant Journal, 61(2010) S. 839-53
DOI:10.1111/j.1365-313X.2009.04110.x

Zimmermann, U., Rüger, S., Shapira, O., Westhoff, M., Wegner, L.H., Reuss, R., Gessner, P., Zimmermann, G., Israeli, Y., Zhou, A., Schwartz, A., Bamberg, E., Zimmermann, D.
Effects of environmental parameters and irrigation on the turgor pressure of banana plants measured using the non-invasive, online monitoring leaf patch clamp pressure probe.
Plant Biology, 12(2010) S.424-36
DOI:10.1111/j.1438-8677.2009.00235.x

Other printed publications:

Attmann, F., Sack, M., Wolf, A., Müller, G.
Measurement of the heat transfer from a spark gap electrode through its connection rod.
3rd Euro-Asian Pulsed Power Conf. (EAPPC2010) and 18th Int. Conf. on High-Power Beams (BEAMS 2010), Jeju Island, Korea, October 11-15, 2010, Book of Abstracts S. 82, Proc. on USB-Stick

Flickinger, B.
Nanosekunden-zeitaufgelöste Messungen der Plasma-membranaufladung pflanzlicher Zellen.
Dissertation, Karlsruher Institut für Technologie 2010.
KIT Scientific Reports, KIT-SR 7562 (November 2010)

Sack, M., Stängle, R., Müller, G.
Over-voltage trigger device for Marx generators.
3rd Euro-Asian Pulsed Power Conf. (EAPPC 2010) and
18th Int. Conf. on High-Power Beams (BEAMS 2010), Jeju
Island, Korea, October 11-15, 2010. Book of Abstracts S.246.
Proc. on USB-Stick

Papers or lectures, which are not available in printed form:

Attmann, F., Sack, M., Müller, G.
Spark gap erosion in Marx generators for electroporation.
12th Int. Conf. on Optimization of Electrical and Electronic
Equipment (OPTIM 2010), Brasov, R, May 20-22, 2010

Attmann, F., Sack, M.
Spark gap erosion in Marx generators for electroporation.
ISP-PhD Congress, Karlsruhe, 17.-18. Februar 2010

Berghöfer, T., Flickinger, B., Eing, C., Sack, M., Hohen-berger,
P., Nick, P., Pacher, M., Puchta, H., Frey, W.
Effects of microsecond- and nanosecond-pulsed-electric-fields
on plant cells.
Frühjahrstagung DPG, Symp. Plasma in Biology and Medicine,
Hannover, 8.-12. März 2010
Verhandlungen der Deutschen Physikalischen Gesellschaft,
R.6, B.45(2010) SYMP 1.7

Berghöfer, T., Eing, C., Flickinger, B., Frey, W., Hohen-berger,
P., Wegner, L., Nick, P.
Effects of nanosecond pulsed electric fields (nsPEF) on the
cytoskeleton of plant cells.
37th IEEE Int. Conf. on Plasma Science (ICOPS 2010), Norfolk,
VA, June 20-24, 2010, Book of Abstracts S. 185

Berghöfer, T., Eing, C., Flickinger, B., Hohenberger, P.,
Wegner, L., Nick, P., Frey, W.
Specific responses of actin filaments and microturbules in plant
cells exposed to nanosecond pulsed electric fields (nsPEF).
Bioelectrics Symp., Norfolk, VA, June 25-26, 2010

Berghöfer, Th., Flickinger, B., Eing, C., Frey, W., Pacher, M.,
Puchta, H.
Nanosecond pulsed electric fields affect the growth of plants
and fungi.
ISP-PhD Congress, Karlsruhe, 17.-18. Februar 2010

Flickinger, B., Berghöfer, T., Eing, C.J., Pacher, M., Puchta, H.,
Frey, W.
Growth stimulation of plants and fungi exposed to ultrashort
electric fields.
Bioelectrics Symp., Norfolk, VA, June 25-26, 2010

Flickinger, B., Berghöfer, T., Eing, C., Frey, W., Pacher, M.,
Puchta, H.
Nanosecond pulsed electric fields affect the growth of plants
and fungi.
37th IEEE Int. Conf. on Plasma Science (ICOPS 2010), Norfolk,
VA, June 200-24, 2010. Book of Abstracts S. 185

Flickinger, B.
Transmembrane potential measurements on plant cells using
the voltage-sensitive fluorescence dye ANNINE-6.
ISP-PhD Congress, Karlsruhe, 17.-18. Februar 2010

Frey, W., Sack, M., Gusbeth, C., Eing, C., Berghöfer, T.,
Sträßner, R., Göttel, M., Stängle, R., Wolf, A., Leber, K.,
Wüstner, R.
Konditionierung von Biomasse mit gepulsten elektrischen
Feldern.
EE-Topictreffen, KIT, Karlsruhe, 20. April 2010, Folien auf CD-
ROM

Frey, W., Flickinger, B., Berghöfer, T.
Measurement of the azimuthal membrane voltage distribution at
by-2 protoplasts exposed to ns pulsed electric fields.
37th IEEE Int. Conf. on Plasma Science (ICOPS 2010), Norfolk,
VA, June 20-24, 2010. Book of Abstracts S.345

Gusbeth, C.A., Sträßner, R., Frey, W.
Lifetime and design considerations for anodes for pulsed
underwater corona discharges.
37th IEEE Int.Conf. on Plasma Science (ICOPS 2010), Norfolk,
VA, June 20-24, 2010, Book of Abstracts S. 416

Müller, G.
Status on application of intense pulsed e-beams and
electrodynamic fragmentation at Karlsruhe Institute of
Technology (KIT).
Int. COE Forum on Pulsed Power Engineering and Young
Researcher Training Camp, Kagoshima, J, Sept. 27-29, 2010

Sack, M., Müller, G.
Electrical design of electroporation reactors.
12th Int. Conf. on Optimization of Electrical and Electronic
Equipment (OPTIM 2010), Brasov, R, May 20-22, 2010

Sack, M., Attmann, F., Müller, G.
EMV-Aspekte beim Entwurf einer Elektroporationsanlage.
Int. Fachmesse und Kongress für elektromagnetische
Verträglichkeit (EMV), Düsseldorf, 9.-11. März 2010

Sigler, J., Sack, M., Eing, C., Müller, G., Waidelich, G.
Elektroporation zum verbesserte Aufschluss von Trauben und
Maische.
Intervitis Interfructa: Int. Technologiemesse für Wein, Obst,
Fruchtsaft und Spirituosen, Stuttgart, 24.-28. März 2010

Wegner, L.H.
Elucidation of membrane transport processes in the giant
marine alga valonia ultricularis by employing the charge pulse
relaxation technique.
BioEM 2009: Joint Meering of the Bioelectromagnetics Society
(BEMS) and the European BioElectromagnetics Association
(EBEA), Davos, CH, June 14-19, 2009. Book of Abstracts S. 51

Patents:

Berghöfer, T., Bluhm, H.J., Eing, C., Sack, M.
Elektroporationsreaktor und Verfahren zum druckbehafteten
Elektroporieren von biologischem Nutz- und Abfallgut.
DE-OS 10 2009 011 755 (2010.09.16)

Giese, H., Hoppé, P.
Aufbau einer elektrodynamischen Fraktionieranlage.
Electrodynamic fractionation plant.
DE-PS 10 346 055 (2004.08.06)
EP-OS 1 667 798 (2006.06.14)
CN-OS 1 863 601 (2006.11.15)
RU-PS 2 311 961 (2007.12.10)
JP-PS 4 388 959 (2009.10.09)
AU-PS 2004 277 317 (2010.01.21)
EP-PS 1 667 798 (2010.12.29)
US-PS 7 677 486 (2010.03.16)

Giese, H., Frey, W., Sträßner, R., Schormann, A., Giron, K.
Verfahren zum Betreiben einer Fragmentieranlage und
Fragmentieranlage zur Durchführung des Verfahrens.
DE-PS 10 342 376 (2005.02.03)
EP-OS 1 663 498 (2006.06.07)
RU-OS 2006 112 208 (2006.08.27)
RU-PS 2 326 736 (2008.06.20)
AU-PS 2004 274 091 (2008.07.17)
US-OS 2008/0283639 (2008.11.20)
CA-PS 2 555 476 (2010.05.18)
EP-PS 1 663 498 (2010.11.17)

Sack, M.
Verfahren für den kontinuierlichen, getriggerten Betrieb eines
Marx-Generators insbesondere von mehreren Marx-
Generatoren zur Druckregelung und Abbranddetektion in den
Funkenstrecken.
DE-OS 10 2005 025 998 (2006.12.21)
EP-OS 1 889 363 (2008.02.20)
EP-PS 1 889 363 (2010.08.04)

Sack, M.
Verfahren zur Reduktion pulsförmiger Erdströme an einem
elektrischen Großgerät und Kompensationsschaltung zur
Erdstromverlagerung.
DE-OS 10 2008 024 348 (2009.12.03)
DE-PS 10 2008 024 348 (2010.04.20)

Schultheiss, C., Kern, M.
Elektroporationsreaktor zur kontinuierlichen Prozessierung von
stückigen Produkten.
DE-PS 10 144 479 (2003.04.03)
EP-OS 1 424 910 (2004.06.09)
EP-PS 1 424 910 (2007.04.25)
HU-OS 0 401 095 (2004.09.28)
PL-OS 367 363 (2005.02.21)
PL-PS 199 833 (2008.11.28)
MD-PS 3640 (2009.08.27)
CA-PS 2 460 569 (2010.05.11)

Schultheiss, C.
Verfahren zum kontinuierlichen nichtthermischen Aufschluß und
Pasteurisieren industrieller Mengen organischen Prozessguts
durch Elektroporation und Reaktor zum Durchführen des
Verfahrens.
Method and reactor for the non-thermal decomposition and
pasteurisation of organic process materials by electroporation.
DE-PS 10 144 486 (2002.11.11)
EP-OS 1 425 104 (2004.06.09)
PL-OS 367 359 (2005.02.21)
US-PS 7 691 324 (2010.04.06)

Program: Efficient Energy Use and Conversion (REUN)

Publications at cross-referenced journals:

Melcher, A., Unser, A., Reichhardt, M., Nestler, B., Pötschke, M., Selzer, M.
Conversion of EBSD data by a quaternion based algorithm to be used for grain structure simulations.
Technische Mechanik, 30(2010) S. 401-13

Van Phan, T., Jöchen, K., Melcher, A., Böhlke, T.
Deep drawing simulations based on microstructural data.
Proceedings in Applied Mathematics and Mechanics, 10(2010) S.69-70
DOI:10.1002/pamm.201010027

Other printed publications:

Van Phan, T., Jöchen, K., Melcher, A., Böhlke, T.
Zweiskalenmodellierung von Umformprozessen.
Graduiertenkolleg 1483: Prozessketten in der Fertigung:
Wechselwirkung, Modellbildung und Bewertung von
Prozesszonen; Begleitband zur 1. jährlichen Klausurtagung,
Bad Herrenalb, 25.-26. Februar 2010

Papers or lectures, which are not available in printed form:

Feher, L.
Neue energieeffiziente Hochfrequenztechnologien für die
industrielle Produktion von CFK-Strukturen im Verkehrswesen.
Mit kalten Öfen zu energieeffizienten Produktionstechnologien
der Zukunft.
Workshop 'Energieeffiziente Mikrowellen-Produktions-systeme
für Luftfahrt und Automobil-Leichtbau' (EEEfCOM 2010), Ulm,
17. Juni 2010
Vortr.: Fraunhofer-.Einrichtung für Polymermaterialien und
Composite PYCO, Berlin, 1. September 2010

Fehler, L.
Einsatz von Nao-Blends for die Aushärtung von
Faserverbundwerkstoffen in kalten Öfen.
8. NanoVision 2010, Karlsruhe, Dezember 8-9, 2010

Patents:

Feher, L., Link, G.
Hochmodiger Mikrowellenresonator zur thermischen
Prozessierung.
DE-PS 10 329 412 (2005.01.031)
DE-OS 10 329 412 (2005.02.03)
EP-OS 1 494 506 (2005.01.05)
EP-PS 1 494 506 (2010.07.14)

The main working fields of the Institute for Pulsed Power and Microwave Techno-logy have been research, development, academic education and, in collaboration with the KIT Division IMA and industrial partners, the technology transfer in the areas of pulsed power technology and microwave technology at high power levels. The projects of the IHM have been conducted within six HGF Programs: Renewable Energies (EE), FUSION, NUKLEAR, NANOMIKRO, Efficient Energy Conversion and Use (REUN) and Technology-Innovation and Society (TIG). R&D work has been done in the following topics: theoretical and experimental basics of pulsed power and high-power microwave technology; theory and experiments on the generation of intensive electron beams, strong electromagnetic fields and waves and their inter-action with plants, materials and plasmas; application of these methods in the area of generation of energy through controlled thermonuclear fusion in magnetically confined plasmas, in materials processing and in energy technology. Research in both divisions of the IHM require the application of modern electron beam optics, high voltage technology and high voltage measurement techniques. The list of 175 publications in 2010 is enclosed at the end of this report. Dr. Georg Müller, orga-nized in collaboration with the International Society on Pulsed Power Applications e.V. an International Pulsed Power PhD-Congress (2010) at KIT. At the 3rd Euro-Asian Pulsed Power Conference (EAPPC) in Korea Dr. Georg Müller has been elected for the Int. Organizing Committee. At the 2010 IEEE International Vacuum Electronics Conference, in Monterey, CA, USA, Dipl.-Ing. Andreas Schlaich, a PhD student of the Institute for Pulsed Power and Microwave Technology (IHM), CN, and at the Institute of High Frequency Techniques and Electronics (IHE), CS, received the „Best Student Paper Award". At the IEEE 37th Int. Conference on Plasma Science in Nor-folk, VA, USA, Prof. Dr. Dr.h.c. Manfred Thumm received the Plasma Science and Applications Award 2010.